Miniaturised Gravity Sensors for Geophysical Monitoring

R. P. Middlemiss, A. Prasad, A. Noack, G. D. Hammond
Institute for Gravitational Research, University of Glasgow, UK

D. J. Paul
School of Engineering, University of Glasgow, UK

Abstract. A miniature gravity sensor is being developed that utilises the fabrication techniques used to make mobile phone accelerometers. These devices will be significantly cheaper than existing commercial gravity sensors used in geophysics. This reduced cost means that networks of gravimeters will be feasible, providing greater spacial resolution to gravity surveys. Here, the latest iterations to the prototype are outlined. A measurement of the Earth tides is presented, demonstrating the sensitivity, and long-term stability of this sensor. The device is shown to have a sensitivity of less than 10 μGal/√Hz (i.e.10^{-7} m/s^{-2} in an integration time of one second).

1 Introduction

Gravimeters are used for various applications within geophysics; prospecting (Barnes 2012), volcanology (Carbone 2017), and hydrology (Naujoks, 2008) being three examples. They can be used to infer subterranean density variations, and hence gather information difficult to find by other means.

Gravimetry has also been used in the mineral exploitation industry (Martinez 2013), but its use has been somewhat limited. Mosher and Farquharson (Mosher 2013) state that one reason for this is the size of existing devices. They explain that borehole gravimetry is of particular use for mineral exploration, but that the size of existing equipment means that this can only be done in holes of a large bore. The development of miniaturised devices could therefore enable wider usage of borehole gravimetry in the industry.

Commercial gravimeters cost upwards of fifty thousand pounds, and generally weigh at least five kilograms. The size and cost of these devices has limited their widespread usage. One exception is a borehole gravimeter developed by Scintrex (Nind 2007), but this device is not available for purchase (only for surveys conducted by the company), and it is not fabricated in a way that enables mass production.

Mobile phones utilise MEMS (micro-electro-mechanical-systems) accelerometers for various purposes. These devices can be mass produced in great numbers. They do not, however, meet the sensitivity requirements of a workable gravimeter by four orders of magnitude; nor would they be stable enough to make long-term measurements over day to week timescales, another essential criterion of commercial gravimeters.

Utilising experience within the gravitational wave community (Abbott 2016), researchers at Glasgow created the first MEMS gravimeter (Middlemiss 2016). This device capable was of long-term measurements, and with a noise floor within an order of magnitude of commercial gravimeters. Since this work was published in 2016, several iterations have occurred in the design of the sensor (Middlemiss 2017; Bramsiepe 2018); each making the device smaller, more rugged, and more sensitive to gravitational acceleration.

This manuscript outlines the significant changes made to the latest design of this device, and a demonstration is made of the current sensitivity of the device.

2 System Description

The MEMS gravimeter is comprised of a mass suspended from four geometrical anti-spring flexures (Acernese 2015). This entire structure is etched monolithically from a single piece of silicon using standard photolithography techniques. As a mass-on-spring system, this structure has a mechanical resonance, which occurs at a frequency of 7.3 Hz. Beneath this resonance peak, the device has a constant relationship between displacement and acceleration. This means that by measuring the displacement of the mass on the springs, one can make a direct measurement of the local gravitational acceleration. This displacement is measured using a capacitive method. Metal electrodes are patterned on the surface of the silicon mass. A second (fixed) plate is then fixed above the mechanical structure. Another set of electrodes are patterned onto this second plate. A sinusoidal signal is driven to the electrodes on the mechanical structure, and the second plate is used to measure the current variations caused by mutual capacitance variations as the mass moves. The mechanical device can be seen in figure 1, with the metal electrodes visible on the surface of the suspended mass.

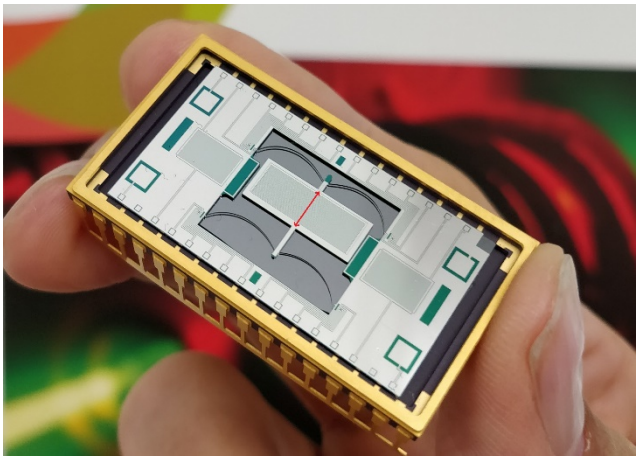

Figure 1. The MEMS device inside a standard enclosure. A mass is suspended from four arched flexures. As the mass displaces, a second plate (not shown) picks up a capacitive signal, that is used to measure the local acceleration due to gravity. The mass oscillates along the axis shown by the red arrow. This axis is aligned vertically to the ground during operation.

Complications are inevitable when constructing a device for such precision measurements. As with any other relative gravimeter (so called because it makes measurements relative to a spring whose spring constant can vary); parasitic signals are a problem. The Young's modulus of silicon varies with temperature (Hopcroft 2010); changing the spring-constant of the flexure; and thus the measurement of gravity. For this reason, it is essential to control the temperature of the structure to within 1 mK using precision measurement and control loop feedback. This is achieved using nested temperature control enclosures. A metal box is controlled at a set-point around five degrees Kelvin above ambient temperature. The MEMS package is enclosed within this box; separated by a peltier device. The peliter allows a second level of thermal control. To further reduce the effect of long-term drifts, it is necessary to use a lock-in amplification technique (Scofield 1994).

The functionality required to implement the signal processing outlined above can now be carried out using a custom-built FPGA (field-programmable gate array) electronics board (Monmasson 2011). This board can be programmed to input multiple data-streams, feedback control signals to maintain temperature, and carry out a lock-in amplification process.

3 Results

To demonstrate sensitivity of the device and its capacitive readout, the system was left in a basement lab for one week. During this time the MEMS did not experience temperature variations larger than 1 mK. The output of the system was monitored continuously. This output was converted into unit of µGal (a unit commonly used by the gravimetry community, where 1 Gal is equal to 1 cm/s^2).

Figure 2 is a time-series of the data recorded during this week-long period. The light grey series is the raw signal (with a polynomial drift removed), the black series is the same data with a running average applied, and the yellow series is the theoretical Earth tide signal, as predicted for our location in Glasgow by the T-Soft software (Van Camp 2005). The Earth tides are periodic fluctuations in the elastic crust caused by tidal forces within the Earth-Moon-Sun system (Farrell 1973). These crustal fluctuations change the distance between the crust, and the centre of the Earth, and thus the surface value of gravity. A clear correlation is seen between the measured data and the theoretical Earth tide signal. Unlike data previously published, these data have not been processed using regression analysis; yet the signal is still clearly observable.

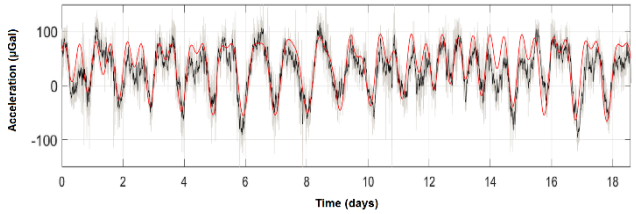

Figure 2. The time-series of the MEMS gravimeter output. The grey series is the un-averaged data, the black series is the same data with a rolling average applied, and the red series is the theoretical Earth tide signal calculated for our location.

To ascertain the noise floor of the system (when controlled using the FPGA board), an amplitude spectral density was plotted (Fig. 3). This figure demonstrates that the device can measure the primary and secondary microseismic peaks (Peterson 1993). In addition to this, it demonstrates that the noise floor of the system lies beneath 10 µGal/√Hz.

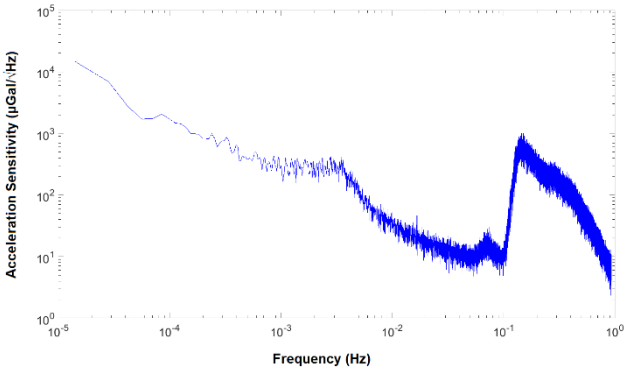

Figure 3. The amplitude spectral density of the system. The primary and secondary microseismic peak are visible.

4 Conclusion

A device capable measuring variations in gravitational acceleration beneath 10 µGal, with a small size/cost will change the way in which gravimetry is carried out, and the people who can do it.

A dramatic cost reduction in gravimeter technology will mean that networks of gravimeters can be placed in an array over an area of geophysical interest, providing increased spacial and temporal data. Work is already underway to do this at Mt Etna Volcano in Sicily, as part of the NEWTON-g H2020 consortium.

The reduced weight of these devices means that they can be flown in drones, to conduct airborne gravity surveys. Work is also underway on a device that can be

drone-mounted.

More generally, by reducing the size/cost of gravimeters, the field of gravimetry can be democtratised; gravity surveys will no longer solely be the remit of oil and gas multinationals or large academic consortia. The mineral exploration industry – which has only used gravimetry sparingly in the past - will be a clear benefactor here.

Acknowledgements

We would like to thank Kelvin Nanotechnology for fabricating the MEMS devices used to gather the data presented in this manuscript. We also wish to thank the staff and users of the JWNC for their support in the development of the MEMS fabrication process.

References

Abbott BP et al (2016) Direct Observation of Gravitational Waves from a Binary Black Hole Merger. Phys Rev Lett 116, 061102. doi: 10.1103/PhysRevLett.116.061102

Acernese F, De Rosa R, Giordano G, Romano R, Barone F (2015) Low frequency inertial control strategy for seismic attenuation with multi-stage mechanical suspensions. Proc SPIE 9431. doi: 10.1117/12.2083352

Barnes G, Barraud J (2012) Imaging geologic surfaces by inverting gravity gradient data with depth horizons. Geophysics 77(1), G1. doi: 10.1190/geo20110149.1

Bramsiepe SG, Loomes D, Middlemiss RP, Paul DJ, Hammond GD (2018) A High Stability Optical Shadow Sensor with Applications for Precision Accelerometers. IEEE Sensors Journal 18(10):4108-4116. doi: 10.1109/JSEN.2018.2818066

Carbone D, Poland MP, Diament M, Greco F (2017) The added value of time-variable microgravimetry to the understanding of how volcanoes work. Earth-Sci Rev 169(April):146-179. doi: 10.1016/j.earscirev.2017.04.014

Farrell WE (1973) Earth tides, ocean tides and tidal loading. Phil Trans R Soc A 274:253–259

Hopcroft M, Nix W, Kenny T (2010) What is the Young's modulus of silicon? J Microelectromech Syst 19(2):229-238. doi: 10.1109/JMEMS.2009.2039697

Naujoks M, Weise A, Kroner C, Jahr T (2008) Detection of small hydrological variations in gravity by repeated observations with relative gravimeters. J Geod. 82:543. doi:10.1007/s00190-007-0202-9

Martinez C, Yaoguo L, Krahenbuhi R & Braga MA (2013) 3D inversion of airborne gravity gradiometry data in mineral exploration: A case study in the Quadrilátero Ferrífero, Brazil. Geophysics 78(1) 1JF-Z24. doi: 10.1190/geo2012-0106.1

Middlemiss RP, Samarelli A, Paul DJ, Hough J, Rowan S, Hammond GD (2016) Measurement of the Earth Tides with a MEMS Gravimeter. Nature 531:614-617 doi: 10.1038/nature17397

Middlemiss RP, Bramsiepe SG, Douglas R, Hough J, Paul DJ, Rowan S, Hammond, GD (2017) Field Tests of a Portable MEMS Gravimeter. Sensors 17(11):2571 doi: 10.3390/s17112571

Monmasson E, Idkhajine L, Cirstea MN, Bahri I, Tisan A, Naouar MW (2011) FPGAs in industrial control applications. IEEE Trans Ind Inf 7(2) 224–243. doi: 10.1109/TII.2011.2123908

Mosher CRW & Farquharson CG (2013) Minimum-structure borehole gravity inversion for mineral exploration: A synthetic modeling study. Geophysics 78(2) 1MA-Z51. doi: 10.1190/geo2012-0373.1

Nind C, Seigel HO, Couteau M & Giroux B (2007) development of a borehole gravimeter for mining applications. First Break 25(7):1143-1147

Peterson J (1993) Observations and modeling of seismic background noise. US Geological Survey Open-file Report Number 93-322. doi: 10.3133/ofr93322

Prasad A, Bramsiepe SG, Middlemiss RP, Hough J, Rowan S, Hammond GD, Paul DJ (2018) A Portable MEMS Gravimeter for the Detection of the Earth Tides. IEEE SENSORS New Delhi 1-3. doi: 10.1109/ICSENS.2018.8589884

Scofield JH (1994) Frequency domain description of a lock in amplifier. Am J Phys, 62 (2) 129-133. doi: 10.1119/1.17629

Van Camp M & Vauterin P (2005) Tsoft: graphical and interactive software for the analysis of time series and Earth tides. Computers & Geosciences 31(5):631-640. doi: 10.1016/j.cageo.2004.11.015

Low volume solution ICP-MS: achieving high-precision geochemical analysis of small amounts of sample

Lewis A. Banks
British Geological Survey and University of Leicester

Simon R. Tapster, Matthew S.A. Horstwood, Simon R. Chenery
British Geological Survey

Daniel J. Smith, Tiffany L. Barry
University of Leicester

Abstract. There is a need to improve geological models for ore deposits. This requires the analysis of ever smaller amounts of material and element, to either increase the spatial (and hence temporal) resolution of the study or bring novel minerals in to the realms of analytical capability. The precision and accuracy of these measurements must be sufficient to resolve the geochemical variation required, e.g. across an orebody. Here we show the application and potential of the novel method of *low volume sampling* for geochemical measurements, by solution mode ICP-MS. Through the analysis of U-isotopes, we demonstrate that by changing the way solutions are introduced to ICP-MS instruments, comparable precision to that achieved using conventional measurement techniques, can be attained by the low volume method, yet utilising ten times less material. This method yields a 2.5 times improvement in measurement precision over the conventional method, for 2 ng U. The analytical time of 10 minutes shows a threefold reduction compared to conventional methods. The potential of low volume sampling greatly improves the analytical efficiency, the spatial resolution of a study or opens novel minerals to routine analysis.

1 Introduction

The challenge facing the progression of analytical geochemistry, and therefore the understanding of ore deposits, is the inability to measure finite amounts of element contained within the volume of a single crystal. These are inaccessible due to instrumental detection limits, impacting the precision of the analysis. This renders small variations in the target system unresolvable.

Inductively coupled plasma mass spectrometry (ICP-MS) is a widely used tool for trace element and isotopic analysis. This is due to its low backgrounds, the ability to ionise most elements, and its adaptability to analytical requirements. This study presents the application of the Teledyne-CETAC MVX 7100 µl Workstation (MVX) to solution ICP-MS. This aims to bridge the gap between conventional solution ICP-MS and laser ablation ICP-MS.

This new method of solution ICP-MS analysis targets and overcomes the inefficiencies of conventional ICP-MS sample introduction. This method relies on the relative preconcentration of the element of interest in the solution to yield an increased signal to noise ratio (SNR; Bauer and Horstwood 2018).

Integrating the ability to achieve high-precision elemental and isotopic analyses on low amounts of sample with petrographic, tracer and geochronological records will better constrain the timing and the sources of the formation of an ore deposit. This will enable a deeper, and higher resolution understanding of their genesis. This method will use geological materials that have previously been impossible to analyse, advancing the understanding or ore forming processes.

2 Sample introduction for solution ICP-MS

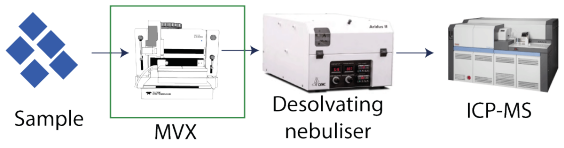

Figure 1. The analytical setup of the low volume method. The green square identifies the sample introduction mode. This can be a conventional autosampler, a laser ablation system or the MVX for example.

Conventional solution sample introduction to ICP-MS instruments (Fig. 1) is a significant source of inefficiency to the analysis, both in terms of time and wasted sample.

Long sample grow in and washout times can lead to significant amounts of the sample not being utilised in the sample measurement. This creates both wasted time and wasted sample.

Another source of wasted sample by conventional sample introduction for ICP-MS is that generally only part of the sample is utilised, e.g., 1500 µl of sample is prepared and only 1000 µl is aspirated. This therefore results in 500 µl of remaining sample solution.

There is also a relatively 'low and long' signal profile when measuring conventionally as the sample solution is dilute. This results in a low SNR whereby the baseline and/or background make up a significant proportion of the total signal intensity.

Beam stability for conventional analyses relies on the stability of the Ar stream aspirating the sample. Fluctuations can lead to variations in signal intensity, which yield inaccurate results if obtaining ratios by some single collector (SC) instruments, whereby spectral skew can be an issue.

3 What is low volume sampling?

The low volume solution sample introduction method aims for a square-wave signal profile whereby the sample grow in and washout are minimised. This leads to more of the sample being used in the analysis, therefore leading to less wasted sample and time.

The low volume method only utilises 100 µl of sample solution, facilitated by relative preconcentration. This method also aspirates the whole sample, so wasted sample is negated.

Contrary to the 'low and long' signal profile of conventional methods, the low volume method utilises a 'high and short' peak signal due to the relative preconcentration of the element of interest. This higher signal intensity results in an increased SNR. As the baseline and background provide less of the total signal intensity with the low volume method, more of the sample contributes to the final measurement precision.

The MVX is a syringe driven autosampler which actively pushes the sample into the ICP-MS. Therefore, any effects of a variable Ar stream affecting the beam intensity are reduced, reducing the chance of spectral skew effects.

4 Example: Uranium isotopes in geological samples

Understanding U-isotopes is a fundamental aspect of geochronology as they underpin U-based dating methods. A well constrained U-isotope value in the sample will provide a more accurate age determination (Hiess et al 2012; Tissot and Dauphas 2015). The U-isotope value of the sample determines the relative abundance of radiogenic Pb in the sample by which it is dated. Therefore, understanding the U-isotope ratio is imperative to an accurate age determination.

Low volume sampling demonstrates the ability to gather high-precision data on 2 ng of natural U with a 2.5

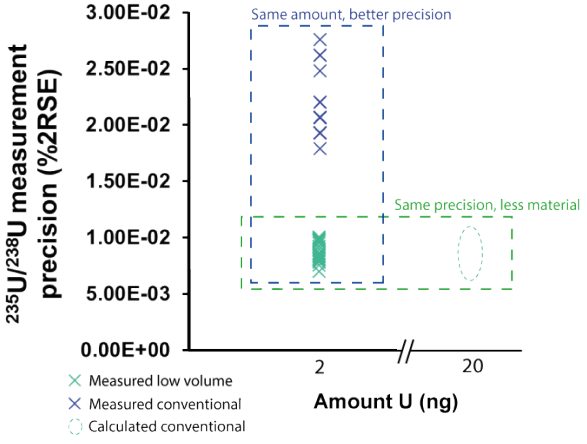

Figure 2. By measuring the same amount of material by both the conventional and the low volume method, it can be shown that there is a 2.5 times improvement in the measurement precision by utilising the low volume method. By calculating the amount of material required by the conventional method to yield the precision achieved by the low volume, it can be shown to be 10 times higher.

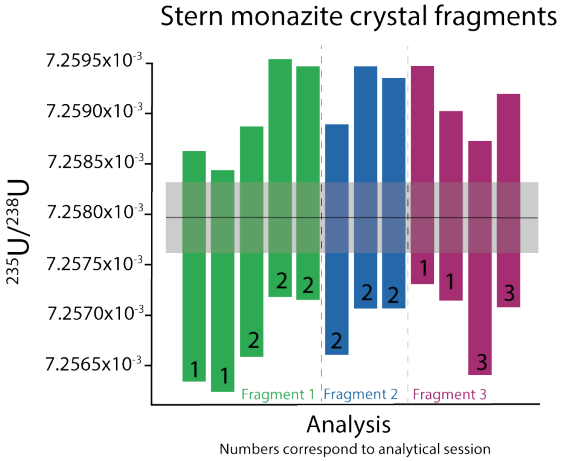

Figure 3. Analysis of three fragments of Stern monazite over three analytical sessions shows that this reference material is homogenous at this scale, whereby each measurement contains 2.5 – 4 ng U. This is representative of a crystal at 600 ppm U with dimensions between 95x95x95 µm and 105x105x105 µm.

times improvement in measurement precision (Fig. 2) over conventional methods. This amount of element is in the realm that is present in single crystals for monazites and large zircons. The ability to measure single crystal U-isotope compositions allows a unique U-isotope value to be applied to measurements, allowing the most accurate age determination possible.

Although 2 ng U may not be enough material to resolve variation in U-isotopes in zircons, the measurement precision achieved facilitates resolving the larger range of variation in $^{235}U/^{238}U$ present in nature, at a higher resolution than the conventional method, when using 2 ng.

Monazite is a REE-phosphate accessory mineral found in igneous and metamorphic rocks. It can also be formed by hydrothermal processes and is found in some orogenic Au deposits. Fig. 3 shows analysis of three single crystal fragments of this mineral by the low-volume method. Stern is a common reference material used during monazite analysis, making full characterization important. Not only does Fig. 3 show that this method is appropriate for this type of measurement, but that the Stern monazite is homogenous at this scale (see Fig. 3 caption). This information was previously outside the realms of analytical capability due to the amount of material required to yield this level of precision.

Further work to characterise a suite of monazite reference materials will establish the homogeneity of U-isotopes within crystals and crystal fragments of the commonly used reference materials. Again, this work will have significant implications to U-based geochronology, whereby the starting U-isotope composition is imperative to an accurate date (Hiess et al 2012). Also, heterogeneity in reference materials introduces a fundamental limitation to uncertainty. For example in laser ablation analysis, there is a fundamental limitation on the uncertainty of monazite reference materials of 1% (2σ). This limits the resolving power of an analysis. Subsequent geochronological measurements will facilitate a better constrained ore deposit genesis at a

higher resolution (Fig. 4) than is previously possible.

5 Advantages of low volume sampling to industry and academia

The low volume sampling method increases the overall efficiency of the measurement by measuring as much of the sample as possible. This results in significant advantages over the conventional method.

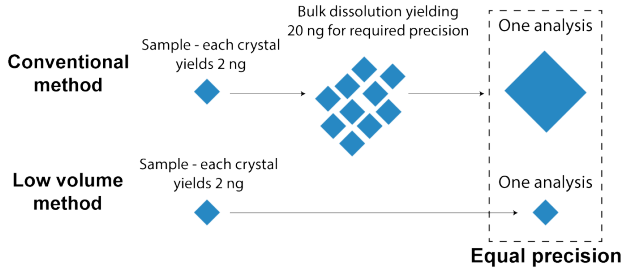

Figure 4. To achieve the same precision as the low volume method, it is calculated that the conventional method requires ten times more material, due to SNR limitations. The low volume method therefore increases the spatial resolution of the study and advances the ability to quantify heterogeneity in the sample.

For the measurement of U-isotopes, it is shown that a tenfold decrease in sample size is required to achieve the same precision by the low volume method, as would be achieved using the conventional method (Fig. 2). This decrease in sample size required has far reaching effects in geochemistry, namely, the spatial resolution of geochemical analysis by solution ICP-MS is greatly increased (Fig. 4). For example, conventional analysis will require a bulk dissolution of ten crystals to yield the amount of U required for the precision needed to resolve variation in the samples. This results in an 'averaging' of the potentially different values in the crystals, yielding one homogenised result. Using the low-volume method however, this can yield ten, single crystal analyses at the same precision as the bulk dissolution, therefore greatly increasing the spatial resolution of the study. It can also bring novel minerals into the realms of analytical capability. These minerals can have concentrations of element previously too low to measure. The advancements facilitated by this new technique will further our understanding of ore deposit genesis by creating a higher resolution model. This is achieved by both low-volume, single crystal analysis of orthodox minerals and routine analysis of novel minerals by the same method.

Further to this, if measuring the same amount of element as the conventional method, but running by low volume, the increase in precision will yield a higher resolution of the study. This means that smaller variations in elemental and isotopic ratios can be defined.

Furthermore, the time taken for the complete sample run by the low volume method is three times faster than that of the conventional method. This means that the throughput of samples for the low volume method is increased over the conventional method, creating a higher efficiency method overall.

The low volume method also produces negligible waste per sample. This results in less potentially hazardous waste being produced, therefore also making this method cheaper and safer.

Acknowledgements

This study is being undertaken with funding by a NERC CENTA studentship. This is a CASE award with Teledyne-CETAC. Thanks to Pete Winship, Niel Williams and Damon Green from Teledyne-CETAC.

References

Bauer AM, Horstwood MSA (2017) Small-volume Lu-Hf and U-Pb isotope determination of complex zircons by solution and laser ablation MC-ICP-MS. Chem Geol 476:85-99.

Hiess J, Condon DJ, McLean N, Noble SR (2012) $^{238}U/^{235}U$ systematics in terrestrial uranium-bearing minerals. Science 335: 1610-1614

Tissot LHF, Dauphas N (2015) Uranium isotopic compositions of the crust and ocean: Age corrections, U budget and global extent of modern anoxia. Geochim. Cosomochim. Acta 167:113-143

Biogeochemical surveys for epithermal Au-Ag exploration in New Zealand

Anthony B. Christie
GNS Science, PO Box 30-368, New Zealand

Colin E. Dunn
Colin Dunn Consulting Inc., North Saanich, British Columbia, Canada.

Abstract. Biogeochemical orientation surveys were undertaken at epithermal Au-Ag deposits in the Coromandel Volcanic Zone – Hauraki Goldfield (CVZ) and Taupo Volcanic Zone (TVZ), and at the Waiotapu geothermal area in the TVZ. Several plant types were sampled including pine tree bark and needles, tree fern fronds and tea tree foliage. The ferns had the most consistent occurrence and were easiest to sample, although tea tree was the main sample medium at Waiotapu. Sampling at the three CVZ Au-Ag prospects, Luck at Last, Pine Sinter and Ohui, was on previous soil geochemistry grids. The biogeochemical element anomalies successfully highlighted most known quartz veins and provided additional anomalies for further investigation. The latter were in many cases not spatially coincident with similar soil geochemical anomalies and these spatial differences are attributed to deeper penetration by the plants or soil creep downslope. At the Goldmine Hill Au-Ag prospect in the TVZ, highest Au, Ag, As and Al in ferns correlated well with the elevated Hg reported previously in soils from this area and with anomalies of pathfinder elements in reconnaissance rock chip geochemistry. At the Waiotapu geothermal area, significantly higher concentrations of Ag, Au, Sb, As, Cs and Rb were present in samples close to Champagne Pool than elsewhere confirming its location as the main outflow source of precious metals and their pathfinder elements.

1 Introduction

Exploration of late Cenozoic, volcanic-related, low sulphidation epithermal Au-Ag prospects in the North Island of New Zealand typically involves soil geochemical surveys as a primary method for siting drilling in areas with sparse outcrop. Between 2013 and 2017, biogeochemical orientation surveys, predominantly sampling ferns (Fig. 1), were carried out in the Hauraki Goldfield - Coromandel Volcanic Zone (CVZ) and in the Taupo Volcanic Zone (TVZ) to test the method as an alternative to soil surveys (Fig. 2). Three Au-Ag prospects were sampled in the CVZ, Luck at Last, Pine Sinter and Ohui, and one in the TVZ, Goldmine Hill (Fig. 2). Additionally, in the TVZ, sampling was carried out in the Waiotapu geothermal area, famous for its Champagne Pool and surrounding Au-As-Sb-Tl-bearing sinter sheet that is used as a modern analogue of epithermal mineralisation processes (e.g. Rowland and Simmons 2012).

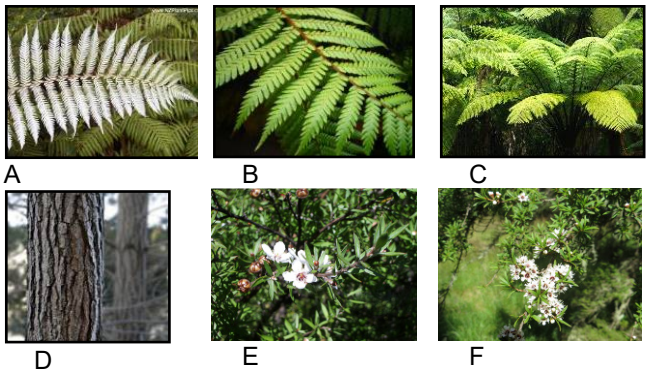

Figure 1. The main vegetation types sampled were tree ferns (A, B, C), pine tree outer bark and needles (D) and tea tree foliage (E and F). A. silver fern (ponga) - *Cyathea dealbata* (silver underneath to fronds, green on top); B. rough fern (wheki) - *Dicksonia squarrosa*; C. black fern (mamaku) - *Cyathea medullaris*; D. pine tree – *Pinus radiata*; E. Manuka tea tree - *Leptospermum scoparium*; and F. Kanuka tea tree - *Kunzea ericoides*.

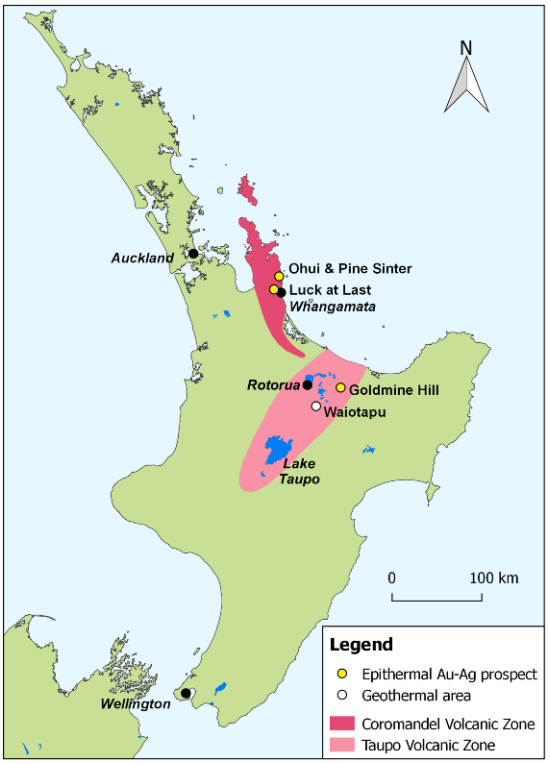

Figure 2. Location of the sampled areas in the North Island of New Zealand: Pine Sinter, Ohui and Luck at Last in the Hauraki Goldfield – Coromandel Volcanic Zone and Gold Mine Hill and Waiotapu in the Taupo Volcanic Zone.

2 Analyses

Samples of plant material were oven-dried and the foliage separated. Some sets of samples were processed as dry tissue, whereas others were ashed by controlled ignition at 485°C for 24 hours. The samples were analysed at Bureau Veritas Laboratories in Canada by method VG104-EXT (52 elements) plus 12 of the REE elements not included in the standard suite, to give a total of 64 elements. The material was digested in aqua regia (HNO_3-HCL-H_2O at 2:02:02) and analysed by inductively coupled plasma emission spectroscopy (ICP-ES) for Ca, Mg, Na, K, and Fe, and inductively coupled plasma mass spectrometry (ICP-MS) for Ag, Al, As, Au, B, Ba, Be, Bi, Cd, Ce, Co, Cr, Cs, Cu, Dy, Er, Eu, Ga, Gd, Ge, Hf, Ho, In, La, Li, Lu, Mn, Mo, Nb, Nd, Ni, P, Pb, Pd, Pr, Pt, Rb, Re, S, Sb, Sc, Se, Sm, Sn, Sr, Ta, Tb, Te, Th, Ti, Tl, Tm, U, V, W, Y, Yb, Zn and Zr. For most elements there are little or no losses during ashing and for others there are small losses (e.g. As and S), and complete loss of Hg. The elements that partially volatilise typically exhibit a consistent loss provided consistent ashing conditions in the laboratory are maintained, and so the patterns of element distributions are meaningful (Dunn and Christie 2014). Ashing concentrates fern tissues by approximately 10 to 15-fold and by determining the ash yield of each sample, the data can be levelled to a dry weight basis.

The QA/QC protocols followed were:

- Control SF1 (swordfern ash) was inserted at irregular intervals throughout the analytical sequence at a frequency of 1 standard per 20 samples.
- Field duplicates were inserted at the same frequency as the control SF1.
- The geochemical laboratory inserted 3 analytical duplicates at a frequency of approximately 1 per 40 samples.
- The laboratory also inserted several of their own controls and blanks at a frequency of approximately 1 of each per 40 samples.

3 Hauraki Goldfield, CVZ

3.1 Luck at Last

At the Luck at Last prospect, west of Whangamata, underground mining over a vertical extent of ~108 m, from 1896 to 1929, produced 13,176 oz of Au-Ag bullion from quartz veins in hydrothermally altered, flow-banded rhyolite and andesitic tuffs. The biogeochemical survey used a previous soil geochemistry sampling grid and sampled pine tree bark and needles, and several fern species at or adjacent to the previous soil sample sites (Dunn and Christie 2014; Dunn et al. 2017). Silver fern ('ponga') proved to be the most widespread and diagnostic of the several species tested.

Concentrations of Rb and Cs were elevated near the mineralised vein, but the highest levels of Au and Zn occurred near the eastern margin of the survey area and around the disturbed ground in the west previously occupied by the stamp mill battery. At the latter site, analysis of adjacent 'ponga' and 'wheki' (rough tree fern) showed that 'ponga' is considerably more enriched in most elements – with the notable exception of Ba being higher in the 'wheki'. Several elements such as Ag (Fig. 3) exhibited anomalies associated with both the quartz veins and the eastern area. The eastern anomalies lie along a northeasterly trend east of the main quartz vein and mine and provide new targets for future exploration.

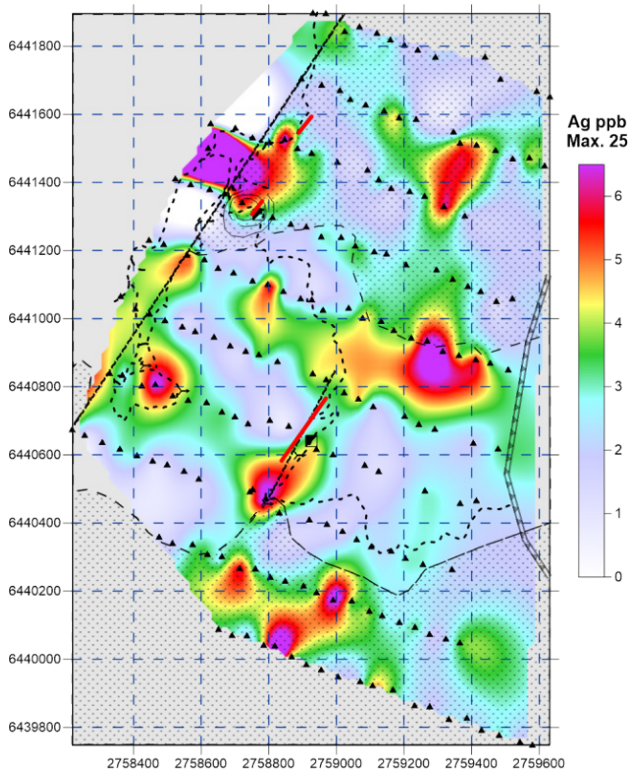

Figure 3. Luck at Last – contours of ppb Ag in silver fern. Black triangles are sample points, red lines are quartz veins and half-blacked square is entrance to the main former underground mine. Grid spacing is 100 m.

3.2 Pine Sinter

The Pine Sinter prospect is a recent discovery and has had no previous mining. A rhyolite dome is overlain by a sequence of rhyolitic tuffs and breccias, and andesitic flows and pyroclastic units. Remnants of a sinter sheet are present on the surface. To the east, the sequence is overlain by post-mineral andesite. Following the positive experience with ferns at Luck at Last, only ferns were sampled at Pine Sinter and they were collected on a previous soil geochemistry sampling grid. Results showed that silver ferns have slightly anomalous Ag content in a north-trending zone located near and parallel to the post mineral andesite contact (Fig. 4). Several elements (Ba, Ca, Sr, Se and REE) are elevated in a parallel trend but ~100 m to the west. All Au levels were low and no definitive trends were obvious.

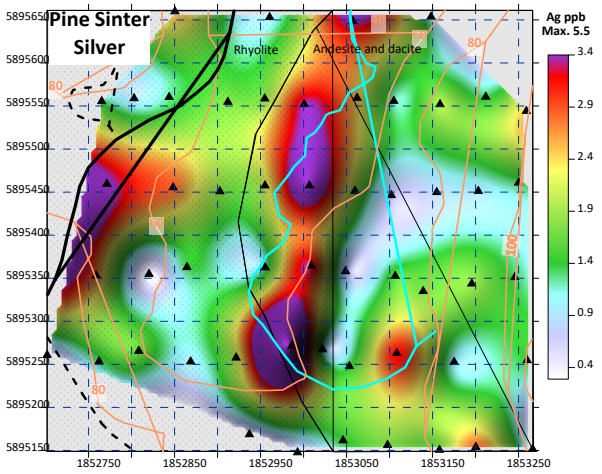

Figure 4. Pine Sinter – contours of ppb Ag in silver fern. Sample points are shown by the black triangles, the thick black line in the top left is a road and the blue line is a stream. Grid spacing is 100 m.

3.3 Ohui

At Ohui, shallow underground mining from the 1890s to 1910 produced 234 oz of Au-Ag bullion from quartz veins hosted in andesite and rhyolite. Ferns were sampled on a previous soil geochemistry grid. The Phoenix and Staircase vein areas are defined by elevated Ag and Sb in the ferns (Fig. 5), but not by Au (Dunn et al. 2018). The Staircase veins also show some weak enrichment of As. Nickel, Co, and to a lesser degree S, Ca and Ag (Fig. 5) define a north-easterly trend between the Phoenix and Staircase areas, providing secondary exploration targets. Earlier soil surveys showed enrichments of Au, As, Sb and Hg near the Great Mexican fault, but these signatures are either not present in the ferns where sampled, or the weak signatures are laterally displaced. A large part of the area of interest was not available for sampling because the vegetation had been cleared by logging operations (shown by area of 'No samples" in Fig. 5).

.

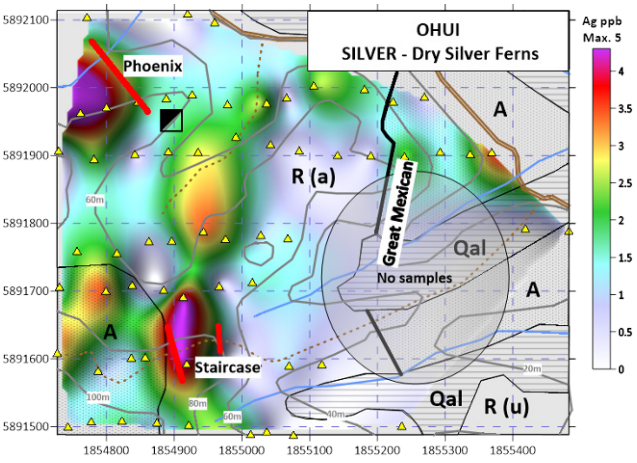

Figure 5. Ohui – contours of ppb Ag in silver fern. Grid spacing is 100 m.

4 Taupo Volcanic Zone

4.1 Goldmine Hill, Puhipuhi

At Goldmine Hill, east of Rotorua, alteration and mineralisation occur in close spatial association with dacitic intrusions, breccias and flows of Pleistocene age (Fig. 6). These rocks are intruded into and erupted onto Okataina Group rhyolitic volcanic and volcaniclastic rocks. They are transgressed by northeast-trending faults. Exploration to date has been of a reconnaissance nature and there has been no past mining or drilling.

Reconnaissance sampling of pine bark and needles, and ferns, on road and stream traverses showed that wheki is the dominant fern species, but there were sufficient ponga and mamaku (Fig. 1) to establish that they absorb substantially different amounts of elements, with wheki having lowest concentrations of most elements. However, the spatial distribution of elements is of greater significance than absolute concentrations, and highest Au, Ag (Fig. 6), As and Al in wheki correlated well with the elevated Hg reported previously in soils from this area and with anomalies of pathfinder elements in reconnaissance rock chip geochemistry (Dunn and Christie 2017).

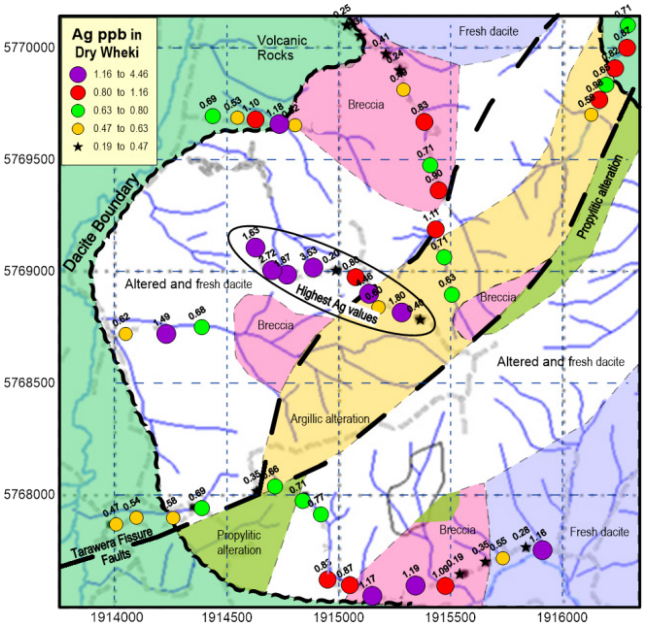

Figure 6. Goldmine Hill, Puhipuhi – ppb Ag in wheki at sampled locations. Grid spacing is 100 m. Base geology map modified after Corbett (2015).

4.2 Waiotapu

The Waiotapu active geothermal area is characterised by a large area of steaming ground and fumarolic activity. Vegetation in the area is dominated by two types of tea tree – Kanuka and Manuka. Kanuka has higher concentrations of the epithermal related elements Ag, Au, Sb and As than Manuka, especially close to Champagne Pool (Fig. 7) where the deep

geothermal alkali chloride water flows out to surface from a hydrothermal eruption crater. The sample taken near Champagne Pool is growing in soil developed on a hydrothermal eruption breccia, although the metal enrichment in the Kanuka is probably also in part a result of precipitation from the metal-enriched mists emanating from Champagne Pool (Dunn et al. 2018).

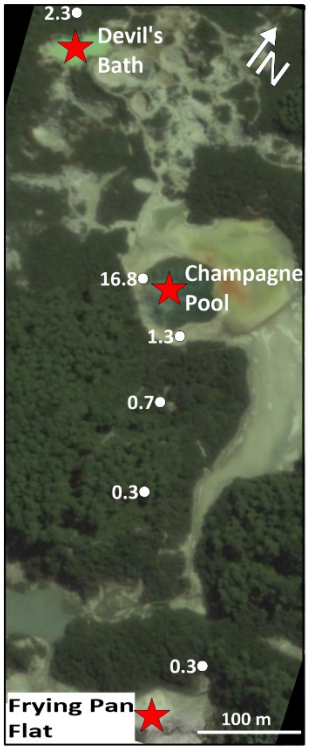

Figure 7. Waiotapu – ppb Au in kanuka shows significant concentration by Champagne Pool.

5 Discussion

5.1 Fern versus pine geochemistry

At Luck at Last, a comparison of median concentrations of elements in ferns, pine bark and pine needle litter showed that many elements were considerably more concentrated in the ferns than in the other media – notably Al, B, Ce, Cr, Cs, Cu, Ga, K, La, Mg, Mn, Mo, Na, Ni, P, Rb, S, Sc and Y (Dunn and Christie 2014). Elements consistently enriched in the pine bark were As, Au, Pb, Ti, and Bi. Pine needles had the highest concentrations of Ag, Ca and Zn.

5.2 Fern versus soil geochemistry

Many of the biogeochemical anomalies were away from known sources (veins, breccia, sinter) and some of these were not spatially coincident with similar soil geochemical anomalies. These spatial differences are attributed to deeper penetration by the plants, or soil creep downslope, with contributions of elements migrating vertically from concealed mineralisation.

5.3 Selection of sample media

A major factor in selecting a suitable plant species to sample is its distribution in the survey area. The plant species must be commonly present and occur throughout the area. It must also have a good response to the elements of interest so that concentrations are significantly elevated above the lower level of detection. This can be improved by ashing to concentrate the elements, but at the loss of Hg. In the epithermal Au-Ag prospect areas sampled here, ferns proved the most useful sample medium.

6 Conclusions

Biogeochemical orientation surveys carried out in New Zealand show that common plant species exhibit anomalous element concentrations in the vicinity of Au-Ag deposits. Different species have different responses and therefore care must be taken in the species selection, preferably through an orientation survey in the exploration area and employment of samplers that are trained in identification of the selected species. Surveys to date have assembled a reference biogeochemical database of common species to assist in future mineral exploration surveys.

Acknowledgements

Access to Luck at Last, Ohui and Pine Sinter was provided by Newmont Waihi Gold and OceanaGold, and facilitated by Rick Streiff, Lorrance Torckler, Rob Theron and Robert Schoonderwoerd. Access to Goldmine Hill was provided by Silver City Minerals and facilitated by Chris Torrey and Gordon McLean. Jenny Black, Holly Harvey-Wishart, Chris Town, Gordon McLean and Rob Theron provided field assistance and John Simes provided laboratory assistance. Jenny Black drafted Fig. 1. Funding was provided by the New Zealand Government and by Silver City Minerals for the analyses of the Goldmine Hill samples.

References

Corbett W (2015) Final relinquishment and annual report for Exploration Permit 56212 “Taupo One” and Prospecting Permit 56147 “Taupo Two” for the period 1 January 2015 to 29 January 2016. Silver City NZ Pty Ltd. Unpublished mineral report MR5302, Ministry of Business, Innovation and Employment, Wellington

Dunn CE, Christie AB (2014) Biogeochemical orientation survey, Luck at Last Mine Area, Coromandel, New Zealand. GNS Science Report 2014/60

Dunn CE, Christie AB (2017) Tree ferns in biogeochemical exploration, Goldmine (Puhipuhi) Hill, North Island, New Zealand. GNS Science Report 2017/21

Dunn CE, Christie AB, Black J (2017) Tree ferns as biogeochemical survey sample media in gold exploration, Luck at Last Mine, Coromandel, New Zealand. GNS Science report 2017/22

Dunn CE, Christie AB, Black J (2018) Biogeochemical Surveys at Ohui and Pine Sinter Epithermal Au-Ag Prospects, Coromandel, and at Waiotapu Thermal Park, New Zealand. GNS Science Report 2018/20

Troubleshooting hydrogeochemical sampling in grassroots mineral exploration: a Case Study from central Australia's Western Amadeus basin

Jennifer A. Roskowski
Generative Exploration Group, First Quantum Minerals Ltd., West Perth, WA, Australia

Nathan Reid
CSIRO Mineral Resources, Kensington, WA, Australia

James Kidder
Department of Geological Sciences, Queen's University, Kingston, ON, Canada

Ryan R.P. Noble
CSIRO Mineral Resources, Kensington, WA, Australia

Abstract. Early-stage exploration for ore deposits has historically included reconnaissance sampling of solid media. Sampling of natural waters for mineral exploration has been increasing since its initial adoption in the 1970s but has not yet become a standard greenfields exploration tool despite increased commercial availability of low detection limit water analyses. A practical field sampling methodology was developed by the CSIRO, and interpreting results appeared fairly straightforward after initial literature review. However, the practicalities of analyzing hydrogeochemical data from real-world mineral exploration samples has led to important learnings regarding the assessment of metal anomalism in natural waters. We present an example of highly base-metal anomalous samples from saline groundwaters in Australia. Several phases of water sampling across different seasons followed by pump testing of the anomalous water bore revealed that the extremely elevated copper anomalism was related to downhole equipment rather than a buried mineral system. We outline the evolution of field work and data interpretation that led to this conclusion as well as share guidelines for how to mitigate the effects of potential downhole contaminants to produce viable, geologically meaningful water sampling results for reconnaissance mineral exploration.

1 Introduction

Geochemical footprints of ore deposits are detectable in groundwaters on a larger scale than is typically visible in solid media (Leybourne et al. 2007). With the advent of lower detection limits in commercially available analytical techniques, hydrogeochemical sampling can now reliably detect and map kilometre-scale footprints of both ore and pathfinder elements (Eppinger et al. 2012). The ability to detect mineral system footprints from farther away or under deeper post-mineral cover is becoming increasingly important in modern-day mineral exploration.

Reconnaissance hydrogeochemical sampling was employed during an initial field program in the Amadeus Basin of arid Western Australia. The Amadeus Basin is a Neoproterozoic to Devonian intracratonic basin formed during the breakup of the supercontinent Rodinia (Walter and Veevers 2000). The Amadeus Basin covers an area of approximately 180,000 km^2 along an E-W axis, and sediment thickness reaches in excess of 12km (Edgoose 2013). Much of the basin lies in the Northern Territory, but the western extent of the basin traverses into Western Australia and is interpreted from regional magnetics to exist under thin cover in an approximately 40,000km^2 area. Copper shows and prospects are known in the eastern and central Amadeus basin, where these Neoproterozoic strata outcrop extensively.

2 Exploration Program Overview

The Amadeus Basin is broadly coeval in time and tectonic setting with the well-endowed Central African Copperbelt, and the western extent of the basin was selected for on-ground exploration for large sediment-hosted copper deposits following desktop review. The western sub-basin was interpreted to contain shallow to outcropping Neoproterozoic strata obscured by a thin veneer of desert sand and has had relatively little historic exploration due to its remoteness and the challenging access conditions.

The presence of relatively thin (generally less than 50m) transported, post-mineral cover on conceptually prospective sedimentary rocks made the western Amadeus a prime location for a wide-spaced, reconnaissance-style hydrogeochemical sampling campaign. Initial levels of base metal anomalism in water samples were very encouraging. Repeat sampling of the most anomalous bore continued to indicate elevated levels of base metals at the site; however, traditional reconnaissance geological mapping and sampling in the region was not compelling.

Before proceeding with more substantial on-ground expenditure, robust evidence supporting a direct relationship between the strongly base-metal anomalous water bore and buried mineralisation was required. Due

diligence work was conducted to assess whether the metal anomalism of the borehole could be due to contamination at the site.

Several types of contamination were hypothesized including historic leaded petrol spills, downhole industrial detritus, sample acidification with contaminated acid, and metallic downhole gear. Re-assay and re-sampling of several bores in the region ruled out any issues with sample preparation or assay laboratories. Hydrocarbon sampling of bore waters ruled out the current presence of any type of hydrocarbon at the site, and Pb isotope sampling was proposed as one possible avenue to test for spills of historic leaded petrol.

However, after correspondence with James Kidder at Queen's University, it became apparent that the suite of anomalous metals and their relative levels of anomalism were very similar to waters measured from various household and industrial water taps with brass fittings. With this information in mind, the downhole gear became the prime suspect for base metal contamination in the water bore. A water bore pump test was designed with input from the CSIRO team in Perth and executed by FQM personnel and contractors. Details of sampling campaigns, methodology, and results are elucidated below.

3 Initial Reconnaissance Water Sampling

3.1 Overview

A helicopter-supported, sub-basin wide water sampling program was conducted in collaboration with Indigenous Aboriginal Traditional Owners and anthropologists during October-November 2013. Sample spacing was entirely dependent on the location of existing surface and subsurface water sources in the region; approximate sample spacing was on the order of 30km.

Knowledge of the location of available water sources was derived mainly from consultation with Ngaanyatjarra Land Council anthropologists and Traditional Owners. Water sources included traditionally known soaks, seeps, and springs; locally administered water bores; and historic gold exploration drill holes. Water bores typically contained varying types of irretrievable downhole equipment. Several of the water bores were ~1950s-60s era hand pump bores.

Sample collection was conducted during the drier months of the year.

3.2 Methodology

Samples were collected according to the procedure in Noble et al. (2011). Samples were stored at camp in an air-conditioned trailer for the duration of the 3 – 4 week program. Samples were sent to ACME Labs in Canada for acidification and low-level hydrogeochemical analysis; however, significant dilution of the salty, Australian cation samples was required at this lab in order to maintain the instrument quality for use on very fresh Arctic waters. This and other analytical challenges prompted FQM to send a split of the cation samples to ALS Chemex Minerals lab in Vancouver for verification purposes. Reassay of cation samples at ALS confirmed anomalism and generally reproduced the ACME results.

Water sample assays were placed into aquifer groups determined by their physicochemical properties and each aquifer group was assessed separately for anomalism. Metal anomalism was evaluated with respect to the pH, Eh, and salinity of the water in question.

3.3 Results

The 2013 water sampling campaign resulted in several Cu anomalous samples; these samples tended to also have high Pb and Zn and variably elevated V, Cd, and U. In both locations with exceedingly anomalous base metal enrichment, the samples were serendipitously collected as field duplicates. The fact that the anomalous metal concentrations were broadly repeatable in field duplicates increased confidence that the metal anomalism was genuine.

Background levels of copper in water for this region are ~30ppb Cu. The highest copper assay in water was 954ppb Cu with a similarly high but slightly depressed duplicate sample; this bore was also strongly anomalous in Zn (3869ppb), moderately anomalous Cd and V, and had concerningly elevated Pb (49.5ppb) given that the water source was a hand pump bore occasionally used for drinking water by local residents during hunting trips.

All other base-metal anomalous water samples were determined to lie broadly along the NaCl - metal enrichment trend, thus downgrading the significance of their high metal content.

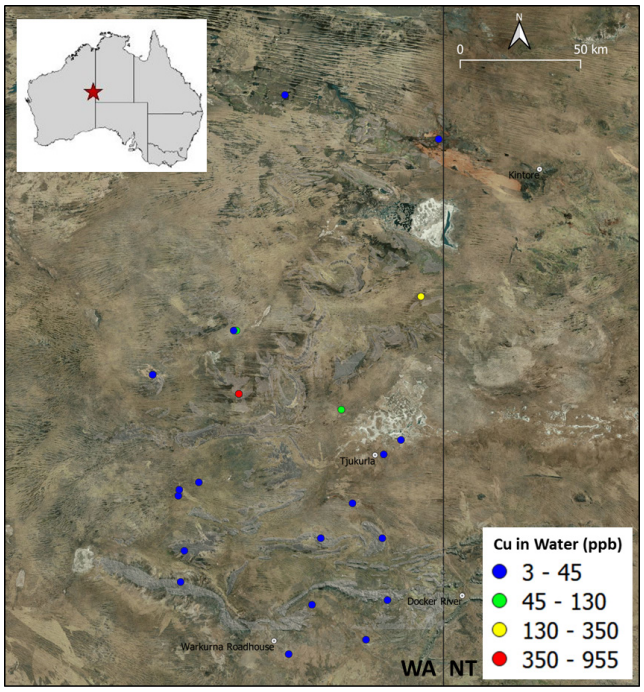

Figure 1. Location map of water samples in western Amadeus Basin. Raw copper values (ppb) on satellite imagery.

4 Re-assay Water Sampling Campaign

4.1 Overview

After significant delays in on-ground access due to protracted negotiations, the field area was again accessed in March 2016. During the execution of an Aboriginal Heritage Cultural Clearance Survey on this tenure, repeat duplicate samples were collected from the anomalous water bore and a background-level water bore also within the license area.

Samples were collected during the wetter part of the year.

4.2 Methodology

Samples were collected according to the procedure in Noble et al. (2011). Samples were stored in a camp cooler in the shade for several days before being transported to Perth via aircraft. Cation samples were acidified at the CSIRO lab in Perth with 1mL clean nitric acid; no substantial precipitate was noted in the samples.

Samples were submitted to ALS Perth for shipment to ALS Chemex Minerals Lab in Vancouver for analysis by high resolution hydrogeochemical package. Duplicates, blanks, and standards were included in sample submittal for lab and method verification.

4.3 Results

Re-assay of both water bores showed similar patterns to the initial assays. Duplicates were reasonably consistent though did show a tendency to have slightly varying levels of metal anomalism between field duplicates.

Whilst water samples from both re-sampled bores showed similar patterns to the 2013 samples, the absolute values of nearly all elements were suppressed by approximately half. This pattern conformed to expectations, as these samples were collected during a wet time in the region whereas the previous sampling campaign was conducted during a dry season.

One exception to this pattern of absolute value suppression was the Pb concentrations. In both bores the Pb values from the 2016 samples were equal to or higher than the Pb values from the 2013 samples. For the background bore this discrepancy could be attributed to a slight change in lab methodologies between the two sample batches; however, one of the samples from the anomalous bore had twice the Pb levels of the initial sample: 98.4ppb Pb. Pb is not particularly soluble in surface waters in similar hydrogeochemical regimes in Australia, so these increasingly high levels suggested Pb contamination (Gray 2001). There was not substantial evidence at this time to suggest contamination of Cu, Zn, or other metals.

5 Pump Test of Anomalous Bore

5.1 Overview

In late 2017 an on-ground work program was conducted within the license area containing the anomalous bore. Rock chip sampling and geologic mapping were conducted on exposed rocks, and systematic surface sampling of solid media completed.

Results of the surface sampling and geologic investigations were interesting but not compelling. A final test of the water bore was planned to determine unequivocally whether the anomalous metal values were related to a mineral system or due to contamination.

In February 2018 a field team conducted a campaign involving a thorough investigation of the bore itself and collection of water samples from the bore by several methods. During on-country work it became apparent that the downhole equipment at the anomalous bore had been removed and replaced; the change in gear reportedly occurred in 2014 or 2015, meaning that the downhole gear in place during the first year of sampling and during the re-sampling campaign in 2016 were not the same.

Inspection of the *in situ* downhole gear and the downhole gear detritus near the site suggested that the old gear was simply replaced with newer gear of the exact same design. Downhole gear was clearly made of copper alloys and brass, and the outflow arm at the surface was constructed of galvanized pipe. Approximate volume of the bore was estimated at 1000L based on collar width and bore depth.

5.2 Methodology

Upon arrival to the site a water sample was collected with a plastic bailer while the downhole gear was still in place. After the downhole gear was retrieved using a block and tackle set up, a plastic waterline connected to a pump at the surface was snaked down the borehole.

Two stages of pump testing were conducted consecutively: 30 min at 0.5L/s and 3.5 hours at 1.5L/s flow rate. Physicochemical measurements were taken at regular intervals throughout the pump tests, and water samples were collected at one times the bore volume (1000L), three times the bore volume (3000L), at a spike in TDS around the 100 minute mark, and at the end of the pump test (7500L).

Following the pump test, the downhole gear was reinserted into the bore. Hand pump apparatus was worked vigorously and a water sample was taken once the water was clear of significant sediment. The bore was allowed to rest overnight. The following morning two samples were collected: the first water from the hand pump which contained some sediment, and a sample of clear water after renewed pumping.

Downhole gear was tested with a Niton portable XRF. Footer valve, actuator arm, pipe fittings, and outflow pipes contained percent levels of Cu, Zn, and Pb and up to 100s - 1000s ppm of Co, Cr, V, and Ag. Sediment retrieved from the footer value was anomalous in Cu, Zn, Pb, V, Cr, and Au.

5.3 Results

Results are shown in Figure 2. Samples taken with the hand pump show extremely elevated levels of copper, while all other methods show background levels. It is

unclear why this particular hand pump is substantially more anomalous than any of the other hand pump bores sampled. High levels of metals may be due in part to fairly saline water conditions. Very low throughput of water from the bore – due in part to its saline nature and in part to its remoteness on a lesser used side track – could contribute to accumulation and precipitation of metals into the lower portion of the water column and into the sediment that has settled there.

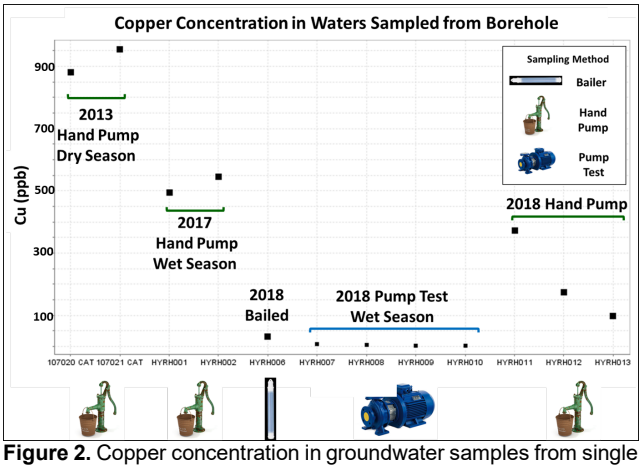

Figure 2. Copper concentration in groundwater samples from single 'anomalous' bore. Note the very high concentrations of Cu in samples collected using the hand pump apparatus. Bailed sample and samples from pump test contain Cu values near regional background. With repeated flushing of hand pump, Cu levels appear to be dropping off to background levels suggesting high base metals in this bore were from downhole contamination.

6 Recommendations

Following multiple hydrogeochemical orientation studies and exploration programs, several guidelines regarding use and interpretation of water sampling data for mineral exploration can be delineated:

1) Cation species important in base metal exploration such as Cu, Pb, and Zn are more prone to influence from contaminants in surface waters than oxyanion species like Mo, U, V.
2) Data interrogation of linked anomalous elements may prove useful. A strong association of cation species in broadly neutral waters can suggest contamination while an oxyanion association with occasional cation spikes may indicate a mineral system.
3) Some elements in a sample or data set may show order of magnitude contamination, e.g. Cu, Pb, Zn. Other pathfinder elements in the same data set may show no or low-level contamination and can thus still be used in the exploration assessment; Co and Cr in this study experience only minor ppb-level shifts.
4) Flush as much water through the sampling apparatus or system as possible to ensure a clean sample. This is not always possible in early-stage surveys, but data assessment methods can mitigate these relatively rare risks.
5) Take two aliquots of water for cation analysis at every sample location. Acidify and store this back-up sample safely for up to a year.

Contamination in hydrogeochemical sampling is a minor concern in most large data sets but can become critical to the success of wide-spaced, reconnaissance-level surveys. An awareness of metal associations and characteristics of potential downhole contaminants can adequately mitigate risk to exploration interpretation. As hydrogeochemistry becomes a more widely used tool, technical teething issues such as the one presented here will become better known and more routine to manage.

The more we use and troubleshoot robust techniques like hydrogeochemical sampling, the more reliable the technique becomes and the more confidence explorationists will have in the consistency and practical utility of this geochemical method.

Acknowledgements

Many thanks to David Gray from CSIRO and Michelle Carey at IMDEX for constructive discussions regarding hydrogeochemical data analysis and potential contaminant test designs.

Pump testing would not have been possible without the Pumps United team in Perth and the multi-faceted expertise of field specialist Geoff Nicholson. Expert field support provided by XM Logistics.

All on-country work was made possible by the collaborative and welcoming spirit of the Ngaanyatjarra Land Council and Tjamu Tjamu Traditional Owners and staff. Special thanks to anthropologists David Brooks and Bryony Nicholson.

References

de Caritat P and Kirste D (2005) Hydrogeochemistry - clues to hidden mineralisation. Geoscience Australia AusGeo News 77

Edgoose, CJ (2013) Chapter 23 – The Amadeus Basin. In: Ahmad M and Munson TJ (compilers) Geology and Mineral Resources of the Northern Territory. NTGS, Special Publication 5

Eppinger RG, Fey DL, Giles SA, Kelley KD, Smith SM (2012) An exploration hydrogeochemical study at the giant Pebble porphyry Cu-Au-Mo deposit, Alaska, USA, using high-resolution ICP-MS. Geochemistry: Exploration, Environment, Analysis 12:211-226

Gray DJ (2001) Hydrogeochemistry in the Yilgarn Craton. Geochemistry: Exploration, Environment, Analysis 1:253-264

Leybourne MI (2007) Aqueous Geochemistry in Mineral Exploration. In: Goodfellow WD (ed) Mineral Deposits of Canada: A Synthesis of Major Deposit-types, District Metallogeny, the Evolution of Geological Provinces, and Exploration Methods. Geol Association of Canada Mineral Deposits Division, Special Publication 5 pp1007-1033

Noble RRP, Gray DJ, Gill AJ (2011) Field guide for mineral exploration using hydrogeochemical analysis. CSIRO Earth Science and Resource Engineering

Walter MR and Veevers JJ 2000. Neoproterozoic Australia. In: Veevers JJ (ed) Billion-year history of Australia and neighbours in Gondwanaland. GEMOC Press, Sydney pp131-153

Application of synchrotron X-rays to ore geology research

Bjorn P. von der Heyden
University of Stellenbosch, South Africa

Abstract. Ore mineralization genetic models, which strongly guide exploration efforts, rely heavily on a full and fundamental scientific understanding of the exposures provided by known ore deposits. To this end, synchrotron-based X-ray techniques represent an emerging class of research technologies that can be used to augment traditional ore geology studies. These techniques provide a unique set of affordances that include micrometer- to sub-micrometer chemical mapping (synchrotron X-ray fluorescence mapping), as well as detailed insights into chemical valence states and local coordination using X-ray Absorption Spectroscopies (XAS). In this contribution, the unique insights provided by synchrotron X-ray techniques are highlighted by referring to their applicability to studying ore fluids, trace element distributions in ore minerals, and supergene/surficial ore-forming processes. As synchrotron science and technology continues to evolve, particularly to include high-resolution three-dimensional capabilities, high brilliance X-ray techniques are expected to play an increasingly important role in ore geology research, ultimately benefitting the efficiency of exploration and mining activities.

1 Introduction

Rampant technological advancements over the last twenty years have seen the emergence and proliferation of third and fourth generation synchrotron light sources (e.g., Ice et al. 2011). Correspondingly, ore geology researchers have increasingly found novel and effective ways in which to apply synchrotron X-rays towards advancing this important field of earth science (Fig. 1).

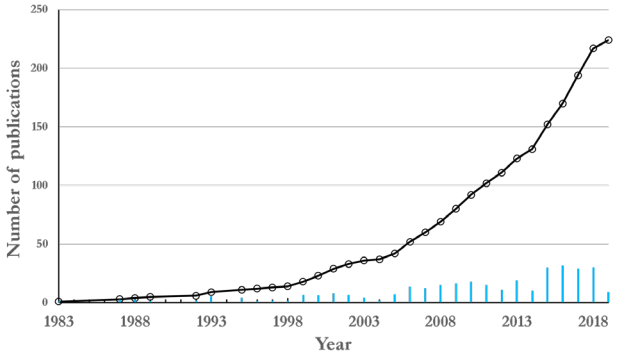

Figure 1. Cumulative curve for the number of scientific articles published that focus on utilizing synchrotron X-rays towards advancing ore geology research. Bars reflect the annual outputs used to generate the cumulative curve.

Relative to standard bench- or laboratory-scale X-ray sources, synchrotron X-rays are characterized by a much higher brilliance, are more energetic, have significantly smaller spot sizes (<10 nm), and can be fine-tuned to provide exceedingly good energy resolution in measured spectra (e.g., 0.05 eV (Merkulova et al. 2019)). These superior X-rays interact with the electrons in the orbital structure of matter (including ore metals) and thus give rise to a host of highly specialized techniques for understanding molecular-scale to sub-micrometer scale properties of ore mineralization (Brugger et al., 2010). These techniques include: X-ray Absorption Spectroscopies (XAS) which probe local coordination (e.g., XANES: X-ray Absorption Near-Edge Structure) and bonding interactions (e.g., EXAFS: Extended X-ray Absorption Fine Structure); synchrotron X-ray Fluorescence (sXRF) used to quantify and map chemical distributions at sub-micrometer resolutions; and synchrotron X-ray Computed Tomography (sXCT) which provides 3D insights into ore parageneses. A limited number of researchers and research groups are currently applying these techniques towards understanding the controls and characteristics of ore mineralization. The aim of the present contribution is to highlight to the broader research community how these techniques can and have been utilized toward enhancing our understanding of the fundamental aspects of ore formation. Results derived from future synchrotron studies are anticipated to result in continuous and incremental improvements in the scientific strength and accuracy of the ore mineralization models that are produced and which are ultimately used to advise minerals exploration.

2 Chemistry of ore-forming fluids

Synchrotron X-rays have been central to two key study methodologies which focus on the chemistry of ore mineralising fluids, viz. fluid inclusion studies and metal complexation studies in experimental fluids. The former approach was pioneered in the 1980's (e.g., Frantz et al. 1988), albeit with large spot sizes and limited detection of chemical concentration. In the last few decades, these two parameters have been significantly improved, and synchrotron XRF (sXRF) is now a quantitative characterisation technique which can be successfully applied to fluid inclusions as small as ~10 - 30 µm (e.g., Cauzid et al. 2006; Berry et al. 2009) Furthermore, recent sXRF fluid inclusion studies are combining element quantification with chemical insights from XANES and EXAFS which reveal the valence and coordination chemistry of metals within mineralising fluids (Berry et al. 2009; Richard et al. 2013). These insights will be particularly important for understanding ore deposit formation, especially those in which reactions between the wall-rock and the chemical moieties in hydrothermal

solution give rise to metal precipitation.

A growing body of experimental work on aqueous metal complexes complements the fluid inclusion analyses described in the previous paragraph. These studies utilise especially-designed high-pressure and high-temperature cells (e.g., Testemale et al. 2005) that enable model aqueous hydrothermal fluids to experience temperatures of 30 – 600 °C and pressures ranging between 0.1 and 200 MPa. These experiments commonly pair quantitative sXRF (for concentration and solubility data) with XANES and EXAFS (for coordination chemistry insights); and often couple these experimental insights with *ab initio* molecular orbital calculations. A recent synthesis of metal coordination chemistry in these model systems highlights the role that temperature-dependent coordination changes play in metal fractionation in natural hydrothermal mineralising systems (Brugger et al. 2016).

3 Speciation and distribution of contained trace metals

The economic viability of an ore deposit is often strongly influenced by the presence of sought-after by-product metals that enhances the economic viability of the deposit, or the presence of deleterious trace elements which detract from the viability of an ore deposit. The affordances of sXRF as a micrometer-scale chemical mapping technique is gaining prominence over LA-ICP-MS mapping (which has a poorer spatial resolution), and SEM-WDS and electron microprobe mapping (which have inferior chemical detection limits). Recently, the temporal scales for collecting sXRF mapping data have been greatly enhanced by the development of multi-detector arrays such as the Maia detector at the Australian Synchrotron (Fisher et al. 2015; Li et al. 2016).

The chemical speciation of contained trace metals has important implications for the ultimate ore processing (i.e., it impacts the metallurgical extraction from the host mineral). The mineralogical siting, valence state designation, and identity of adjacent atoms in the bulk lattice structure are parameters which are best probed using XANES and EXAFS spectroscopies. For example, two recent papers by Bonnet et al. (2016) and Belissont et al. (2016) investigate the speciation of germanium in natural sphalerite minerals sampled from two different ore deposits. Germanium was identified in three different coordination environments, viz. Ge^{2+} and Ge^{4+} in tetrahedral coordination to sulphur, and Ge^{4+} in octahedral coordination with oxygen ligands (Fig. 2). The differences between the two studies are tentatively attributed by Bonnet and coworkers (2016) to the controls of Fe on oxygen fugacity within the mineralising system.

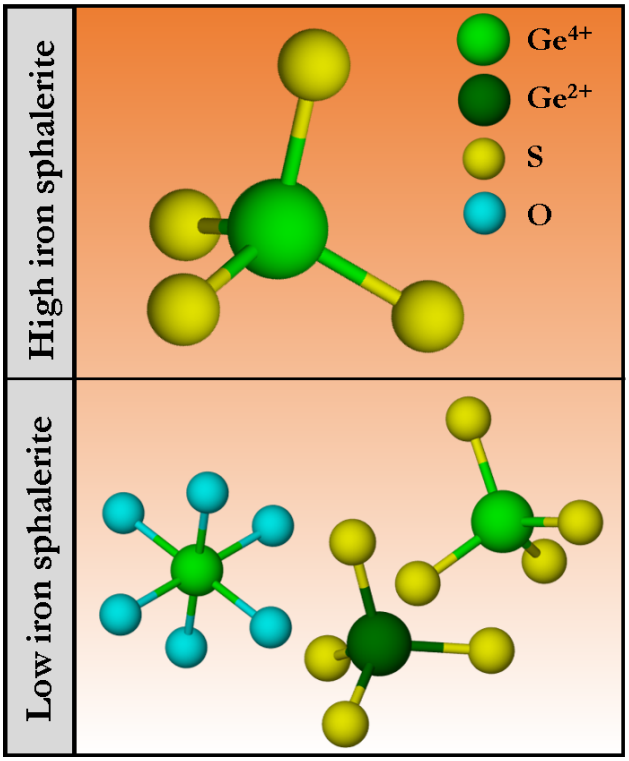

Figure 2. Chemical coordination environments of Ge in sphalerite identified for high Fe sphalerite (Belissont et al. 2016) and low Fe sphalerite (Bonnet et al. 2016).

4 Mineralization in low temperature environments

Low-temperature biogeochemical mineral transformations and precipitation reactions generally give rise to small and poorly-crystalline mineral assemblages. One such example is the mineralogy of laterite deposits (important for Al, Ni and Cr resources), which have thus far received significant attention from ore geology-focussed synchrotron user bases. Studies of these deposits include EXAFS finger-printing of Ni speciation with depth into the laterite profile (Dublet et al. 2012), and mechanistic insights into the adsorption of Ni to highly-adsorptive oxide surfaces (Robbins et al. 2015; Hens et al. 2019).

Poorly crystalline precipitates also form actively during the growth of ferromanganese nodules on the sea-floor. These nodules represent rich resources of Mn, and are associated with the presence of adsorbed (and then included) trace metals such as Co, Cd, Zn, Ni and PGE (e.g., Manceau et al. 2014). Synchrotron XRF and XANES and EXAFS studies respectively help to identify the distribution of these trace metals and the local bonding coordination associated with relevant adsorption reactions. Finally, a growing body of work is focussed on the mineral-microbe interactions which primarily take place in low-temperature surficial environments (e.g., Yang et al. 2014, Shuster et al. 2015, SGA 2019 (this conference) session: '*Coevolution of Life and Ore Deposits*). These interactions take place on exceedingly small scales and involve complex biogeochemical

transformation reactions, thus requiring the small spot size and chemical characterisation capabilities enabled by synchrotron techniques.

5 Conclusions and envisaged future directions

Because of their high tuneability, excellent spatial resolution, sub-ppm detection limits, and provision of chemical insights into molecular level bonding environments; synchrotron X-rays have found fruitful application to several specialised aspects of ore geology research. Most of these applications have been constrained to two spatial dimensions (e.g., detailed chemical mapping on the Maia detector). Recent studies, however, have highlighted the power of mapping chemical distributions and speciation across three dimensions (e.g., Sayab et al. 2016). 3D studies provide much clearer insights into the chemical, mineralogical and textural associations within ore parageneses. Studies conducted over higher-order dimensions also include those that evaluate temporal timescales (e.g., to evaluate reaction kinetics), and those that track geochemical changes across temperature and pressure dimensions (e.g., using experimental P-T cells). These high-level affordances all ensure that synchrotron science will continue to contribute meaningfully to the development of ore geology as a science in which micro- and sub-micrometer scale observations help to explain macroscale phenomena. Rigorous scientific contextualisation and grounding of mineralisation models will in turn lead to more tightly constrained and efficient minerals exploration undertakings.

Acknowledgements

This work was supported by the National Research Foundation (NRF Grant number 106006) with additional support from NRF-DST CIMERA. The African Lightsource (AfLS) organisation is also acknowledged for the useful discussions that served to motivate for this review.

References

Belissont R, Munoz M, Boiron MC, Luais B, Mathon O (2016) Distribution and oxidation state of Ge, Cu and Fe in sphalerite by u-XRF and K-edge u-XANES: insights into Ge incorporation, partitioning and isotopic fractionation. Geochemica Cosmochim. Acta 177:298–314.

Berry AJ, Harris AC, Kamenetsky VS, Newville M, Sutton SR (2009) The speciation of copper in natural fluid inclusions at temperatures up to 700°C. Chem Geol 259:1–6. https://doi.org/10.1016/j.chemgeo.2008.10.018

Bonnet J, Cauzid J, Testemale D, Kieffer I, Proux O, Lecomte A, Bailly L (2017) Characterization of Germanium Speciation in Sphalerite (ZnS) from Central and Eastern Tennessee, USA, by X-ray Absorption Spectroscopy. Minerals 7:79. https://doi.org/10.3390/min7050079

Brugger J, Pring A, Reith F, Ryan C, Etschmann B, Liu W, O'Neill B, Ngothai Y (2010) Probing ore deposits formation: New insights and challenges from synchrotron and neutron studies. Radiat Phys Chem 79:151–161. https://doi.org/10.1016/j.radphyschem.2009.03.071

Brugger J, Liu W, Etschmann B, Mei Y, Sherman DM, Testemale D (2016) A review of the coordination chemistry of hydrothermal systems, or do coordination changes make ore deposits? Chem Geol 447:219–253. https://doi.org/10.1016/j.chemgeo.2016.10.021

Cauzid J, Philippot P, Somogyi A, Ménez B, Simionovici A, Bleuet P (2006) Standardless quantification of single fluid inclusions using synchrotron radiation induced X-ray fluorescence. Chem Geol 227:165–183. https://doi.org/10.1016/j.chemgeo.2005.09.012

Dublet G, Juillot F, Morin G, Fritsch E, Fandeur D, Ona-nguema G, Brown GE (2012) Ni speciation in a New Caledonian lateritic regolith : A quantitative X-ray absorption spectroscopy investigation. Geochemica Cosmochim Acta 95:119–133. https://doi.org/10.1016/j.gca.2012.07.030

Fisher LA, Fougerouse D, Cleverley JS, Ryan CG, Micklethwaite S, Halfpenny A, Hough RM, Gee M, Paterson D, Howard DL, Spiers K (2015) Quantified, multi-scale X-ray fluorescence element mapping using the Maia detector array: application to mineral deposit studies. Miner Depos 50:665–674. https://doi.org/10.1007/s00126-014-0562-z

Frantz JD, Mao HK, Zhang YG, Wu Y, Thompson AC, Underwood JH, Giauque RD, Jones KW, Rivers ML (1988) Analysis of fluid inclusions by X-ray fluorescence using synchrotron radiation. Chem Geol 69:235–244. https://doi.org/10.1016/0009-2541(88)90037-X

Hens T, Brugger J, Cumberland SA, Etschmann B, Frierdich AJ (2018) Recrystallization of Manganite (γ-MnOOH) and implications for trace element cycling. Environ. Sci. Technol. 52:1311–1319. https://doi.org/10.1021/acs.est.7b05710

Ice GE, Budai JD, Pang JWL (2011) The race to X-ray microbeam and nanobeam science. Science 334:1234–1239. https://doi.org/10.1126/science.1202366

Li K, Etschmann B, Rae N, Reith F, Ryan CG, Kirkham R, Howard D, Rosa DRN, Zammit C, Pring A, Ngothai Y, Hooker A, Brugger J (2016) Ore Petrography Using Megapixel X-Ray Imaging : Rapid Insights into Element Distribution and Mobilization in Complex Pt and U-Ge-Cu Ores. Economic Geology 111:487–501.

Manceau A, Lanson M, Takahashi Y (2014) Mineralogy and crystal chemistry of Mn, Fe, Co, Ni, and Cu in a deep-sea Pacific polymetallic nodule. Am Mineral 99:2068–2083.

Merkulova M, Murdzek M, Mathon O, Glatzel P, Batanova V, Manceau A (2019) Evidence for syngenetic micro-inclusions of As3+-and As5+-containing Cu sulfides in hydrothermal pyrite. Am Mineral 104:300–306.

Richard A, Cauzid J, Cathelineau M, Boiron MC, Mercadier J, Cuney M (2013) Synchrotron XRF and XANES investigation of uranium speciation and element distribution in fluid inclusions from unconformity-related uranium deposits. Geofluids 13:101–111.https://doi.org/10.1111/gfl.12009

Robbins LJ, Swanner, ED, Lalonde SV, Eickhoff M, Paranich ML, Reinhard CT, Peacock CL, Kappler A, Konhauser, KO (2015) Limited Zn and Ni mobility during simulated iron formation diagenesis. Chem Geol 402:30–39. https://doi.org/10.1016/j.chemgeo.2015.02.037

Sayab M, Suuronen JP, Molnár F, Villanova J, Kallonen A, O'Brien H, Lahtinen R, Lehtonen M (2016) Three-dimensional textural and quantitative analyses of orogenic gold at the nanoscale. Geology 44:739–742. https://doi.org/10.1130/G38074.1

Shuster J, Johnston CW, Magarvey NA, Gordon RA, Barron K, Banerjee NR, Southam G (2015) Structural and chemical characterization of placer gold grains: Implications for bacterial contributions to grain formation. Geomicrobiol J 32:158–169.

Testemale D, Argoud R, Geaymond O, Hazemann JL (2005) High pressure/high temperature cell for x-ray absorption and scattering techniques. Rev Sci Instrum 76:4–9. https://doi.org/10.1063/1.1884188

Yang Y, Harmer S, Chen M (2014) Synchrotron X-ray photoelectron spectroscopic study of the chalcopyrite leached by moderate thermophiles and mesophiles. Miner Eng 69:185–195.

Garnierite characterisation for open data bases for nickel laterite exploration

Nicolas Maubec, Pierre Gilles Blaineau, Cédric Duée, Anthony Da Silva Alves, Xavier Bourrat, Guillaume Wille
BRGM, 3 avenue Claude Guillemin, BP 36009, 45060 Orléans Cédex, France

Beate Orberger
GEOPS, Université Paris Saclay, Bât 504, 91405 Orsay Cedex, France
CATURA Geoprojects, 2 rue Marie Davy, 75014 Paris, France

Monique Le Guen
ERAMET IDEA, 1 avenue Albert Einstein, 78190 Trappes, France

Cristina Villanova-de-Benavent
Departament de Mineralogia, Petrologia i Geologia Aplicada, Facultat de Geologia, Universitat de Barcelona (UB), C/Marti i Franquès, s/n -08028, Barcelona, Spain

Abstract. In order to develop a mineralogical and chemical database, which will be associated with an on-line-on mine instrument, for nickel mining exploration, several garnierite samples were studied in laboratory. The collected samples are Ni-bearing laterites from New Caledonia and Dominican Republic and are mainly composed of serpentine-like and/or talc-like and/or sepiolite-like phase. These three types of phases are clearly differentiated by X-ray diffractometry (XRD). The presence of Ni within the crystallographic structure of these phases can be observed from the infrared or Raman spectra, where the effect of Mg/Ni substitutions causes shifts in some bands. The relative intensity of these bands can be correlated with the Ni content. These different parameters are a reliable indicator to define the nature of garnierite and to have an indication on the Ni content.

1 Introduction

On-line–real time drill core scanner may comprise sensors such as Red – Green – Blue (RGB) cameras, profilometer, X-Ray Fluorescence (XRF) and hyperspectral cameras, X-Ray diffractometer (XRD) and Raman spectrometer. The analyses are performed on-line, and data interpretation relies on data bases with accurate and precise analyses on reference samples. Some data bases are available via the USGS Spectral Library (Kokaly et al. 2017) or CSIRO Mineral Spectral Libraries (Laukamp et al. 2019). However, these databases are not necessarily suitable for mining industries that need custom databases tailored to their specific ore types.

Nickel laterites are the most important Nickel source for the industries. It represents 60-70% of the total nickel resource in the world (Dalvi et al. 2004). They are complex soils with heterogeneous grain sizes (nanometric minerals to centimetric large aggregates or concretions). Nickel is present in several types of phyllosilicates (serpentine, chlorite, clay minerals and talc), which are sometimes agglomerated to garnierite (Gleeson et al. 2004; Soler et al. 2008).

The SOLSA project develops a coupled expert system comprising a sonic drill module, a core-scanner including RGB camera, profilometer, a XRF spectrometer and VNIR and SWIR cameras, and a XRD-XRF-Raman-benchtop system. The core scanner will define regions of interests (economic or for processing designs), while combined XRD-XRF-Raman will only analyze the regions of interest.

In this paper, we present detailed analyses on garnierites from different laterite sites in the world with the aim to calibrate and evaluate optical, chemical and mineralogical characteristics of the garnierite varieties, and to quickly categorize it for mining and processing purposes. All analyses will be entered in the Open Data Bases developed in the frame of the SOLSA H2020 project (www.solsamining.eu), and available for mining companies.

2 Sample material

A set of representative Garnierites of different facies and mineralogies from New Caledonia and the Dominican Republic were used for this work (Fig.1).

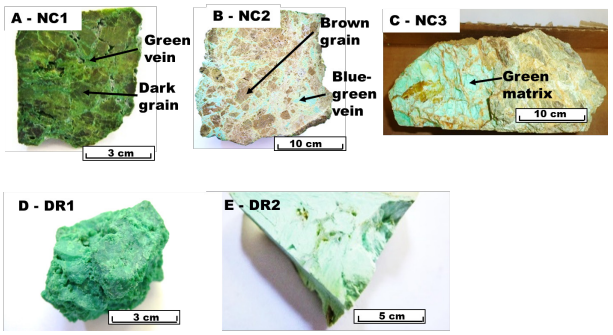

Figure 1. Selected samples from New Caledonia (A-C) and from Dominican Republic (D-E)

Three samples, referenced NC1 to NC3, are from New Caledonia (Fig. 1A-C). Samples NC1 and NC2 are characterized by the occurrence of green veins (dark green for NC1, blue-green for NC2) surrounding darker grains. The third sample (NC3) does not have veins but has a blue-green matrix associated with brown regions. Samples DR1 and DR2 are from the Falcondo deposit in Dominican Republic (Fig. 1D-E). Sample DR1 features green blocs within bulky lighter grains while sample DR2 displays light blue fibbers.

3 Methodology

3.1 Sample preparation

The samples were analyzed by electron probe micro-analysis (EPMA), XRD, Fourier Transform, Infrared (FTIR) and micro-Raman spectroscopies for their chemical and mineralogical characterizations. Raman spectroscopy and EPMA were performed on polished thin sections, representing the different areas of interest (garnierites and associated phases).The XRD and FTIR analyses were carried out on powders. Because of the heterogeneity of the samples, it was decided to hand-pick a few tens of milligrams from different areas of each sample, in order to obtain “pure” phases. The targeted areas were greenish veins and matrices, as well as dark grains. The powder samples were ground in an agate mortar and sieved to 63 µm.

3.2. Analytical methods

Quantitative electron probe microanalyses were performed with a CAMECA SX FIVE electron microprobe equipped with five vertical spectrometers. The analyses were performed on carbon-coated (20 – 30 nm) polished thin sections using a 15 kV acceleration voltage, 20 nA probe current and 1-2 µm spot size. For each sample, the chemical composition was obtained from about ten measurement points.

The XRD analyses were performed on randomly oriented samples. For each sample, tens milligrams of powders were set on a zero-background sample holder. The diffractograms were acquired with a Bruker D8 Advance DA VINCI diffractometer equipped of a CuKα source (λ = 1.5406 Å), operating at 40kV and 40mA, and a LYNXEYE XE 1D detector with a 3.3° opening. The XRD patterns were measured in continuous scan mode over the 4-75°2θ range with a step size and a measuring time of 0.03°2θ and 576 seconds per step, respectively.

FTIR spectra were obtained using a Bruker Equinox 55 FTIR spectrometer, equipped with a middle-infrared (MIR) source and a KBr beam splitter. For each sample, 30 scans in the 4000-400 cm^{-1} spectral range were recorded with a resolution of 4 cm^{-1}. The analyses were carried out on pellets discs consisting of a mixture of 0.5 mg of sample and 150 mg of KBr. Before being analyzed, the pellets were stored at 60°C to minimize the absorption of water on KBr and on the sample.

Raman measurements were performed with a Renishaw InVIA Reflex microspectrometer coupled to a DMLM Leica microscope. Three different lasers were used (λ0 = 514.5 nm; 633 nm and 785 nm). The analyses were carried out using thin-sections observed with a x100 objective (NA = 0.90) or x50 objective and exposed to a laser beam with a power of around 1 mW at the sample surface. The Raman spectrometer was operated using continuous scanning mode with large spectral windows from 100 to 4000 cm^{-1}. Acquisition times (generally over 10 seconds) and accumulations of spectra vary depending for instance on the mineral type.

4 Results

The chemical compositions of the different samples, obtained by EPMA, are presented in Table 1. Each sample is mainly composed of Si, Mg, Ni. These are the main elements of the silicate phases found in garnierites. Only NC1_dark grain and NC2_brown grain contains some percents of Fe.

From a mineralogical point of view, the clay minerals found in garnierites form solid solutions by substituting Mg with Ni. The Ni(Ni+Mg) ratio gives an indication of these substitutions. In the present study, this ratio varies from 14% to 97% and indicates a fairly wide diversity in composition from one sample to another. It is also interesting to note that for samples that come from the same piece, such as NC1 and NC2, the Ni content is much higher in the veins than in the grains.

Table 1. Average composition of samples measured EPMA

	Wt %	SiO_2	Al_2O_3	MgO	Cr_2O_3	MnO	FeO	CoO	NiO	Total	Ni/(Ni+Mg) (%)
NC1_dark grain_1	Av	40.97	0.09	32.73	0.02	0.05	2.41	0.11	9.34	85.73	27
	σ	0.72	0.02	1.28	0.04	0.04	0.18	0.02	1.37	1.50	
NC1_green vein_2	Av	33.06	0.02	2.21	0.03	0.01	0.10	0.56	50.84	86.91	97
	σ	1.22	0.02	1.07	0.02	0.03	0.13	0.21	2.92	2.60	
NC2_Brown grain_3	Av	37.77	0.01	34.62	0.00	0.05	5.62	0.03	4.17	82.32	14
	σ	1.16	0.01	2.26	0.00	0.05	1.33	0.03	1.54	2.76	
NC2_green vein_4	Av	50.73	0.04	23.11	0.00	0.03	0.14	0.01	8.91	83.06	33
	σ	2.58	0.02	2.59	0.01	0.03	0.24	0.01	1.50	3.78	
NC3_green matrix_5	Av	54.53	0.01	19.86	0.00	0.00	0.00	0.01	18.97	93.52	55
	σ	1.69	0.01	1.14	0.01	0.00	0.00	0.02	1.70	0.73	
DR1_green matrix_6	Av	40.93	0.01	5.61	0.00	0.01	0.11	0.02	41.68	88.52	91
	σ	1.49	0.02	0.76	0.01	0.02	0.09	0.04	1.20	0.85	
DR2_green matrix_7	Av	47.15	0.03	16.43	0.00	0.02	0.04	0.00	23.14	86.95	65
	σ	2.85	0.02	2.88	0.00	0.02	0.08	0.00	4.79	1.62	

Mineralogical analyses obtained by XRD allow identifying the main mineralogical families featured into garnierite. These families are often called according to their basal d_{001} reflection: “serpentine-like” phase (7Å), “talc-like” phase (10Å) as well as “sepiolite-like” phase (12 Å) (Villanova-de-Benavent et al. 2014). In the present study, the three families are detected by peaks located at 7.3 Å, 10.2 Å and 12.1 Å (Figure 2). The two powders obtained from NC1 sample are mainly composed of serpentine-like minerals. Between the two diffractograms (NC1_dark grain and NC1_green vein), only a difference in peak width is visible. This difference is probably related to the significant presence of Ni into the veins in contrast to the grain.

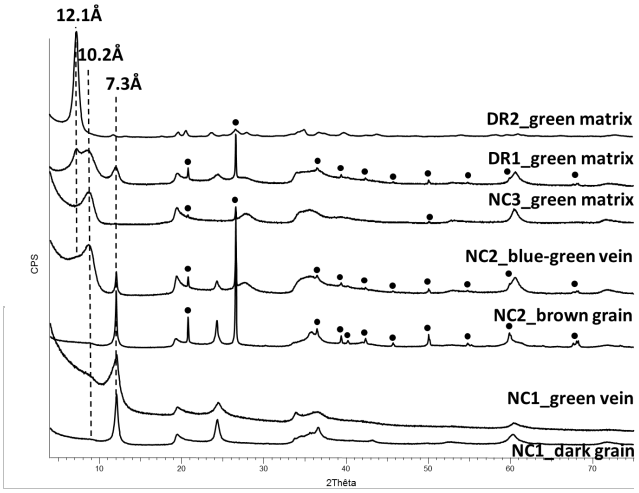

Figure 2. X-ray diffractograms of selected samples, with basal (interlayer) distances of serpentine-like, talc-like and sepiolite-like phases at 7.3Å, 10.2Å and 12.1Å, respectively. Black circles correspond to quartz peaks.

The two samples taken from the NC2 sample have a different mineralogical composition. NC2_brown grain is mainly composed of serpentine and quartz, while NC2_blue green vein is a mixture of talc-like, serpentine-like phase and quartz and probably also sepiolite-like phase. The NC3_green matrix sample is a relatively pure sample of talc-like phase with only traces of quartz detected. As for the NC2_blue green vein sample, the characteristic peaks of talc-like phase are broad. The DR1_green matrix sample has a complex composition consisting of the three types of clay minerals (serpentine-like, talc-like and sepiolite-like) as well as quartz. According to EPMA analyses, Ni is very abundant in relation to Mg and can be located within the crystallographic structures of the three clay phases. The DR2_green matrix is a pure sample of sepiolite-like phase characterized by a main peak at 12.1 Å.

The spectra obtained by FTIR, on the spectra ranges between 3000-3800 cm^{-1} and 500-1200 cm^{-1} (Fig. 3).

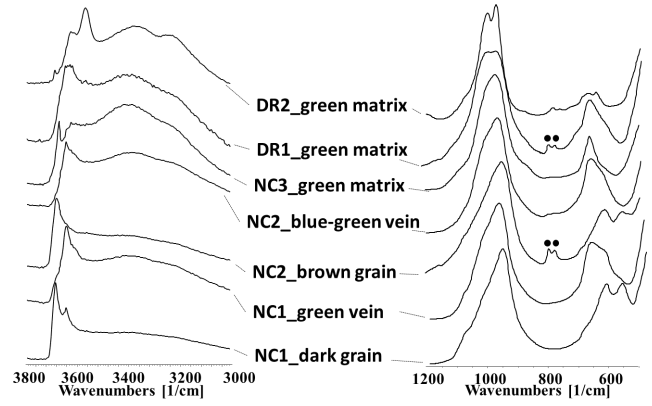

Figure 3. Infrared spectra of selected samples, in the 3000-3800 cm-1 and 500-1200 cm-1 spectral ranges. Black circles correspond to quartz bands.

Each spectrum shows three series of absorption bands; one between 500 and 700 cm-1, the second between 900 and 1100 cm-1 and the third between 3500 and 3700 cm-1. Between 500 and 700 cm-1, the results show that there are similarities between the samples NC1_dark grain and NC2_brown grain. For these two samples, there are two absorption bands located around 550 cm-1 and 605 cm-1. The similarity between these two samples is consistent with the previous data indicating that they are Mg-rich serpentines. On the other hand, the comparison with a Ni-rich serpentine, such as that present in the NC1_green vein sample, shows a difference in the position of these bands. For this sample, the bands are around 660 cm-1 and 610 cm-1. In the case of a sample rich in talc-like phase (NC3_green matrix), there is a characteristic band centered around 665 cm-1 with a shoulder towards 610 cm-1. These are the same positions as those observed for the Ni serpentine. This similarity is certainly related to an environment around Ni that is comparable between the two clay structures. Compared to the other samples, sepiolite-like phase (DR2_green matrix) is characterized by two bands of low intensities at 643 cm-1 and 670 cm-1. For samples consisting of phase mixtures, the bands are relatively broad and poorly resolved. They consist of the association of the different absorption bands that characterize the different clay minerals. In the 900-1100 cm-1, the spectra have very similar characteristic. Except for sepiolite-like phase, the samples are characterized by an asymmetric band with a maximum located between 950 and 975 cm-1, and a shoulder around 1080 cm-1. In this absorption domain, it is the vibration modes of the SiO4 tetrahedra that are at stake (Suarez and Garcia-Romero 2006). Only sepiolite is distinguished by the presence of two well-defined bands at 974 cm-1 and 1002 cm-1. These bands are perceptible in DR1_green matrix which also contains sepiolite. The 3500-3800 cm-1 range is characteristic of the vibrations of hydroxyl groups associated with R-(O,OH) octahedra (where R = Mg or Ni) (Baron and Petit 2016; Suarez and Garcia-Romero 2006). The position of the bands will depend on the Mg/Ni substitutions. This is particularly the case when comparing the spectra between the Mg-rich serpentines (NC1_dark grain or NC2_brown grain) and the Ni-rich serpentine (NC1_green vein); the bands present at 3687 cm-1 and 3646 cm-1 shift towards lower frequencies in the presence of Ni (3646 cm-1 and 3608 cm-1, respectively). In the talc-like sample (NC3_green matrix), there are similarly located bands. The difference with serpentines comes from the presence of very broad bands between 3100 and 3500 cm-1 attributed to the vibrations of the water molecules present in the structure (Gerard and Herbillon 1983). The sepiolite-like sample (DR2_green matrix) differs from the other samples by the presence of two well-defined bands at 3628 cm-1 and 3569 cm-1 in addition to broad bands due to water molecules.

In addition to FTIR analyses, Raman spectroscopy makes it possible to differentiate between the different types of clay minerals (Figure 4).

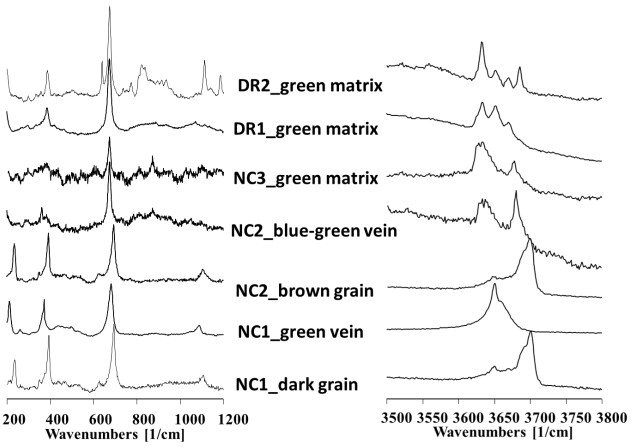

Figure 4. Raman spectra of selected samples, in the 200-1200 cm^{-1} and 3500-3800 cm^{-1} spectral ranges.

Serpentine-like sample (NC1_dark grain and NC2_brown grain) are characterized by four main bands in the range 200 - 1200 cm^{-1}, located around 230 cm^{-1}, 390 cm^{-1}, 690 cm^{-1} and 1105 cm^{-1}, as well as several bands between 3650 and 3700 cm^{-1}. In the presence of a high Ni content (in the case of the NC1_green vein sample), all the bands are shifted towards lower wavenumbers compared to those present in Mg-rich serpentines (NC1_dark grain and NC2_brown grain). Compared to serpentines, talc-rich samples (NC2_blue green vein and NC3_green matrix) are marked with a main band at 675 cm^{-1}. Bands with low intensity around 380 cm^{-1} and 870 cm^{-1} may also be visible. In the 3500 - 3800 cm^{-1} range, the two samples are characterized by a well resolved band at 3678 cm^{-1} accompanied by a broad band centered at 3632 cm^{-1}. The only visible difference between these two samples is the intensity ratio between these two bands (I_{3632} / I_{3678}). This ratio is higher for the sample with a higher Ni content, namely NC3_green matrix (Table 1). Sepiolite minerals (DR2_green matrix) are clearly distinguished from other samples by the presence of four well-defined bands located at 3633 cm^{-1}, 3651 cm^{-1}, 3669 cm^{-1} and 3686 cm^{-1}. Most of these bands are found in the DR1_green matrix sample but with different relative intensities.

4 Discussion and conclusions

A set of Ni-bearing laterites samples from New Caledonia and the Dominican Republic representative of the diversity of Ni-bearing clay minerals has been characterized using different analytical techniques (EPMA, XRD, FTIR and Raman micro spectroscopy).

The garnierites characterized in this study are composed of either serpentine-like, and/or talc-like and/or sepiolite-like phase(s). These three types of clay phases (serpentine-like, talc-like and sepiolite-like) can form series of solid solutions by substituting Mg for Ni (Gleeson et al. 2004). The presence of nickel is first visible to the naked eye where the areas enriched in this element tend to be green or blue green. Then, in analytical point of view, the effect of the substitutions of Mg by Ni generates a structural disorder which results in the broadening of diffraction peaks (Baron and Petit 2016). This is the case for Ni-rich serpentine (NC1_green vein) and talc-like phase where Ni is important. Then the presence of Ni within the crystallographic structures induces differences (peak shift) on the spectra obtained by FTIR and Raman spectroscopy. The observed shifts are due to the nature of the cations (Mg^{2+} or Ni^{2+}) which will have an influence both on the environment of the SiO_4 tetrahedra and on the properties (lengths, forces) of the R-O,OH bonds, where R = Mg or Ni (Baron and Petit 2016; Petriglieri et al. 2015).

All these data are important because they are indicators to define the nature of garnierite and to have an indication on the presence of Ni into the samples. These data are entered into the SOLSA Open data bases, which will be online by the end of the SOLSA project 2/202 and will be able to assist mining and metallurgical companies in exploration and mining exploitation.

Acknowledgements

This study received grants from the EU H2020 project SOLSA N°689868. Samples were provided by ERAMET, BRGM and University of Barcelona.

References

Baron F, Petit S (2016) Interpretation of the infrared spectra of the lizardite-nepouite series in the near- and mid-infrared range. American Mineralogist 101:423-430

Dalvi AD, Bacon WG, Osborne RC (2004) The past and the future of nickel laterites. PDAC 2004 International Convention, Trade Show and Investors Exchange, Canada, 1-27

Gerard P, Herbillon AJ (1983) Infrared studies of Ni-bearing clay minerals of the kerolite-pimelite series. Clays and Clay Minerals 31 : 143-151

Gleeson SA, Herrington RJ, Durango J, Velasquez CA, Koll G (2004) The mineralogy ang geochemistry of the Cerro Matoso SA Ni laterite deposit, Montelibano, Colombia. Economic Geology 99: 1197-1213

Kokaly RF, Clark RN, Swayze GA, Livo KE, Hoefen TM, Pearson NC, Wise RA, Benzel WM, Lowers HA, Driscoll RL, Klein AJ (2017) USGS Spectral Library Version 7. US Geological Survey Data Series 1035, 68 p.

Laukamp C, Lau I, Warren P (2019) CSIRO Mineral Spectral Libraries. CSIRO Mineral Resources https://mineralspectrallibraries.csiro.au/Home/Samples

Petriglieri JR, Salvioli-Mariani E, Mantovani L, Tribaudino M, Lottici PP, Laporte-Magoni C, Bersani D (2015) Micro-Raman mapping of the polymorphs of serpentine. Journal of raman spectroscopy 46 : 953-958

Soler JM, Carma J, Gali S, Melendez W, Ramirez A, Estanga J (2008) Composition and dissolution kinetics of garnierite from the Loma de Hierro Ni-laterite deposit, Venezuela. Chemical Geology, 249, 191-202

Suarez M, Garcia-Romero E (2006) FTIR spectroscopic study of palygorskite: influence of the composition of the octahedral sheet. Applied Clay Science 31: 154-163

Villanova-de-Benavent C, Proenza JA, Gali S, Garcia-Casco A, Tauler E, Lewis JF, Longo F (2014) Garnierites and garnierites: Textures, mineralogy and geochemistry of garnierites in the Falcondo Ni-laterite deposit, Dominican Republic. Ore Geology Reviews 58: 91-109

It's not easy being green – detecting arc-related mineral system fingerprints using mineral chemistry in 'propylitic alteration' in a Cambrian arc terrane Victoria, Australia

Rob Duncan, David Taylor
Geological Survey of Victoria, Melbourne, Victoria, Australia

Sebastien Meffre, Ivan Belousov, Leonid Danyushevsky, David Cooke
Centre for Ore Deposit and Earth Sciences, University of Tasmania, Hobart, Australia

Abstract. Epidote and chlorite compositional data were collected using laser ablation inductively-coupled mass spectrometry (ICP-MS) on samples from two mineral prospects in the Cambrian Stavely Arc, western Victoria. The aim was to distinguish between regional metamorphic and hydrothermal alteration origins for epidote-chlorite-bearing assemblages. At the Thursday's Gossan Porphyry Cu(-Au-Ag) Prospect, chlorite signatures are similar to both propylitic hydrothermal and regional metamorphic origins, however, elevated Zn and Sr contents are associated with the former. Application of the chlorite proximitors (predicted distance to a hydrothermal centre) identify a likely hydrothermal centre at depth. At the Eclipse Cu-Zn(-Au) VHMS Prospect, epidote As and Sb and chlorite Zn, Cu and Pb contents are consistent with propylitic alteration in most samples. Systematic variations in chlorite Cu and Pb and As and Cu in epidote contents identify a portion of the prospect for follow-up exploration. This study demonstrates that even a limited epidote-chlorite mineral chemistry dataset can provide fertility and vectoring information for mineral exploration targeting. These data are consistent larger-scale geochemical data and geodynamic models that predict the Stavely Arc has significant arc-related mineral system potential.

1 Introduction

Hydrothermal alteration patterns in mineral systems have long been used in mineral exploration. Visibly altered rocks extend beyond the mineralized footprint, and recent efforts have shown geochemical anomalies in epidote and chlorite extend even further than whole rock geochemical anomalism and can also be used to predict the location of hydrothermal deposit centres (e.g., Wilkinson et al., 2015). As part of an effort to de-risk mineral exploration in the, largely covered, Stavely Arc of western Victoria, epidote and chlorite geochemical analyses were undertaken on 'green rock' samples from two mineral prospects. The aim of this work was to use these data to assess mineral system fertility and prospect-scale mineral exploration vectors.

2 Geological setting

Arc-related mineral systems formed in the Stavley Arc during the ~525 to 495 Ma collision between the Palaeo-Pacific Plate and the eastern margin of the Proto-Australian Continent (e.g., Schofield et al., 2018). Originally, the Stavely Arc consisted of four sub-parallel volcanic belts (~1,200 km in total strike length) that contain Cambrian low- to high-K boninitic, tholeiitic and calc-alkaline volcanic and intrusive rocks separated by panels of Cambrian metasedimentary rocks – these rocks record a transition from a thinned continental margin through to a more Andean-style tectonic environment (Cayley et al., 2018).

The Stavely Arc was affected by two major structural rearrangements; D_{1a} related to sinistral transpression (pre-505 Ma – Delamerian Orogeny) and D_4 related to dextral transtension (~400 Ma – Bindian Orogeny). These events are responsible for the current distribution of volcanic belts (Fig. 1). Sinistral transtension (D_{1b}) during the Delamerian Orogeny (post-505 Ma) was accompanied by porphyry intrusion emplacement into (D_{1a}) thrust-bound arc-slices. Mineral occurrences of porphyry-, epithermal-, and volcanic-hosted massive sulphide-(VHMS) affinity have been identified in the Stavely Arc in small portions of (poorly) exposed Cambrian bedrock, although the majority (>99%) of Cambrian rocks are concealed by younger cover. 'Green rock' mineral assemblages have been recognized at numerous mineral occurrences in the Stavely Arc. It is unknown if these occurrences are related to propylitic hydrothermal alteration or low-grade regional metamorphism. Material for this study was collected from the Thursday's Gossan and Eclipse prospects (Fig. 1).

2.1 Thursday's Gossan Porphyry Cu-Au(-Ag)

Thursday's Gossan is located at the northern end of the exposed Stavely Belt (Fig. 1) and is hosted by andesitic to rhyolitic volcanic rocks, volcaniclastics and sedimentary rocks that have been intruded by a series of dacitic to tonalitic sub-volcanic porphyry stocks (Buckland, 1987). An inferred, supergene resource of 28.1 Mt at 0.4% Cu at 0.2% cut-off grade has been estimated (Stavely Minerals, 2019). Supergene mineralization is thought to be associated with hypogene porphyry-style mineralization at depth. A series of nested hydrothermal alteration zones are present at Thursday's Gossan – the largest is a ~8 km^2 propylitic assemblage (chlorite-epidote-calcite±zeolite-sericite-illite-pyrite) which envelops a 3 km^2 phyllic assemblage (quartz-sericite-illite-pyrite) and a 0.5 km^2 central advanced

argillic assemblage (kaolinite-dickite-quartz). Mineral exploration is on-going at Thursday's Gossan and has intersected wide zones of M-veins veins, potassic assemblages and chalcopyrite-bornite mineralization associated with D-veins (Stavely Minerals, 2019). Significant intersections, such as 952 m at 0.23% Cu, 283 m at 0.16 % Cu and 124 m at 0.35% Cu and 0.18 g/t Au (Stavely Minerals, 2019) demonstrate the porphyry potential at Thursday's Gossan. Timing of mineralization is best constrained by Re/Os molybdenite model ages of ~503 to 501 Ma from chalcopyrite B-veins – these accord with ~505 to 501 Ma U/Pb zircon ages for pre-mineral diorite and dacite porphyries (Schofield et al., 2018; Lewis et al., 2016).

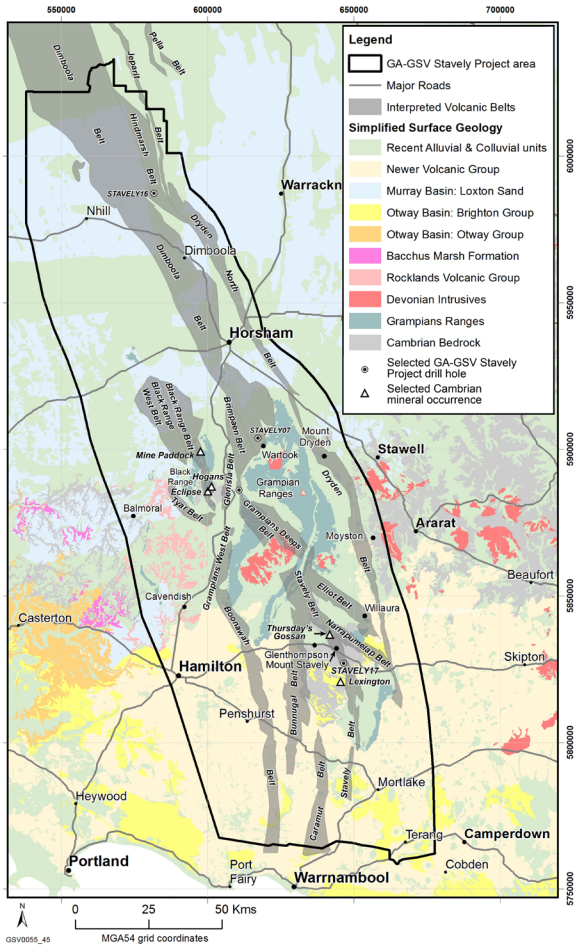

Figure 1. Map to show location and distribution of volcanic belts that comprise rocks of the Stavely Arc, western Victoria, ~250 km west from Melbourne. Only small portions of the Stavely Arc are exposed at surface, mostly southwest of Thursday's Gossan and east of the Eclipse prospects

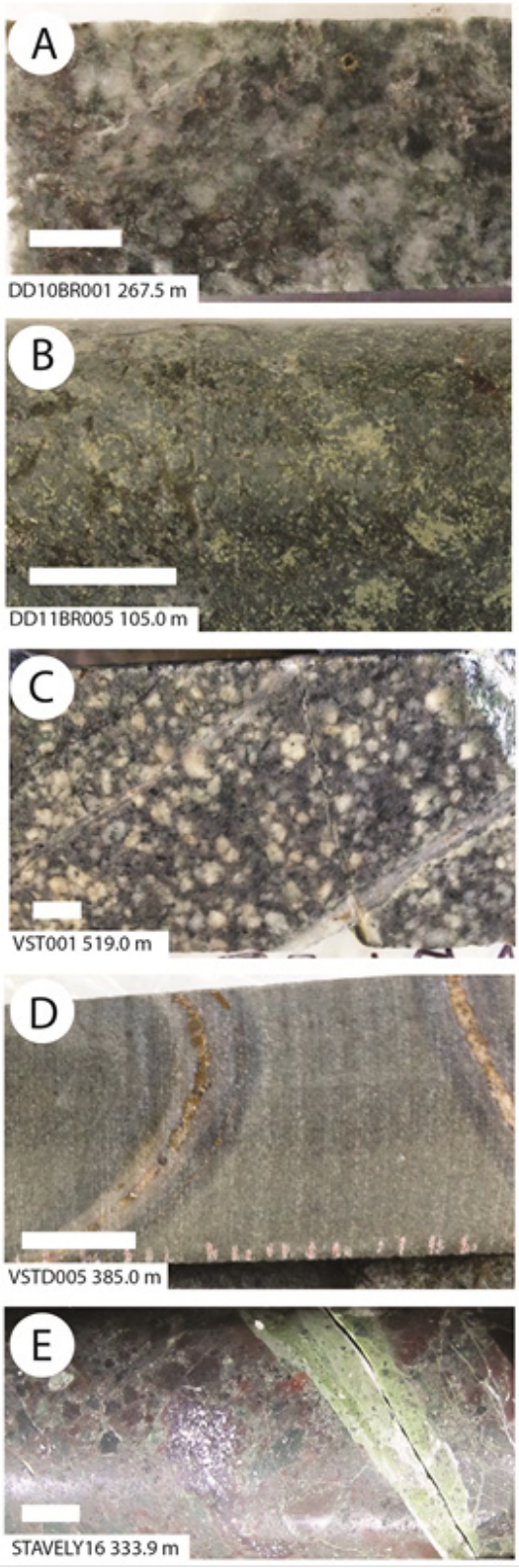

Figure 2. Examples of chlorite and epidote alteration assemblages in Stavely Arc rocks analyzed during this study. (A) to (B) Chlorite-epidote-pyrite assemblages in volcanic rocks from Eclipse. (C) to (D) Chlorite-bearing assemblages in porphyritic phases and greywackes. (E) Epidote-chlorite assemblages from heterolithic volcanic rocks far removed from known mineralization. Annotation shows drillhole and downhole depth – scale bars are 1 cm.

2.2 Eclipse Cu-Zn(-Au) VHMS

Eclipse is located at the southern portion of the exposed Black Range Belt (Fig. 1). No resource has been estimated. Supergene copper mineralization is partly covered by post-mineral cover and has developed above an intense phyllic (quartz-sericite-pyrite) zone that hosts massive, stratabound chalcopyrite-sphalerite-pyrite and later quartz-calcite-sulfide veins in dacitic to rhyolitic volcanic and volcaniclastic rocks (Navarre Minerals, 2014). Laterally the phyllic alteration transitions to a chlorite-sericite assemblage. Significant intersections include 267.1 m at 0.3% Zn, 2 g/t Ag and 0.1 g/t Au from 1.3 m (including 6 m at 1% Zn, 1 g/t Ag. 1 g/t Au from 147 m depth) and 5 m at 0.2% Cu, 3.9% Zn, 2.7 g/t Ag and 1.4 g/t Au (Navarre Minerals, 2014). The age of mineralization is unresolved but is likely ~503 Ma based on the U/Pb zircon age of the similar unit that hosts similar style mineralization in the Stavely Belt (Fig. 1).

3 Materials and methodology

Polished rock mounts of propylitic alteration assemblages from eight (four from each prospect) diamond drill core samples were prepared and imaged using scanning electron microscopy (SEM) to: examine textural and paragenetic relationships; determine potential intra-grain epidote and chlorite group mineral compositional variations; and identify included mineral phases. Materials from Thursday's Gossan (Fig. 2) consists of two equigranular, porphyritic, feldspar-phyric intrusive phases and two medium-grained greywackes – chlorite in these samples is typically fine-grained and intergrown with quartz in the groundmass and no epidote is present. Materials from Eclipse (Fig. 2) consists of dacitic to andesitic coherent lavas with variable grain sizes – chlorite and epidote are typically intergrown with each other and sericite-pyrite. The samples were analyzed for major, minor and trace elements using LA ICP-MS with New Wave™ 193 nm solid-state laser coupled to an Agilent 7500cs quadrupole mass spectrometer housed at The University of Tasmania (CODES). Calcium for epidote and Al for chlorite data derived from SEM energy dispersive spectra were applied as internal standards to convert the laser ablation data.

4 Results and interpretation

Forty-eight epidote and 122 chlorite analyses were undertaken. Filtering using in-house tolerance parameters removed complete (or portions) of contaminated spectra generated by mineral intergrowths and/or micro-inclusions. Filtering removed more chlorite than epidote analyses – 25 out of 60 Eclipse and 26 out of 62 Thursday's Gossan chlorite analyses were acceptable compared with 41 out of 48 Eclipse epidote analyses. This highlights the potential issues of applying this technique in fine-grained rocks. Limitations of this data include: the relatively small dataset; a lack of

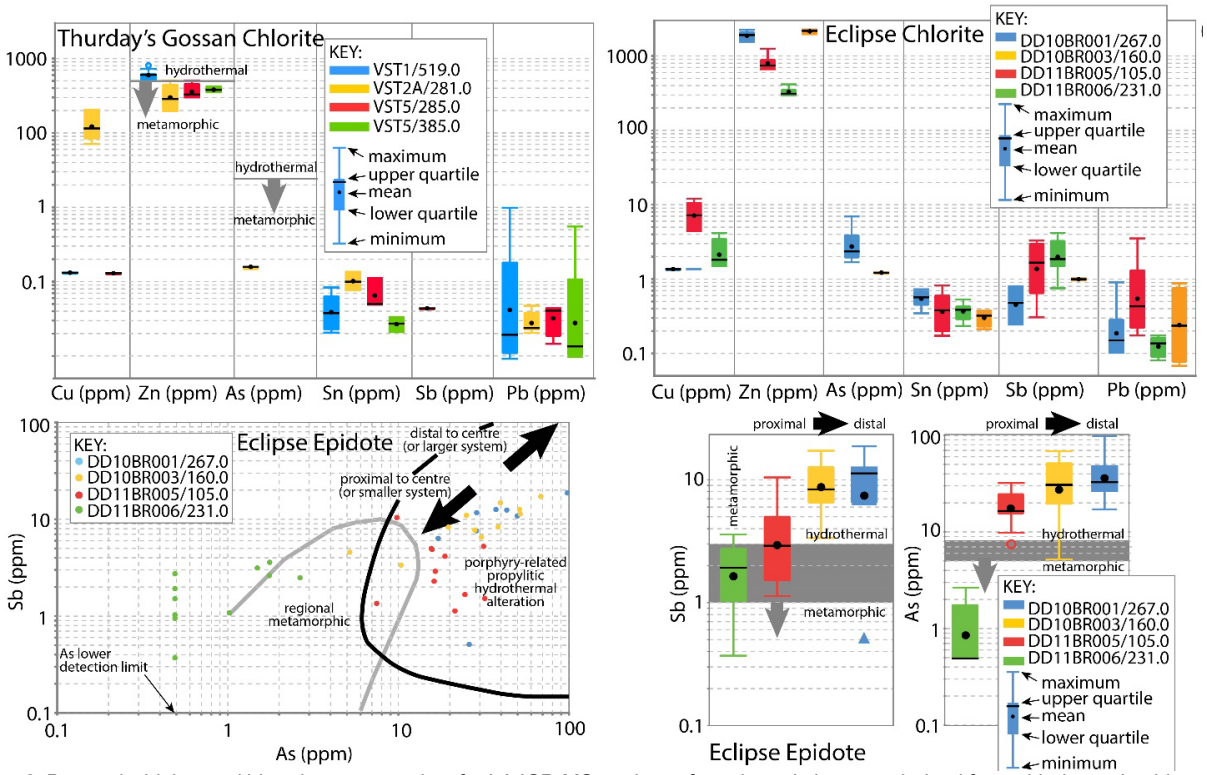

Figure 3. Box and whisker and bi-variate scatter plots for LA ICP-MS analyses for selected elements derived from chlorite and epidote samples from the Thursday's Gossan Porphyry Prospect and the Eclipse VHMS Prospect, Stavely Arc, western Victoria. Fields for (regional) metamorphic, hydrothermal and porphyry-related propylitic alteration after I Belousov pers. comm., 2015. Box and whisker plot bars divided into four parts by calculating median, 25th and 75th percentiles – the box contains 50% of analytical data. Below detection values not plotted and statistical outliers may plot outside the whiskers

regional metamorphic background epidote and chlorite benchmark data; and the lack of chlorite-epidote data from VHMS systems worldwide. Selected elemental results are plotted here (Fig. 3).

4.1 Thursday's Gossan – chlorite only

Chlorite from Thursday's Gossan are similar to both copper-gold porphyry-related and regional metamorphic compositions. Elevated Zn (510 to 806 ppm) and Sr (2.2 to 32 ppm) in two samples are indicative of hydrothermal chlorite compositions – the other two samples have <350 ppm Zn and <2 ppm Sr (Fig. 3). Arsenic in all chlorites is relatively low compared with porphyry-related chlorites worldwide. Applying the chlorite proximitor (Wilkinson et al., 2015) yields conflicting results from the sample position relative to a predicted hydrothermal centre – in this case, typically 800 to 1600 metres. This could reflect the presence of several discrete hydrothermal centres or may result from the heterogeneous rock package (e.g., ultramafic rocks may locally buffer Ni, Co and V in chlorite) – the original proximitors were developed in a largely heterogeneous rock package. A comparison of the proximitors derived from two samples from within a single drillhole indicate that the deeper sample is relatively proximal to the predicted hydrothermal centre – this indicates a vertical temperature component to the hydrothermal system. This observation accords with the notion that porphyry mineralization was post-thrusting and no significant vertical rotation has occurred since mineralization (Cayley et al., 2018), and is supported by mineral exploration at Thursday's Gossan that continues to intersect relatively thick zones of mineralization at depth (Stavely Minerals, 2018).

4.2 Eclipse – epidote and chlorite

The Eclipse epidote-chlorite data are interpreted in the context of data available from copper-gold-porphyry systems – notwithstanding that the mineralization at Eclipse is of VHMS affinity. Epidote and chlorite from Eclipse share similarities with porphyry and metamorphic-related compositions. One sample contains <3.6 ppm Sb and <2.6 ppm As is metamorphic in origin, the other epidotes are classified as hydrothermal in origin and contain up to 18.7 ppm Sb and 97.9 ppm As (Fig. 3). Within this hydrothermal group decreasing As and Sb values (Fig. 3) related to increasing proximity to the predicted hydrothermal centre – as increasing sulfide contents partition Sb and As over epidote. The hydrothermal epidotes are elevated in LREE, Y and Pb and Na-Mg (and low in Mo) compared with mineralized porphyry compositions. The significance of this is unclear but may be result from enrichment in some Stavely igneous rocks (Schofield et al., 2018) and may be important for fingerprinting VHMS-style mineralization.

Chlorite is typically elevated in Sr (>5 ppm) compared with regional metamorphic chlorite – indicative of a hydrothermal origin (Fig. 3). Chlorite from the sample with metamorphic epidote, is also likely metamorphic in origin due to low As and Zn contents (<1 ppm and <300 ppm, respectively (Fig. 3)). Systematic variations in Cu, Pb and Zn in the hydrothermal chlorites can be used to interpret relative sample position with respect to mineralization (Fig. 3) – this identified a (relatively) poorly explored area of the Eclipse Prospect for follow-up mineral exploration.

Mineral exploration significance

The Stavely epidote-chlorite dataset, albeit relatively small, has provided spatial information to assist in mineral exploration decision-making. The data accord with pyrite LA ICP-MS data (Steadman and Large, 2015) that reveal: a transition from oscillatory zoned, Co-Ni-Se associated with relatively high temperature magmatic fluids through relatively lower temperature magmatic-hydrothermal fluids characterized by deposition of a Cu-Sb-Zn-Ag-Au-Bi-Mo assemblage at Thursday's Gossan; and a VHMS-like assemblage of Mn, Hg and Tl (along with relatively high Au) in pyrite at Eclipse. More broadly, in terms of fertility, a series of Cambrian intrusions across the Stavely Arc have Sr/Y and V/Sc (relative to SiO_2 content) that typify relatively hydrous magmas that contribute to the significant metal endowment in large porphyry systems worldwide (Loucks 2014). Additionally, portions of the Stavely Arc volcanic rocks yield major and trace element ratios (e.g, Zr/Nb, Nb/Y, $La/Yb_{(cn)}$) associated with productive VHMS elsewhere (Piercey, 2010). Early thrusting that generated significant dislocation of original volcanic belts during the Delamerian Orogeny, explains why porphyry and VHMS mineral systems appear to be closely associated spatially in the Stavely Arc.

References

Buckland GL (1987) Geology and mineral potential of the Mount Stavely Volcanic Complex. Geol Sur Vic Report 80

Cairns CP, Middleton MJ, Weatherman ML, Haydon SJ, Duncan RJ, Say MM (2018) Stavely Project – Historical Mineral Expl. Data Comp^{n}. Stavely Project Report 2 – Geol Surv Vic

Cayley RA, McLean MA, Skladzien PB, Cairns CP (2018) Stavely Regional 3D Model. Stavely Project Report 3 – Geol Surv Vic

Lewis CJ, Cayley RA, Duncan R, Schofield A, Taylor D (2016) New SHRIMP U-Pb zircon ages from the Stavely region, western Victoria: July 2014-June 2016. Geosci Aust Rec 2016/027

Loucks R (2014) Distinctive composition of copper-ore-forming arc magmas. Aust J Earth Sci 61: 5-16

Navarre Minerals (2014) Navarre extends copper zone at Eclipse, western Victoria. ASX Announcement 6 August 2014

Piercey SJ (2010) An overview of petrochemistry in the regional exploration for volcanogenic massive sulphide (VMS) deposits. Geochem: Explor, Enviro, Anal 10: 119-136

Schofield A et al. (2018) Regional geology and mineral systems of the Stavely Arc, western Victoria. Geosci Aust Rec 2018/002

Stavely Minerals (2019) Knocking on the Door to Discovery in Western Victoria. RIU Explorer's Conference 2019. Available at www.stavely.com.au

Steadman G, Large RR (2015) Geochemical study of pyrite from the Stavely district, Western Victoria. In: Schofield A et al. (2017) Regional geology and mineral systems of the Stavely region, western Victoria: Data release 5 – Geochemistry Data. Geosci Aust Rec 2017/002

Wilkinson JJ, et al. (2015) The chlorite proximitor: a new tool for detecting porphyry ore deposits. J Geochem Explor 152:10-26

Remote sensing based geological mapping and mineral exploration of the area of North Waziristan Pakistan

Adil Nawaz
Faculty of Geology Geophysics and Environmental Protection, AGH University of Science and Technology, Poland

Janusz Magiera, Dr. Inż.
Akademia Górniczo-Hutnicza im. Stanisława Staszica Krakow, Department of Economic and Mining Geology, Faculty of Geology, Geophysics and Environmental Protection

Abstract. In mineral exploration, remote sensing tools are important and cost effective. Minerals occur in a variety of genetic associations but commercial deposits of minerals are limited in genetic types and modes of occurrences which forms the basis of modern concept based prospecting and is also responsible for the significant role of remote sensing in exploration. Remote sensing data can help to differentiate melogenic provinces/belts/sides and mineral guides in a larger terrain. Keeping In view the importance of RS Tools, digitally enhanced OLI Landsat 8 images are applied to find alteration zones and for geological mapping of North Waziristan Pakistan. The territory is rough with sparse vegetation; the exposure of the Waziristan ophiolite, related sedimentary-igneous lithologies and inaccessibility to the area made the utilization of Landsat information helpful in this investigation. Spectral signatures recorded by Landsat 8 data were used to differentiate different rock units and alteration zones. RS tool i.e. band ratios, band combinations, principal component analysis and image classification are helpful in this regard; multispectral images were prepared and investigated for this study. Final detection of the lithology and alteration zones is based on correlation between classes generated in the thematic map and the referenced geological map. On the basis of the image classification techniques; unsupervised classification, band ratios, five principles lithological units and alteration zones with highest percentage of clay and iron ratios are identified which are giving satisfactory results with overall accuracy 63.07 % in comparison with referenced geological map using confusion matrix analysis. The results are subject to discussion and need to examine about the utility and confinements of remote sensing strategy on the investigation zone.

1 Introduction

Waziristan is situated close to the intersection of the western edge of the Himalayan orogeny and western transpressional margin of the Indo-Pakistani craton. Due to security reasons and lack of infrastructure, access to this territory is difficult. This area is globally always under discussion due to geostrategic and geo environment position. In view of economic geology, region held unprecedented mineral resources. According to FATA research center so for 19 minerals including Gypsum, Iron Ore, coal, limestone, marble, lead, barite, emerald graphite, Soapstone, dolomite, feldspar, quartz, silica sand, bentonite and marl have been reported here. Region includes west and south-west of Peshawar between the Kurram River (Tochi River) toward the north and the Gomal River toward the south, bordering some portion of Pakistan's Federally Administered Tribal Areas (FATA). Study zone lies in North Waziristan with path 152 and row 37. Zone has been portrayed as a place where there are high and troublesome slopes with deep and rough terrains. Exposures of Cretaceous and early tertiary structures like Main Waziristan thrust and stratigraphic connections in the zone are noticeable however not obvious in numerous different territories of the Asian intersection zone, mainly in parts of the ranges of the North Himalayan mountain chain. In North Waziristan, mountains are geographically isolated from the larger mountain frameworks of Koh-e-Sufaid in the North and Koh-e-Sulaiman in the South. The normal stature of the slopes in Waziristan is 1,500– 2,500 meters (4,900– 8,200 ft.) above ocean level.

Study area is characterized with dry climate, almost no vegetation cover, vast and clear exposures of rocks and sediments are being a good subject to remote sensing spectral analysis. The aim of the project is remote sensing based mineral exploration and to create a map of lithology of rocks, sediments and their residuals exposed on the land surface. The new map which depends on unsupervised classification and color composite studies, expands limited mapping of the ophiolite, approves and enhances past general conclusions and uncovers new prospects in the territory. The use of multispectral imaging to remote district, for example, northwest Pakistan makes the construction of definite geologic maps economical and efficient. The use of appropriate band Rationing and Principal Component analysis is part of examination which permits auxiliary and lithologic information to be extrapolated from the ground. Modified map is verified with available referenced data; including geological map published by geological survey of Pakistan, high resolution airborne ortho photomap and different field reports.

2 Research problem and methodology

The study goes in four stages. First three stages are iterative.

a. Creating updated lithological map with the use of image processing and analysis

b. Highlighting alteration zones.
c. Rectification of the map obtained by comparison and statistical validation with referenced data.
d. Modification of processing parameters.
e. Final rectification of the map.

The ophiolite belt of Waziristan is economically potential for certain type of ore deposits, consisting VMS type of copper deposits, podiform chromite & banded manganese. Remote sensing tools are being applied on target area to identify VMS type deposits. The occurrences of these deposits in the ophiolite belt of Waziristan was first reported by Asrarullah of Geological survey of Pakistan, Taher Kheli, Aftab Ahmed (1959), Afzal (1970). A number of principal geological criteria, which are helpful in this study, have been setup for mineral prospecting (McKinstry 1948; Peters 1978; kreiter 1968) that can be observed on remote sensing data including: 1-statigraphical–lithological, 2 Geomorphology, 3-Structural, 4-Rock alterations, 5-Geobotnical etc. (Gupta 1991)

3 Regional geology and tectonic setting

Indo Pakistani landmass is encased by two giant global alternatives; Indian Ocean and the Himalayas having standard origin. Northern most region of the Pakistan lies in Tethyan domain and delineates a troublesome geology while southern part has a place with Gondwana area and is supported by Indo-Pakistani crustal plate. Around 130 million years back, The Indo-Pakistan sub-continent isolated from the motherland Gondwana (Jhonson et al. 1976). The study area (Survey of Pakistan topographic sheet No. 38-H/13) falls in the North Waziristan agency and is a part of the Federally Administrated Tribal Area (FATA). The average rainfall is 250 mm per annum. The area is covered by igneous and sedimentary rocks and can broadly be divided into two distinct tectonic blocks:

- Shelf slope sediments of the Indian plate, Waziristan Kurram Block (WKB)
- Waziristan Ophiolite (WO)

4 Methodology

Seven clear, cloud free Landsat-8 images were downloaded from online repository of the USGS (United States Geological Survey) in tiff format, the study area (Path/row-152/37) is captured by Landsat 8 scenes acquired on 15 May, 2016. Figure 1 shows the Landsat image of the study area representing band ratio in the area. Geology and alteration zones' interpretation is based on the following remote sensing techniques; color composites, Band ratios for quantitative analysis (clay, iron-oxide, NDVI and its derivatives). To classify multispectral images, unsupervised classification (ISO CLASS) is applied with 70 number of classes and different classification parameters; results are verified visually and statistically with reference data, color composites and band ratios.

Composite in Figure 2 shows false colour RGB 653 which creates an enhanced image with strongly green vegetation, blue or black water and red-to-brown rock or soil. RGB 753 and 652 are alternatives of this combination. Quaternary fan deposits are clearly visible in brownish colour, Red to brown or purple colour shows barren earth.
In NDVI (Bannari, 1995) b5/b4 band is used while In PC1 Mudrova, M. 2010) bands from 1-7 are used. Clay ratio (figure 3) is produced through the combination of b6/b7 bands. Clays, carbonates and micas can produce the light grey to white zones in greyscale images. In pseudo color, clay with red colour is showing maximum value which is 1.65. It can be due to the reason that hydrous minerals or alteration zone have high absorption as compare to band 7.

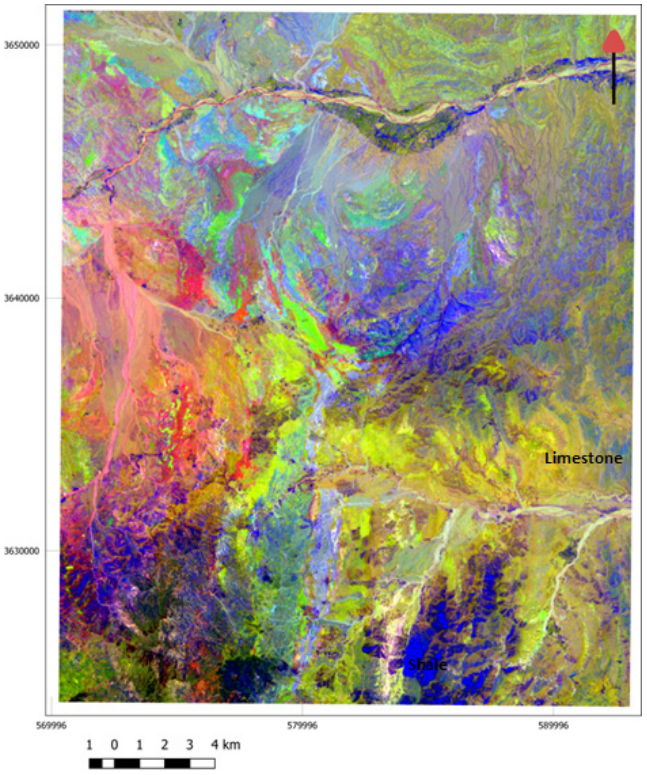

Figure 1: Colour Composite created through Band Ratio with B7/B6 in red, B6/B5 in Green and B2/B3 in Blue.

Unsupervised classification is executed using Iterative Self Organizing Data Analysis Algorithm Technique (ISODATA) (Tou & Gonzalez, 1974). In this classifier we don't use training samples data as a base for classification. Instead, these classifiers involve algorithms. Undefined pixels are analyzed by these algorithms in the image and collect them into number of classes established on the natural clusters or grouping present in the image values. Geological referenced map is reclassified in ER mapper using algorithms.

Colour composites; false or true colour, are created to differentiate geological zones. The false colour display assignment can be done in an absolutely random way for any band of a multispectral image so that the colour of a target in the displayed image does not show any resemblance to its actual colour. The resultant image is known as a false colour composite. However, some methods can be more appropriate for the detection of certain features in the image. False colour composite schemes for exhibiting a Landsat 8 OLI multispectral image used in this research are RGB 653 and RGB 543.

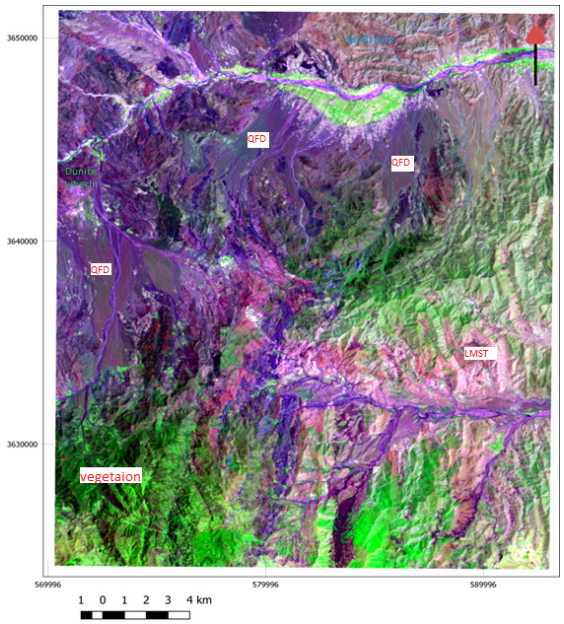

Figure 2. Geological color composite with RGB 653.

5 Result and discussion

The purpose of the study was to generate a revised Map of the rocks revealed on the surface in geologically Complex area and to identify VMS type deposits using RS tools. Geological referenced map was having 20 major lithologic units; JUM, QFD, JPS, JUM, JWV, QFD, QTG, JSD, DOLORITE DYKE, KML, JVV, JG, QRS, JPG, ZEF, TKF, JAF, JZF, TRF and QAL (See end page for details). 5 potential areas are identified using RS tools and a revised map is setup (fig 4) having uniform distribution of 5 major lithologic units. Study showed that on a broad scale, the use of 70 classes in unsupervised classification produced more precise distribution of lithology. The result of study are satisfactory enough to apply remote sensing as a tool to differentiate lithological units and marking alterations zones. Within the ophiolite complex different igneous rock types like gabbroic rocks, ultramafic rocks, and the sheeted dike complex are differentiated on the basis of spectral ratios, false color composites, ISO classification and PCs. Error (Confusion) Matrix (Awad, N.M.A., 2011) analysis allows for quantitative estimation of the overall accuracy of classification and this analysis is giving us quite satisfactory result ~73%. Alterations zones are identified by using Clay ratios and iron oxide ratios (fig 1 and 3) in

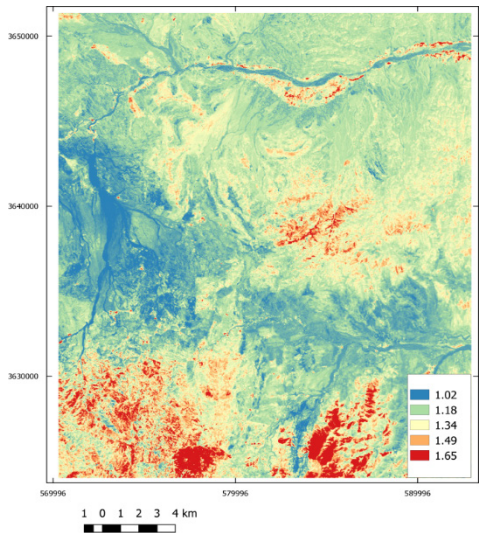

Figure 3. Reddish color shows Clay ratio content in rocks with highest value which is 1.65.

the rocks, such alterations zones could be perspective zones for minerals occurrences. The reference data used in this study was the geological map of North Waziristan on the scale 1:50,000. For further studies and to minimize uncertainties caused by vegetation, complex geologic history and local landscape evolution events, it would be valuable to use other data (field data, geophysical data) for reference purposes. Keeping in view the complex geological history of the area, I suggest that a combination of remote sensing with sampling on ground and geophysical data; magnetics and gravity could produce more accurate results. Information could be changed due to geomorphic processes and different factors; erosion and deposition, so evaluating the accuracy of unsupervised classification, results of Landsat 8 OLI data through error matrix and kappa hat shows that remote sensing using digital image processing techniques can generate moderate to high level results

In lithological mapping and finding alteration zones especially in arid regions.

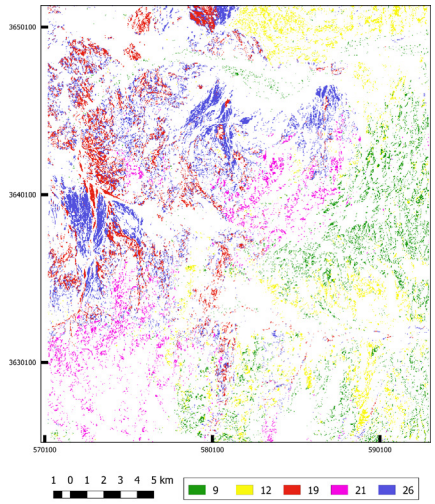

Figure 4. ISO reclassified thematic map 9-JAF: Jurassic Alexandra Formation, 12-TRF: Triassic Raghazii Formation, 19: JUM: Ultramafic Rocks, 21-JPS: Pelagic Sediments, 26-QFD: Quaternary Fan Deposit.

Abbreviations

Raghzai Formation (TRF Triassic)
Kishai Formation (TKF Triassic)
Zebe Formation (JZF Jurassic)
Alexandra Formation (JAF Jurassic)
Zargar Khel Formation (JZF Jurassic)
Mami Rogha Limestone Formation (KML Cretaceous)
Waziristan Ophiolite (WO)
Ultramafic rocks (JUM)
Gabbro (JG)
Plagiograinte (JPG
Sheeted dyke complex (JSD)
Vizhada sar volcanic (JVV
Wala Volcanic (JWV)
Terrace deposit (QTG)
Fan deposit (QFD
Quaternary alluvium (QAL)
River bed QRS)

Acknowledgements

I am grateful to all faculty Professors for providing assistance during my studies. I am thankful to my supervisor Dr. Janusz Magiera for his understanding, endless support and encouragement.

References

Abrams MJ, Brown D, Lepley L, Sadowski R (1983) Remote sensing for porphyry copper deposits in southern Arizona. Economic Geology, 78:591–604.

Anwar M, Fatmi AN, Hyderi IH, (1993) Stratigraphic Analysis of the Permo Triassic and Lower Middle Jurassic Rocks from the "Axial Belt" Region of the Northern Baluchistan, Pakistan. The Geological Bulletin of the Punjab University, 28:1–20.

Awad NMA (2011) Evaluating the effectiveness of multi-spectral remote sensing data for lithological mapping in arid regions: A quantitative approach with examples from the Makkah Neoproterozoic region, Saudi Arabia. Master's Thesis, Missouri University of science and technology, p.24.

Badshah MS (1985) Development of Waziristan. FATADC, Record. 3:15

Bannari A, Morin D, Bonn F, Huete AR (1995) A review of vegetation indices. Remote Sensing Reviews, 13:95–120.

Beck RA (1995) Late Cretaceous ophiolite obduction and Paleocene India-eurasia collision in the westernmost Himalaya, doctoral thesis, University of Southern California, p.550.

Fatmi AN (1974) Lithostratigraphic units of the Kohat-Potwar range, Indus basin, Pakistan. Memoirs of the Geological Survey of Pakistan, 10:1–80

Jensen JR (2005) introductory digital image processing 3rd edition. In Upper saddle river: Prentice hall.

Johnson BD, Powell, C.M.A. and Weavers, J.J., 1976, Spreading history of the Eastern Indian Ocean and greater India's nortward flight from Antarctica and Australia. GSA Bull., Vol. 87:1560–1566.

Kazmi AH (1977b) Application of ERTS-1 imagery to recent tectonic studies in Pakistan. US Geol. Survey. Project Report, CENTO Invest. (IR) CENT, 10:144.

Khan SR (1999) Stratigraphy of the passive margin of the indian plate, Waziristan, NW Pakistan, Geologica, 4:47–68.

Khan SR, (2000) Petrology and Geochemistry of a part of the Waziristan ophiolite complex NW Pakistan. PhD. Thesis, Peshawar University, p.253.

Knepper DH, Simpson SL (1975) Remote sensing in Geology and mineral resources of the Altiplano and Cordillera Occidental, Bolivia. USGS Bulletin, p.47–55.

Mudrov´a MA (2010) Principal component analysis in image processing, Institute of Chemical Technology, Prague, Department of Computing and Control Engineering, p. 2–5.

Petterson, M.G. and Windley, B.F., 1985, RbSr dating of the Kohistan arc-batholith in the Trans-Himalaya of north Pakistan, and tectonic implications. Earth and Planetary Science Letters, 74:45–57.

Patria, P, Achache J (1984) India-Eurasia collision chronology and its implication for crustal shortening and driving mechanism of plates. Nature, Vol. 311, p. 615–621.

Powell CM (1979) A speculative tectonic history of Pakistan and surroundings: Some constraints from the Indian Ocean. In Farah, A and DeJong, K.A. (eds.) Geodynamics of Pakistan. Geol. Surv. Pakistan, p. 524.

Gupta, R.P., 2017. Remote sensing geology. Springer.

Robinson J, Beck R, Gnos E, Vincent RK(2000), New structural and stratigraphic insight for NW Pakistan from field and Landsat Thematic Mapper data. Geol. SOC. Am. Bull., 112:364–374.

San BT, Sumer EO, Gurcay B (2004) Comparison of band ratioing and spectral indices methods for detecting alunite and kaolinite minerals using ASTER data in Biga region, Turkey. In Proceedings ISPRS.

Searle (1991) Geology and tectonic of Karakoram mountains. John Wiley & Sons, New York, p. 358.

Sibson, R.H., 1987. Earthquake rupturing as a mineralizing agent in hydrothermal systems. Geology, 15(8), pp.701-704.

Tou JT, Gonzalez RC (1974) Pattern recognition principles. New York, Addison-Wesley, Reading, MA, p. 377.

Treloar PJ, Izatt CN (1993) Tectonics of the Himalayan collision between the Indian plate and the Afghan block: A synthesis, in Treloar, P. J., and Searle, M. P., eds., Himalayan tectonics: Blackwell, Geological Society of London Special Publication 74: 69–87.

Vincent RK (1997) Fundamentals of geological and environmental remote sensing. Englewood Cliffs, NewJersey, Prentice Hall, p. 366.

Lithium prediction using reflectance spectroscopy in Jiajika area of western Sichuan province, China

Jingjing Dai, Denghong Wang, Hongzhang Dai
MLR Key Laboratory of Metallogeny and Mineral Assessment, Institute of Mineral Resources, Chinese Academy of Geological Sciences

Abstract. The Jiajika ore deposit has become one of the areas with the richest Li resources in China and even in the world. Based on the spectral measurement of representative drill hole ZK1101 in X03 vein, the spectral characteristics of spodumene, pegmatite containing spodumene, pegmatite without spodumene and surrounding schist were analyzed. They indicated that the spectrum of spodumene had three absorption at 1413 nm, 1910 nm, 2207 nm, and the discrimination of these three kinds of rocks can be achieved using the 1910 nm spectral absorption feature. Then a quantitative estimation model was built based on the correlation analysis between absorption depth on 1910 nm and content of lithium which reveals that they were linear positive correlated with R^2=0.75. It will provide spectral basis for prediction of lithium in the feature.

1 Introduction

Reflectance spectroscopy is a rapidly advancing technique used to acquire spectral reflectance data in the visible-near infrared (VNIR) and short-wave infrared (SWIR) wavelength regions (0.35-2.5 nm) for material characterization (Van der Meer 2018). The spectral reflectance method as an analytical tool has such advantages as rapid data acquisition, non-destructive sample measurement and low operational cost. Electronic transition and charge transfer processes associated with transition metal ions cause absorption of incident light in the visible and infrared region, producing diagnostic spectral features (Clark et al. 2013). Much research has been taken on the spectral characteristics of altered minerals such as muscovite, chlorite, alunite and kaolinite with regards to their application in hydrothermal deposits exploration (Biel et al. 2012; Carrino et al. 2015; Mathian et al. 2018). Lithium is currently an important rare metal due to the increasing demand of emerging industries (Wang et al. 2013). However, little research has been undertaken on the diagnostic absorption features of lithium, and few data has been published on the relationship between absorption features and chemical composition of lithium. In this paper, spodumene from the Jiajika area of western Sichuan province, China was studied using reflectance spectroscopy to provide theoretical principles for lithium prediction.

2 Geological setting

Jiajika lithium-polymetallic ore is located at the junction of kangding, Yajiang and Daofu county, which is on the southeast margin of Tibetan Plateau (Liu et al.2017). The main stratum in this area is sandy shale of Triassic Xikang Group, which is converted to biotite schist, xantholite schist, andalusite schist, cordierite schist by regional and contact metamorphism. Two-mica granite shaped like a horse neck is the main metallogenetic rock in this area, with numerous pegmatite veins around it. Among these veins, the X03 vein, known as the “new No.3 vein”, is the most important vein with regards to the Li2O resource with up to 643100 tons, much higher than that of the No.3 vein in Keketuohai, Xinjiang (Wang et al. 2016). The main Li-bearing mineral is spodumene, including comb-like spodumene type, micro-crystalline spodumene type, hair-like fine grain spodumene type and giant crystal column spodumene type (Fu et al. 2015). Drill hole ZK1101 in new No.3 vein with depth of 126.49 m was chosen for our study.

3 Spectral measurement

The spectral reflectance data were acquired using an ASD FieldSpec-4 portable spectroradiometer in a darkroom. The FieldSpec-4 spectroradiometer measures dispersive reflectance at wavelengths from 0.35 nm to 2.5 nm. For reference, a Spectralon plate was measured every ten minutes. A 8° field-of-view fore optics lens was used for spectral data acquisition. Five spectral scans were repeated for each sample and an average spectrum was recorded.

4 Discussion

4.1 Spectral analysis

The spectral characteristics of rocks and minerals including biotite schist, xantholite schist, cordierite schist, andalusite schist, granite, pegmatite containing spodumen, pegmatite without spodumene, spodumene, aquamarine were analyzed. The spectra of surrounding rocks including biotite schist, xantholite schist, cordierite schist, andalusite schist had no diagnostic absorption features with the lowest recorded reflectance. The spectra of spodumene samples had three absorption at 1413 nm, 1910 nm, 2207 nm which was coincident with the USGS spectral library (Fig.1), and the spectral characteristics of pegmatite containing spodumene was similar to the spectra of spodumene (Fig.2). The pegmatites and granites without spodumene and granites showed two deep absorption features at 1413 nm, 2207 nm and a weak absorption feature at 1910 nm whereas mineralized pegmatite showed a deep 1910 nm

absorption feature. Therefore, the absorption at 1910 nm could discriminate ore-bearing or ore-barren (Fig.2)

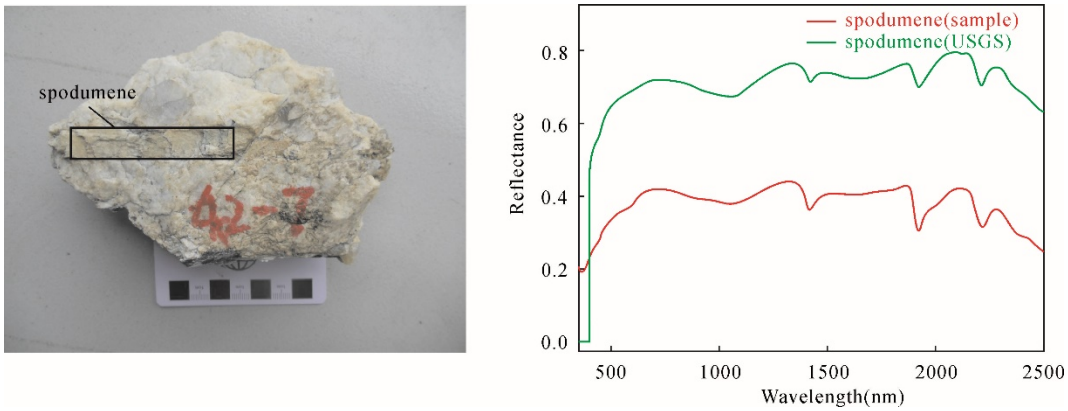

Figure 1. The photo and spectral characteristics of spodumene mineral

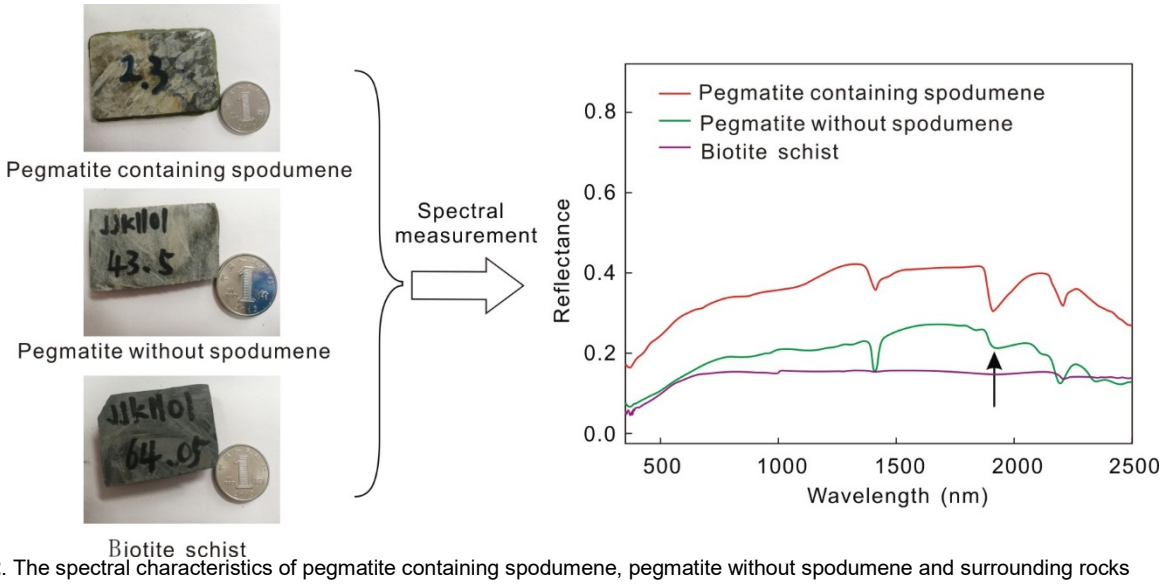

Figure 2. The spectral characteristics of pegmatite containing spodumene, pegmatite without spodumene and surrounding rocks

4.2 The relationship between reflectance spectra and content of lithium

The absorption depth on 1910 nm of thirty-eight samples at different depth of ZK1101 drill were calculated, and the content of lithium were also acquired using ICP-MS (inductively coupled plasma mass spectrometry) which was conducted with the sample powder at each depth, then the relationship between absorption depth and content of lithium was charted (Fig. 3). It revealed that the content of lithium was few hundred to 2000μg/g in the surrounding rocks, and their absorption depth were less than 0.01; while the content of lithium in the ore-bearing rocks were 5000-18000μg/g, and their absorption depth were 0.02-0.08, which were well above the surrounding rocks. The absorption depth on 1910 nm was positive correlated with the content of lithium, and R2 was 0.75 (Fig.4).

5 Implications

The spectral characteristics of lithium deposit in Jiajika were studied, and it provide a new method for lithium prediction. The spectra of surrounding rocks, ore-bearing rocks and ore-barren rocks can be distinguished by the absorption depth on 1910 nm, which can be applied to lithium prediction for hyperspectral remote sensing.

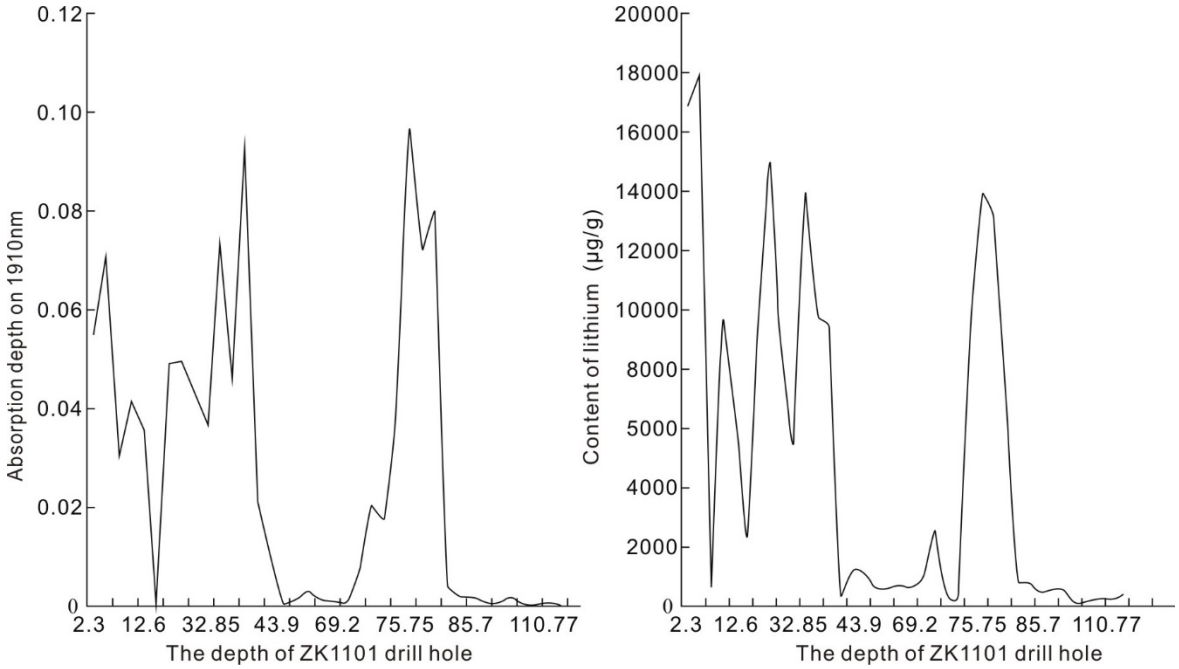

Figure 3. Chart of absorption depth and content of lithium according to depth of ZK1101 drill hole

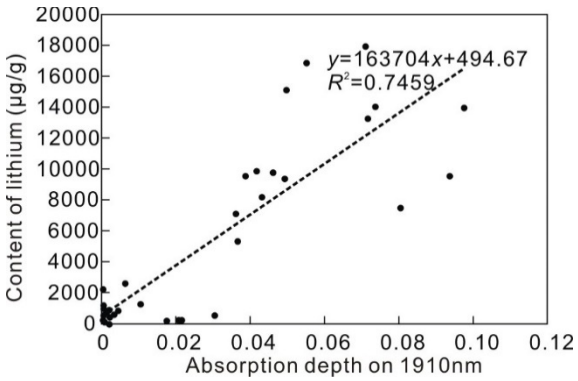

Figure 4. The quantitative inversion model of content of lithium based on absorption depth on 1910nm

Acknowledgements

This work was supported by the China geological survey project “Survey of lithium deposit in Jiajika area of western Sichuan province, China” (Grant No.DD20160055). I would like to thank Miss Liu Lijun (China University of Geosciences (Beijing)) for assisting in sampling in Jiajika deposit, and Prof. Yan Bokun (China Aero Geophysical Survey and Remote sensing Center for Land and Resources) for the valuable comments and suggestions leading to improvement of the paper.

References

Biel C, Subías I, Acevedo RD, Yusta I, Velasco F. (2012) Mineralogical, IR-spectral and geochemical monitoring of hydrothermal alteration in a deformed and metamorphosed Jurassic VMS deposit at Arroyo Rojo, Tierra delFuego, Argentina. Journal of South American Earth Sciences 35:62-73.

Carrino TA, Crósta AP, Toledo CLB, Silva AM. (2015) Unveiling the hydrothermal mineralogy of the Chapi Chiara gold prospect, Peru, through reflectance spectroscopy, geochemical and petrographic data. Ore Geology Reviews 64:299-315.

Clark RN, Swayze GA, Livo KE, Kokaly RF. (2003) Imaging spectroscopy: Earth and planetary remote sensing with the USGS Tetracorder and expert systems. Journal of Geophysical Research 108:5131.

Fu XF, Yuan LP, Wang DH, Hou LW, Pan M, Hao XF, Liang B, Tang Y. (2015) Mineralization characteristics and prospecting model of newly discovered X03 rare metal vein in Jiajika orefield, Sichuan. Mineral Deposits 34:1172-1186.

Liu LJ, Wang DH, Hou KJ, Tian SH, Zhao Y, Fu XF, Yuan LP, Hao XF. (2017) Application of lithium isotope to Jiajika new No.3 pegmatite lithium polymetallic vein in Sichuan. Earth Science Frontiers 24:167-171.

Mathian M, Hebert B, Baron F, Petit S, Lescuyer J, Furic R, Beaufort D (2018) Identifying the phyllosilicate minerals of hypogene ore deposits in lateritic saprolites using the near-IR spectroscopy second derivative methodology. Journal of Geochemical Exploration 186:298-314.

Van der Meer F (2018) Near-infrared laboratory spectroscopy of mineral chemistry: A review. International Journal of Applied Earth Observation and Geoinformation 65:71-78.

Wang DH, Fu XF (2013) A significant lithium resources discovery in outside of Jiajika area, Sichuan. Rock and Mineral Analysis 32:987.

Wang DH, Wang RJ, Fu XF, Sun Y, Wang CH, Hao XF, Liu LJ, Pan M. Hou JL, Dai JJ, Tian SH, Yu Y. (2016) A discussion on the major problems related to geological investigation and assessment for energy metal resources base: a case study of the Jiajika large lithium mineral resource base. Acta Geoscientica Sinica 37:471-480.

Soil magnetic susceptibility mapping as a vectoring tool for mineral exploration: an example from southern New Zealand

Adam P. Martin
GNS Science

Christian Ohneiser
University of Otago

Rose E. Turnbull
GNS Science

Delia T. Strong
GNS Science

Philip Rieger
GFZ Potsdam

Abstract. Element concentration patterns in soil are a commonly used vectoring tool in mineral exploration as they are both time- and cost-effective to collect and can be useful at district- to prospect-scales. However, complications can arise in interpreting patterns if the soil parent material is distal, or a mix of distal and proximal sources. Proxies can be used to link soil back to its parent material, such as physical properties, isotopic composition or its volumetric composition (e.g. organics, lithics, clays and minerals). In this study, the magnetic mineralogy of soil was tested as a proxy for soil provenance on samples in a 20 000 km^2 region of southern New Zealand at 323 sites, on both topsoil and subsoil. Samples were measured for volume-specific magnetic susceptibility using a handheld device, and for mass-specific magnetic susceptibility in the laboratory, with results being strongly, positively correlated. Additional hysteresis, isothermal remanence and thermomagnetic measurements were made on a sample subset. The soil provenance using magnetic minerals can be traced back to likely sources in outcrops of igneous rocks within the same catchment, terrane or rock type in southern New Zealand: <100 km but frequently <1 km.

1 Introduction

Understanding the pattern of dispersion related to ore-forming processes is fundamental to mineral exploration (Hawkes and Webb 1962). The footprint from an ore body is typically larger than the ore-body itself, with landscape-surface dispersion of said footprint related to processes of soil formation, sediment movement, weathering and/or hydrothermal pathways (Groves et al. 1998). Proxies in the soil can be used to trace it back to its parent, which in mineral exploration helps vector towards mineralisation. Proxies include pathfinder elements, isotopic composition, physical properties or volumetric composition (minerals, lithics, clays, etc; Cullers et al. 1998). This study focuses on a specific aspect of the latter, the magnetic mineralogy in soil, to test the hypothesis that soil magnetism is both a time- and cost-effective soil provenance tool useful to mineral exploration (Martin et al. 2018). The measurement of magnetic minerals in soil has been undertaken several times in European (e.g. Rachwal et al. 2017; Dearing et al. 1996) and Chinese (e.g. Bian et al. 2014) regional studies.

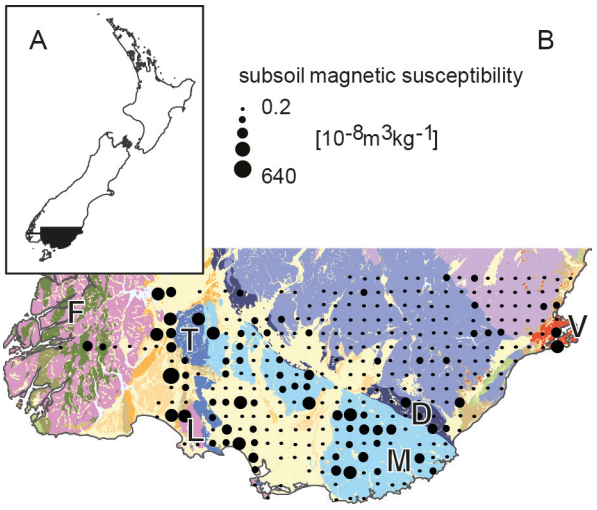

Figure 1. Location, range and pattern of mass-specific magnetic susceptibility in subsoil (50-70 cm). **A**. Position of the survey within New Zealand. **B**. Subsoil magnetic susceptibility values shown as point data overlain on a 1:1 million geological map of southern New Zealand. D: Dun Mountain Ophiolite Belt; F: Fiordland National Park; M: Murihiku Terrane; T: Takitimu Mountains; L: Longwood Range; V: Dunedin Volcanic Group. The reader is referred to online resources for a full discussion of the geology of southern New Zealand (data.gns.cri.nz/geology/).

A study area in southern New Zealand (Fig. 1) was

chosen as a test locality because of a wide range in magnetic susceptibility values from potential bedrock sources in the region. Sample sites with a regional (c. 20 000 km^2) coverage at grid sites spaced at eight km intervals were chosen. Topsoil (0–20 cm) and subsoil (50–70 cm) samples were measured for magnetic susceptibility (323 sample sites), and a subset (21 sample sites) of soil magnetic (hysteresis, isothermal remanence and thermomagnetic) measurements were also made.

2 Geological setting and environment

Sites in this study occur above eight major basement terranes of southern New Zealand (Fig. 1). The basement terranes are characterized by rocks of distinctive composition and age relating to the formation and evolution of Gondwana and include a variety of continental-sourced quartzofeldspathic metasedimentary rocks, calcalkaline volcanic rocks, island arc igneous and sedimentary rocks, ultramafic ophiolite rocks and I-, S- and A-type plutonic rocks. In the west of the survey area, plutonic rocks of the Median Batholith (pink lithologies in Fig 1) occur mostly in Fiordland National Park. Igneous mafic to ultrabasic rocks form prominent hills in the west and southwest of the survey area about the Takitimu Mountains and the Longwood Range. In the north of the survey area, the Dun Mountain Ophiolite Belt is made up of ultramafic to mafic lithologies, with rivers draining through these lithologies to the centre and southern parts of the survey area. The Murihiku Terrane in the centre and east of the survey area comprises several volcaniclastic units and tuff units. Together these, and other units in part makeup the Austral Superprovince.

Overlying the Austral Superprovince are the younger rocks of the Zealandia Megasequence (yellow in Fig. 1), which in the study area is comprised mainly of Quaternary aged river gravels, flood plain deposits and alluvial deposits. In the east of the survey area, Cenozoic, alkalic rocks make up volcanoes and lava flows of the Dunedin Volcanic Group, also part of the Zealandia Megasequence.

Five of the 14 major soil orders found in New Zealand occur within the study area. Cambisols and luvisols are particularly common in the study area, with regosols, gleysols and podzols also well represented. Of interest in this study are soils derived from igneous parent material, which include mafic cambisols and allophanic soils. The latter contains allophane minerals as well as ferrihydrite and imogolite and typically occur as the weathering products of igneous rocks.

Catchments in the survey area drain southwards, eroding and redepositing sediment over distances of ≤100 km. The climate is cool temperate, with rainfall decreasing eastwards from >4000 mm yr^{-1} to 250–500 mm yr-1. Of the *c.* 220 000 people that live in the study area, 73 per cent live within two cities. The rest of the land area is sparsely populated and used for agriculture (beef, sheep, deer and dairy) or exotic forestry.

3 Magnetic measurements

The handheld magnetic susceptibility results range between 1.1 and 424 x 10^{-8} S.I. for the topsoil and between 1.2 and 594 x 10^{-8} S.I. for the subsoil. The laboratory data results range between 0.5 and 534 x 10^{-8} m^3 kg^{-1} for topsoil samples and 0.2 and 640 x 10^{-8} m^3 kg^{-1} for subsoil samples. The isothermal remanent magnetization (IRM) analyses resulted in a coercivity of remanence (Hcr) of between 25 and 77 mT and a saturation remanent magnetization (Mrs) of between 0.12 and 131 mAm^2 kg^{-1}. Hysteresis analyses revealed a coercivity (Hc) of between 2.3 and 19 mT, saturation magnetization (Ms) of between 0.85 and 938 mAm^2 kg^{-1} and remanent magnetization (Mr) of between 0.10 and 134mAm^2 kg^{-1}. Hysteresis loops are narrow waisted with all samples saturating at low fields.

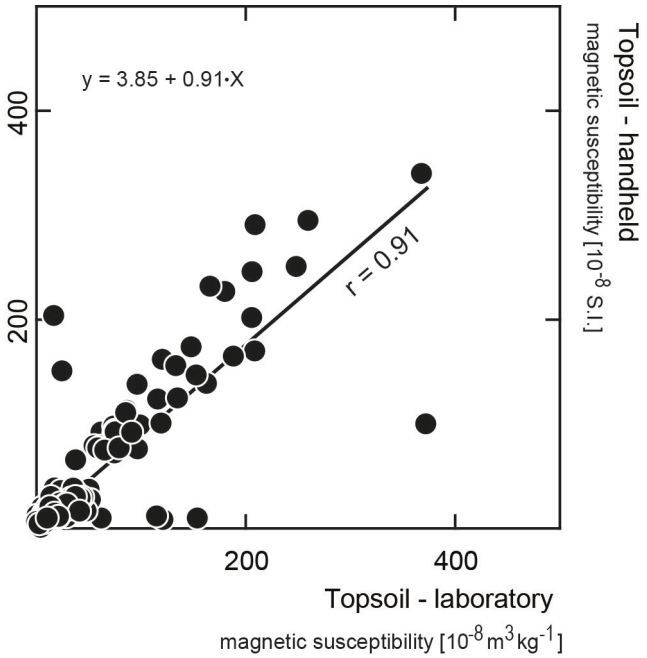

Figure 2. Topsoil mass-specific magnetic susceptibility (laboratory method) versus topsoil volume-specific magnetic susceptibility (handheld method). The strong correlation (r = 0.91) allowed a linear regression to be calculated as shown on the diagram.

4 Discussion

4.1 Handheld versus laboratory techniques

There is a strong, positive relationship between mass-specific susceptibility measured in the laboratory and volume-specific susceptibility measured by handheld techniques (Fig. 2). A linear regression equation calculated for this data (including outliers; Fig. 2) means the handheld data can be converted into mass-specific values (10^{-8} m^3 kg^{-1}). This is important for studies where budget, time or laboratory access are issues, such as for exploration personnel, science students or other researchers where magnetic susceptibility is a secondary concern. The associated costs in personnel and laboratory times are an order of magnitude less using a handheld magnetic susceptibility meter. The advantages to the laboratory technique are higher precision. A range

of additional data about remanence, mineralogy, etc. can also be determined in the laboratory, assuming the time and equipment are available. Using a handheld meter in the field is thus acceptable for studies of soil magnetic susceptibility where an appropriate regression can be calculated or studies where high precision is a lower priority.

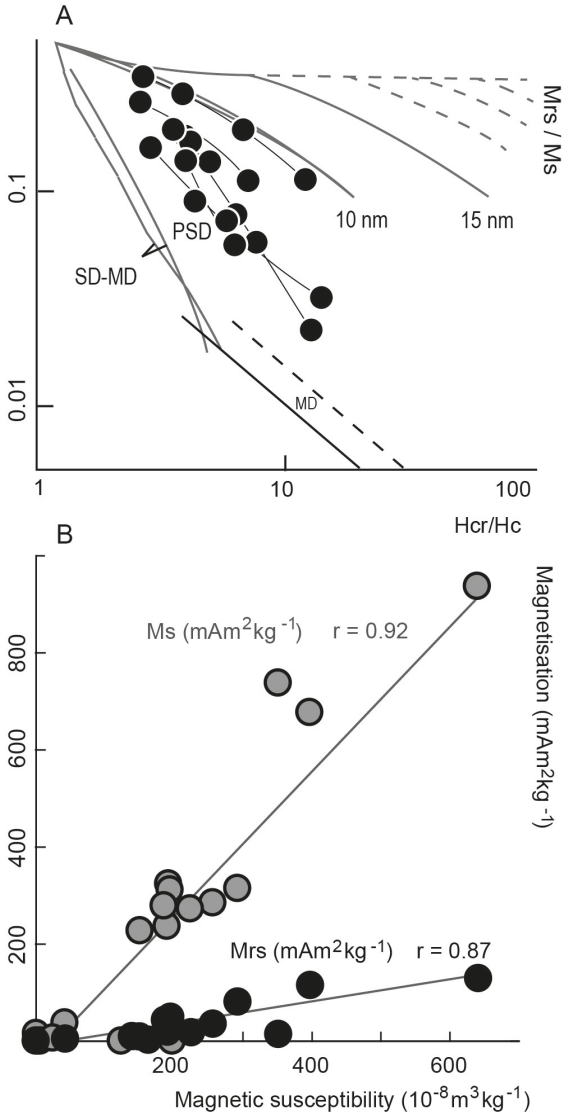

Figure 3. Subsoil magnetic data. **A**. A day plot indicating pseudo-single domain (PSD) magnetite is the dominant remanence carrier (Dunlop 2002a,b; Day et al. 1977). Some analyses which approach the PSD-single domain (SD) mixing line may be biased by minor contributions of higher coercivity grains and a single sample from near the Longwood Range plots in the multidomain (MD) field and likely indicates a geogenic contribution of large titanomagnetite grains. **B**. Magnetic susceptibility versus hysteresis and IRM determined magnetic concentration parameters (Ms and Mrs), which demonstrates a good correlation between magnetic mineral specific concentrations (Ms and Mrs) and magnetic susceptibility, which can be sensitive to contributions from paramagnetic and diamagnetic components in soil.

4.2 Nature of magnetic minerals

The Hcr values are consistent with magnetite mineralogy where values can vary depending on grain size and composition (Day et al. 1977). Overall, the median coercivity of 41 mT indicates magnetite is the dominant remanence carrier at anomalous sites. A minor contribution from haematite may be present in some samples with higher Hcr values above 60 mT (Özdemir and Dunlop 2014). A day plot (Fig. 3A) indicates magnetic grains are mostly in the pseudo-single domain (PSD) and single domain (SD) grain size range, with the exception of one sample which falls in the multidomain (MD) field. A biplot of magnetic susceptibility versus Ms and Mrs (Fig. 3B) reveals a close correlation between the two, indicating that magnetic susceptibility for most samples is controlled by changes in mineral concentration rather than changes in mineral type, or in the proportions of ferromagnetic versus para/diamagnetic contributions. Samples with a higher average Hcr value of 61 may indicate a greater quantity of high coercivity grains.

4.3 Source of the magnetic susceptibility minerals in soil

Three different approaches, the difference method, Tukey boxplot method and geoaccumulation index (Igeo) method, were used to identify the background magnetic susceptibility of soil in the survey area. Sites with anomalous magnetic susceptibility could also be identified using this method. The threshold for identifying anomalies is as follows: difference method < Tukey boxplot < Igeo, such that the difference method detects many more anomalies than the Igeo method, as has been found in other studies (e.g. Reimann 2005). Below, areas with anomalously high magnetic susceptibility (i.e. above background) are discussed.

In the west of the survey area, the provenance of magnetic minerals in soil in the catchment is suggested to be from igneous rocks of the Median Batholith, sourced from the upper part of the catchment in Fiordland National Park. Median Batholith rocks are moderately to strongly magnetic with I-type granites, gabbros and peridotites. The provenance of the magnetic soils in these rocks is therefore 1 to 30 km.

In the west and southwest of the survey area there is likely local input from the Takitimu Mountains, and in the southwest part of the survey area, input from the Longwood Suite in the Longwood Range may be the dominant source. The Takitimu Mountains contain likely titanomagnetite-bearing rocks and this study suggests they are an unrecognized source of a high coercivity mineral such as haematite. The basic and ultrabasic rocks of the Longwood Suite that are known to contain titanomagnetite-bearing rock types. The magnetic minerals in these soil samples have travelled ≤20 km.

Sample sites in the centre of the survey area occur along river flood plains above Late Pleistocene river gravels in cambisol or regosol soil types. The main river catchments in this region drain the Dun Mountain Ophiolite Belt and Takitimu Mountains, both of which have high concentrations of magnetic minerals. It has been shown elsewhere that heavy minerals from the ophiolite belt have been eroded and redeposited along these flood plains (Martin et al. 2016) and a similar

explanation is envisioned to explain the magnetic susceptibility anomalies in the central part of the survey area. Namely, magnetite has been eroded and redeposited along the river floodplains, a distance ≤100 km.

Other anomalously high magnetic susceptibility sights sampled above the Murihiku Terrane have formed in magnetic, allophanic soils and cambisol soils. These formed adjacent to tuffaceous beds and volcaniclastic sandstone units derived from a basaltic–andesitic volcanic arc that are known to contain magnetite, haematite and pseudomorphs after haematite. This suggests the provenance of magnetic minerals at these sights is proximal, certainly less than the terrane width (maximum 80 km), but most likely <1 km.

In the east of the survey area, several high magnetic susceptibility results are from mafic melanic soils and mafic cambisol soils formed from igneous protoliths. These occur either directly above or adjacent to Dunedin Volcanic Group rocks that are known to contain titanomagnetite and are relatively magnetic. The provenance of magnetic minerals in these anomalous sites is proximal (<1 km).

5 Discussion and conclusions

The volume-specific magnetic susceptibility (handheld method) and mass-specific magnetic susceptibility (laboratory method) of topsoil and subsoil were measured in a regional study of southern New Zealand. A strong correlation between the volume- and mass-specific methods suggests the faster and more economic handheld method could be justifiably used in future soil studies in New Zealand. A linear regression calculation on the data in this study could be used in the future to convert volume- to mass-specific magnetic susceptibility.

The magnetic mineralogy is dominated by magnetite, but certain areas around the Takitimu Mountains and Longwood Range in the west, and Dunedin Volcanic Group in the east, indicated variable magnetic mineralogy, e.g. a minor contribution of haematite.

The provenance of magnetic mineralogy is generally confined to the rock type, catchment or terrane the sample was taken in. This is a distance ≤100 km and frequently much closer (<1 km). In the west of the survey area, the source of magnetic mineralogy is from Median Batholith rocks from within or near Fiordland National Park, with proximal sources from the Takitimu Mountains or Longwood Range becoming significant, or even dominant, in the southwestern areas of the survey. In the centre of the survey area the dominant source of magnetic minerals is the Dun Mountain Ophiolite Belt or volcaniclastic rocks or tuffs in the Murihiku Terrane. In the east, the Dunedin Volcanic Group rocks are an important source of magnetic minerals in soil.

The study of soil magnetic susceptibility allows a more thorough understanding of soil distribution and is a powerful tool for provenance studies in regions where the magnetic susceptibility of the soil parent material is sufficiently varied. This study suggests that handheld magnetic susceptibility measurements will be sufficiently accurate and precise for field based mineral exploration. Magnetic susceptibility of soil should be used in conjunction with other parameters (chemistry, soil type, colour, etc.) during mineral exploration campaigns, when the source of soil parent material is in question.

Acknowledgements

This work was funded by the Government of New Zealand through a GNS Science strategic development fund. Amy Beatson and Chantelle Hillier assisted with sample collection and processing.

References

Bian Y, Ouyang T, Zhu Z, Huang N, Wan H, Li M (2014) Magnetic properties of agricultural soil in the Pearl River Delta, South China — Spatial distribution and influencing factor analysis J Appl Geophys 107:36-44

Cullers RL, Basu A, Suttner LJ (1988) Geochemical signature of provenance in sand-size material in soils and stream sediments near the Tobacco Root batholith, Montana, USA Chem Geol 70:335-348

Day R, Fuller M, Schmidt VA (1977) Hysteresis properties of titanomagnetites: Grain-size and compositional dependence Phys Earth Planet Inter 13:260-267

Dearing J, Hay K, Baban S, Huddleston A, Wellington E, Loveland P (1996) Magnetic susceptibility of soil: an evaluation of conflicting theories using a national data set Geophys J Int 127:728-734

Dunlop DJ (2002a) Theory and application of the Day plot (Mrs/Ms versus Hcr/Hc) 1. Theoretical curves and tests using titanomagnetite data Journal of Geophysical Research: Solid Earth 107:EPM 4-1-EPM 4-22

Dunlop DJ (2002b) Theory and application of the Day plot (Mrs/Ms versus Hcr/Hc) 2. Application to data for rocks, sediments, and soils Journal of Geophysical Research: Solid Earth 107:EPM 5-1-EPM 5-15

Groves DI, Goldfarb RJ, Gebre-Mariam M, Hagemann SG, Robert F (1998) Orogenic gold deposits: A proposed classification in the context of their crustal distribution and relationship to other gold deposit types Ore Geol Rev 13:7-27

Hawkes HE, Webb JS (1962) Geochemistry in mineral exploration. Harper and Row, New York

Martin AP, Ohneiser C, Turnbull RE, Strong DT, Demler S (2018) Soil magnetic susceptibility mapping as a pollution and provenance tool: an example from southern New Zealand Geophys J Int 212:1225-1236

Martin AP et al. (2016) The regional geochemical baseline soil survey of southern New Zealand: Design and initial interpretation J Geochem Explor 167:70-82

Özdemir Ö, Dunlop DJ (2014) Hysteresis and coercivity of hematite Journal of Geophysical Research: Solid Earth 119:2582-2594

Rachwał M, Kardel K, Magiera T, Bens O (2017) Application of magnetic susceptibility in assessment of heavy metal contamination of Saxonian soil (Germany) caused by industrial dust deposition Geoderma 295:10-21

Reimann C (2005) Sub-continental-scale geochemical mapping: sampling, quality control and data analysis issues Geochemistry: Exploration, Environment, Analysis 5:311-323

The new approach for kimberlite pipes exploration based on passive seismic and radiometric methods (the example of the Arkhangelsk province)

Konstantin Danilov, Evgenii Iakovlev, Nikita Afonin
N. Laverov Federal Centre for Integrated Arctic Research RAS (FCIARctic)

Abstract. Kimberlite pipes are objects, which are difficult to explore for due to their shapes and sizes. The effectiveness of traditional exploration methods for kimberlite pipes significantly decreases in complex landscape-geological conditions in remote and covered environments. That is why developing of new exploration methods for kimberlite pipes is crucial. In this paper, we present the results of a study of a new model for exploration for industrial diamond pipe based on joint using several geophysical methods: microseismic sounding, passive seismic interferometry, the H/V method, gamma-spectrometry and emanation survey. The studies were carried out using the Lomonosov kimberlite pipe named after M. Lomonosov of the Arkhangelsk diamondiferous province. The main result of our work focus on the model for kimberlite pipe and near pipe medium and their main structural elements. The model includes the kimberlite-caused fault, obtained by passive seismic methods. Radiometric data shows the kimberlite pipe as local radio-geochemical anomalies of an isometric shape. Thus, we shown that the proposed set of methods can be useful in planning exploration. In addition, the robustness of the results suggests that the applicability of these joint methods during exploration.

1 Introduction

Physical properties of kimberlites and enclosing rocks can vary over a wide range. For example, the Lomonosov pipe is characterized by a difference in rock composition differences of near 30% compared to samples extracted from neighbour pipes (Verzhak et al. 1983). Therefore, using geophysical methods for prospecting and exploration of diamond pipes is difficult (Milashev 1984; Kutinov and Chistova 2004). Because of this reason, the effectiveness of exploration in the territory of the Arkhangelsk diamondiferous province using traditional methods is low. In the early 80s, the effectiveness of the verification of magnetic anomalies was 20%. Today, it is now it is less than 0.5% (Korotkov 2011). Therefore, it is necessary to improve the methods for kimberlite pipes exploration. To that instance, the effectiveness of using passive seismic methods and emanation survey was shown earlier by Kiselev et al. (2018) and Francuzova and Danilov (2018). These methods have not been tested together in the same area. Moreover, these approaches were tested using an example of 1-2 profiles on each pipe (Kiselev et al. 2018). The purpose of this work is to examine the possibility of obtaining a model of a pipe, based on the joint use of passive seismic and radiometric methods.

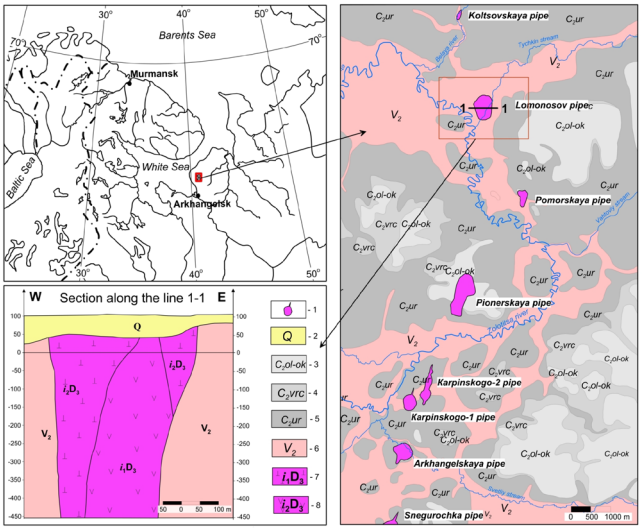

Figure 1. Studied area. Geological scheme of the area. 1 - pipes; 2 - Quaternary fluvioglacial sediments; 3-5 - Middle Carboniferous sediments: 3 - Ursug suite; 4 - Voevchensky suite; 5 - Olmugo-Okunev suite; 6 - Upper Vendian sediments; 7 - kimberlites of first explosion phase; 8 - kimberlites of second explosion phase.

2 Geology

The Lomonosov kimberlite pipe named is part of the Zolotitskoe ore field of the Arkhangelsk diamondiferous province (Bogatikov et al. 1999). We used this pipe in this study as it is a well studied pipe by various geological (including drilling) and geophysical methods (Verzhak et al. 1987). The pipe was previously studied using microseismic sounding method and emanation survey, which made it possible to estimate the repeatability of the results.

Upper Vendian sediments (sandstones, siltstones) with a thickness of about 920 m are hosting the Lomonosov pipe and Neogene-Quaternary sediments (sand and gravel mix) are overlained the pipe (Eremenko and Nenakhov 2002).

The pipe is 202,198 m^2 (585×441 m) and has an oval shape. In the vertical section, the pipe is a cone-shaped body slightly narrowing with depth. The pipe is completely devoid of the crater facies and is composed of two main varieties of the kimberlites - tuff breccias and autolithic breccias (Bogatikov et al. 1999)

The age of the pipe estimated by the K-Ar method is about ~ 355 Ma (Eremenko and Nenakhov 2002)

3 Methods

3.1 Passive seismic methods

Passive seismic interferometry with advanced method of stacking (Afonin et. al. 2019), H/V method (Nakamura, 1989) and microseismic sounding method (Gorbatikov et al. 2013) were used. The passive seismic interferometry allows evaluating empirical Greens function by cross-correlation of seismic noise and stacking of cross-correlation functions. Method H/V allows the estimation of depth of the kimberlite boundary by analysis of resonance frequencies of seismic noise (Lane et al. 2008; Ibs-von Seht and Wohlenberg 1999). The microseismic sounding method (Gorbatikov et al, 2013) based on spectral analysis of a vertical component of ambient noise and aims to isolate sub-vertical inhomogeneities inside the studied medium. This method have been used to isolate fault fractures, intrusive bodies, magma focuses, igneous pipes (Gorbatikov et al. 2013; Francuzova and Danilov 2018).

3.2 Radiometric methods

Radon activity measurements were carried out along sub latitudinal profiles with an outlet beyond the pipe. The distance between stations was about 100 m and the distance between each measurement was about 50 m. Measurements of the volumetric activity of radon (VAR) in the soil were carried out using an automated radiometer PRA-01M-03, following the methodology (VNIIFTRI 2006). In total, over 200 measurements of VAR over the kimberlite pipe were measured.

Gamma-spectrometry measurements were performed in situ using the high-precision mobile scintillation gamma-spectrometry complex RS-700 (RSI 2016). The measurements were carried out at a height of 0.7 m above the ground in the pedestrian variant using a profile system on a scale of 1:10 000 using the same points as the microseismic measurements.

4 Results and discussion

4.1 Passive seismic interferometry

We used the surface wave part of the empirical Greens function to extract the dispersion curve. Model of the dispersion curve inversion has been selected according to general geological conditions of the studied area. According to the calculated model, the medium presented by three layers with boundaries on depths of about 70 m and 750 m. The shear-wave velocities in the layers are about 400 m/s, 1200 m/s and 1900 m/s, respectively. These boundaries correspond to the boundaries between the Quaternary and Vendian deposits (70 m) and the surface of the crystalline basement (750 m) (Verzhak et al. 1983).

The values obtained in the Vendian sediments are close to the model. Nevertheless, velocities in the crystalline basement are one-third less than typical for the studied region.

4.2 Microseismic sounding and H/V methods

Method H/V allowed revealing boarders on depths of 20m, 50m and 800m (Fig. 2). The shallowest boarder feature disappears above the pipe

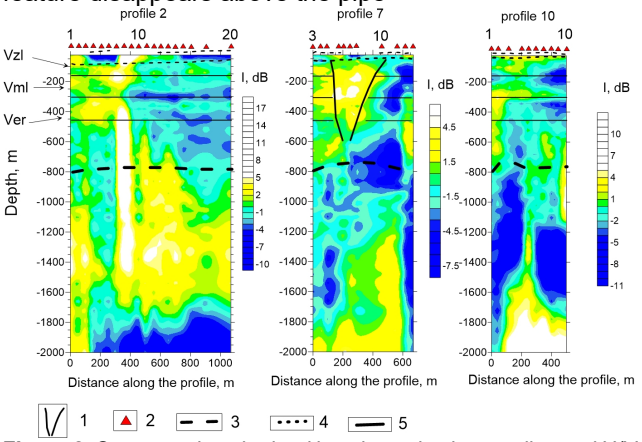

Figure 2. Cross-section obtained by microseismic sounding and H/V methods, 1 – known boarders of the pipe from previous studies, 2 – measurements points of ambient seismic noise, 3 – interpreted surface of bedrock, obtained by H/V method, 4 – interpreted boarders in overburden rocks, obtained by H/V method, 5 – known local stratigraphic units of the Vendian (Vzl - Zolotitskaya suite, Vml - Melskaya suite, Ver –Yerginskaya suite).

According to microseismic sounding result, the pipe correspond to low-velocity cone-shaped heterogeneity with the relative intensity of microseisms 1.5-2 dB. The anomaly appeared in depths between 100 m and 500 m. The heterogeneity is partially out of the boundary, obtained from previous study results at depths 250-450 m on the west and in depths more than 450 m on the east. This part of heterogeneity could not found in previous geological studies Verzhak et al. 1983)

The east vertical border of the pipe has the strongest contrast with the medium. Probably, the reason for this is more consolidate medium , bordered with the west part of the pipe. According to the shape of heterogeneity and variation of microseisms intensities, the pipe has east and west blocks bordered in point 8 of the profile 3 (Fig. 2). The most contrast fault zone located under point 2 of the profile 8. From the south of the pipe, there is also fault under point 10 (profile 5). These faults located inside the sediment and the bedrock. Points 2 and 3 of the profile 8 and point 10 of the profile 5 located along the one line. Relatively both faults and pipe, the near pipe medium separated to more fractured on the west part and more consolidate on the east part. Therefore, one can assume, that kimberlite-caused fault crossed the points marked above. In the same time, the low-velocity heterogeneities in bedrock may be a feed channel.

4.3 Radon method and gamma spectrometry

The VAR of soil over the pipe varies from <1 to 133 kBq·m^{-3}, with average VAR value at ~ 15 kBq·m^{-3} (Fig. 3).

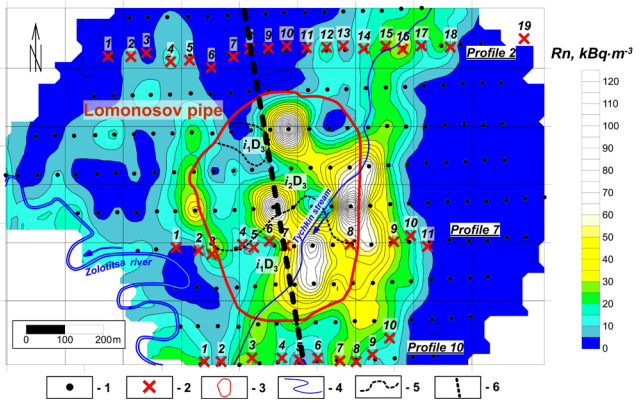

Figure 3. Distribution of VAR in soil gas near the studied pipe. 1 - radon measurement points; 2 - microseisms measurement points; 3 - projection of the pipe contour onto the surface; 4 - water channels; 5 - boundary of the explosion phases; 6 - kimberlite-caused fault.

The standard deviation of the VAR values is 19.7 kBq·m^{-3}. Therefore, according to the 3-sigma rule the values exceeding 59.1 kBq·m^{-3} are anomalous for the local studied area. The pipe stands out in contrast to the field of soil radon. Local anomalies are within the contour of the pipe, as well as on its eastern boundary. The increased values of radon well contoured the pipe from the west, east and southeast and correspond to the sub-vertical boundaries of the pipe according to the section in Figure 1 (section along the line 1-1). Probably, these boundaries correspond to the zones of increased fracturing of the enclosing rocks. Outside the pipe, the VAR decrease significantly to less than 20 kBq·m^{-3}. Nevertheless, when approaching the channel of Zolotitsa river the radon activity increases slightly, which, probably associated with an increase of the radium content in the near-channel sediments. In addition, a linear zone of increased activity of radon in the soil air is clearly distinguished, crossing the pipe in the direction of the north-east - south-west. Spatially, this zone coincides with a channel of small taiga stream - Tuchkin. The formation of elevated values in this linear zone may be due to an increase in the concentration of radium in the near-channel sediments of the Tuchkin stream. However, due to the fact that the Tuchkin stream has a width of only 0.5-1 m, the thickness of its channel sediments is significantly less than that of the Zolotitsa river, but the activity of radon in the riverbed is 2-3 times higher. In addition, the Tuchkin stream has a relatively straight channel that can trace a fault with increased radon permeability.

To verify the data on the VAR, an in-situ gamma-spectrometric survey was performed over the studied pipe, since the activity of radon in soils depends not only on the permeability of sediments but also on the concentration of uranium (radium) in the soil (fig.4).

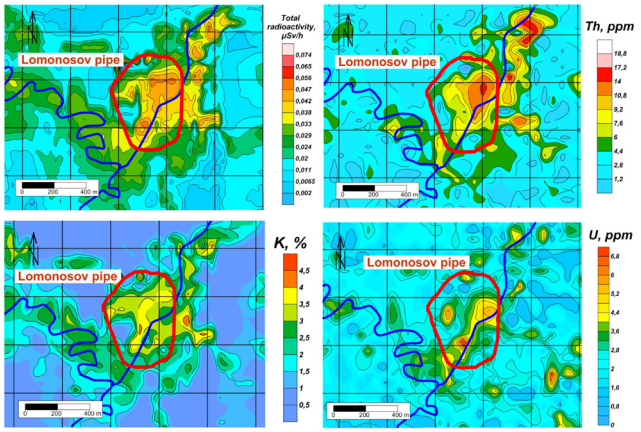

Figure 4. The distribution of total radioactivity, concentration of thorium, potassium and uranium over the studied pipe.

Total radioactivity is characterized by relatively low values, up to a maximum of 0.075 μSv/h, which is typical for the Russian North (Titaeva 2005).

Nevertheless, the kimberlite pipe is clearly distinguished by the values of total radioactivity of more than 0.03 μSv/h. The total radioactivity is due to the content of potassium and thorium since the halos of their distribution are close to the pattern of distribution of total radioactivity. The concentration of thorium over the pipe reaches values of up to 18 ppm, while the background concentration does not exceed 5 ppm. The highest potassium concentrations are also observed above the pipe and reach values of about 4.5%, while background values are less than 2%. According to the gamma-spectrometry data, the near-channel sediments of the Zolotitsa river are clearly recorded, which are allocated as a wide band in the field of total radioactivity and potassium content. According to the content of thorium and uranium, near-channel sediments of the Zolotitsa river are allocated much more weakly. A linear zone with increased total radioactivity that crosses the studied pipe in the direction of the north-east - south-west is noteworthy. This zone locates along the eastern side of the Tuchkin stream and is clearly distinguished by the increased thorium and potassium. At the same time, this zone is not clearly manifested in the radium content. The total radioactivity data, potassium and thorium content are in good agreement with the radon content in the soil. At the same time, the emanometric data substantially complement the gamma spectrometry data. This is clearly seen from the comparison of the distribution patterns of uranium (radium) and radon in soil. For example, the western boundary of the pipe is contoured by an area of increased radon activity, which has a sub-circus morphology. In the data on uranium, this area was not manifested in any way, which may be due to the increased permeability of the medium because of the presence of faults. In addition, the eastern and northern boundaries of the pipe are poorly distinguished in the uranium data, but the maximum of values the VAR (more than 120 kBq·m^{-3}) are observed on these elements of the pipe. Thus, we can conclude that the pipe named after M. Lomonosov is well distinguished in the gamma-spectrometric data, as well as on the activity of radon. By

the activity of radon, some boundaries of the kimberlite pipe are well fixed, which may indicate the presence of permeable zones in the near-pipe space of the kimberlite pipe associated with faults.

4.4 Comparison of the results

The horizontal boundaries inside the medium, obtained by inversion of dispersion curve fully corresponds to results of data processing by the H/V method. In the same time, the boundaries, obtained by H/V method, correspond to microseismic sounding result. The dispersion curve, calculated from surface wave part of an empirical Greens function, allowed to calculate the depths in microseismic sounding and in H/V method.

Moreover, the velocity heterogeneity, caused by the pipe body, totally corresponds to the drilling data, that prove our results. The low-velocity character of the bedrock may be caused by fractured zones near the studied pipe. The points with anomaly values of radon volumetric activity, located within pipe along the kimberlite-caused fault. This fault localised by the microseismic sounding method. This fact also proves the results of interpretation.

5 Conclusion

The kimberlite pipe named after M. Lomonosov appeared as the low-velocity anomaly in Vendian deposits. On the ground surface, the pipe looks like the field of relatively high radon, potassium, thorium concentration and total radioactivity. Nevertheless, anomaly values of radon emanation concentrated near vertical borders of the pipe, borders of injection phases and along the kimberlite-caused fault (Fig. 3). Moreover, above the pipe, there is disruption of the overburden boundary. Joint interpretation of results allowed revealing kimberlite-caused fault and, probably, supplying channel.

Joint application of described methods allows significantly increasing the effectiveness of pipes exploration because of study not only shallow, but also deeper elements of a structure. In the same time, joint using of the methods allows increasing of provability of obtained results.

Acknowledgements

The presented study was funded by RFBR according to the research project № 19-05-00481 A «Structure and dynamics of the lithosphere of the White Sea» and the research project of state assignment « The evolution of island and continental territories of the European Arctic sector under the influence of natural and anthropogenic factors» (0409-2015-0134, № AAAA-A16-116052710105-1).

References

Afonin N, Kozlovskaya E, Nevalainen J, Narkilahti J (2019) Improving quality of empirical Greens functions, obtained by cross-correlation of high-frequency ambient seismic noise, Solid Earth Discuss., https://doi.org/10.5194/se-2019-29, in review.

Bogatikov OA, Garanin VK, Kononova VA, Kudryavtceva GP, Vasil'eva EP, Verjak VV, Posuhova TV (1999) Arkhangelsk diamondiferous province (geology, petrography, geochemistry, and mineralogy). MGU, Moscow.

Eremenko AV, Nenakhov V M (2002) Geology and geodynamic model of the formation of the volcanic pipes of the Arkhangelsk diamond province. Vestn. Voronezh. Gos. Univ, (1), 36-42.

Francuzova VI, Danilov KB (2018) The location of the S10 and Chidviya Kimberlite Pipes from Inhomogeneities in the Host Rock Structure of the Nenoksa and Chidviya–Izhmozero Fields in the Arkhangelsk Diamond Province as Detected by Background Microseisms. Journal of Volcanology and Seismology, 12(5):332–340.

Gorbatikov AV, Montesinos FG, Arnoso J, Stepanova MYu, Benavent M, Tsukanov AA (2013) New Features in the Subsurface Structure Model of El Hierro Island (Canaries) from Low-Frequency Microseismic Sounding: An Insight into the 2011 Seismo-Volcanic Crisis. Surveys in Geophysics. 34: 463–489. DOI 10.1007/s10712-013-9240-4.

Ibs-von SehtM, Wohlenberg J (1999), Microtremors measurements used to map thickness of soft soil sediments. Bulletin of the Seismological Society of America. 89:250-259.

Kiselev GP, Yakovlev EYu, Druzhinin SV, Galkin AS (2018) Local variations of the volume activity of radon over kimberlite pipes of the Arkhangelsk diamondiferous province. Environmental Earth Sciences 77:568.

Kutinov YG, Chistova ZB (2004) Ierarkhicheskii ryad proyavlenii shchelochno-ul'traosnovnogo magmatizma Arkhangel'skoi almazonosnoi provintsii. Ikh otrazhenie v geologo-geofizicheskikh materialakh. Pravda Severa, Arkhangelsk

Lane JW et al. (2008) Estimation of bedrock depth using the horizontal-to-vertical (H/V) ambient-noise seismic metho. Near Surface 2008-14th EAGE European Meeting of Environmental and Engineering Geophysics.

Milashev VA (1984) Trubki vzryva (Explosion Pipes). Nedra, Leningrad.

Nakamura YA (1989) Method for dynamic characteristic estimation of subsurface using microtremor on the ground surface. Quarterly Report of Railway Technical Research Institute. 30(1):25-33.

RSI (2016) RS-700 Mobile Radiation Monitoring System. Radiation Solutions Inc., Ontario, Canada.

Titaeva NA (2005) Geochemistry of Natural Radioactive Decay Series. GEOS, Moscow.

Verzhak VV, Medvedev VA, Verichev EM (1983) Otchet o rezul'tatakh razvedki kimberlitovykh trubok mestorozhdeniya im. MV Lomonosova v 1983–1987, Arkhangelsk.

VNIIFTRI (2006) The method of express measurement of volume activity of radon in soil air. Central Research Institute of Physical and Technical Measurements (VNIIFTRI), Moscow.

Delineation of the permissive tract using computational mineral prospectivity modelling

Johanna Torppa, Kalevi Rasilainen
Geological Survey of Finland

Abstract. We test two mineral prospectivity modelling based approaches for delineating regions favorable for the occurrence of specific types of mineral deposits. We adopt the term *permissive tract* to mean the favorable region, and call the left-over region non-permissive. The idea behind the permissive tract defined using mineral prospectivity modelling is identical to the permissive tract that is generally defined manually in the *three-part quantitative assessment* for estimating mineral resources. The motive for using mineral prospectivity modelling is the possibility to use more complex data sets than in manual tract delineation. One of the mineral prospectivity modelling approaches we use integrates continuous fuzzy memberships of each evidence data set to generate continuous prospectivity values across the study area. The non-permissive and permissive areas are delineated by setting a suitable prospectivity threshold. The other approach uses clustering to produce a number of regions, each one representing homogenous bedrock properties. Prospectivity of a region is defined using the frequency of known mineral occurrences and deposits within the cluster, and the non-permissive region is defined as the region with zero prospectivity.

1 Introduction

Identifying regions that are geology favorable for mineral occurrences is crucial, for instance, in land-use planning and quantitative mineral resource assessment. To describe such regions, we have adopted the term *permissive tract* from the *three-part quantitative assessment* for mineral resource estimation (Singer 1993; Singer and Menzie 2010).

The three-part quantitative assessment is a widely used method for evaluating mineral resources on regional scale. So far, the permissive tract has generally been defined manually by experts, based on geological maps and complimentary information, such as geophysical, geochemical and drill core data. The process of defining the permissive tract can be affected by biased expert opinions, and the decisions or choices made by the expert are sometimes hard to justify and even harder to track after years have passed. Due to the constantly increasing amount and improving quality of data, along with the increased efficiency of computers, the possibility to use computational mineral potential modelling (MPM) methods for defining the permissive tract has become worth considering. MPM is used to integrate information from a number of different data sources to generate prospectivity scores across the study area. Methods for computational MPM were presented already in the 80's and 90's (e.g., Agterberg 1989; Agterberg 1990; Bonham-Carter et al. 1990), and they have become a popular tool for evaluating the prospectivity of specific minerals. Due to their usefulness, the development of MPM methods has been rapid in the past few decades (Carranza 2017). Using MPM to target mineral exploration and make quantitative estimates of mineral resources transfers the focus of the expert work from routine data processing towards interpretation of the data and the results. It also makes it possible to efficiently derive information from large and complex data sets.

The United States Geological Survey (USGS) has implemented software to carry out the three-part quantitative assessment. Currently, however, running the entire assessment procedure requires executing a number of different computer programmes, which has been considered to be complicated. A more user-friendly version of the assessment software, based on the existing USGS code, is currently being developed in the European Institute of Innovation and Technology RawMaterials-funded project "Mineral Resource Assessment Platform" (MAP) coordinated by the Geological Survey of Finland (GTK). Besides generating an easy to use interface to the method, additional tools are implemented for documenting the assessment process and reporting the results. Also, an important step forward is an addition of the possibility to define the permissive tract using MPM.

Comparison of permissive tracts delineated manually by experts to tracts generated using computational MPM has been done previously by Raines (1999), who used the weights of evidence MPM, and Raines and Mihalasky (2002), who used the weights of evidence and weighted logistic regression MPM. Both studies suggest that computational MPM provides tracts comparable with manual delineation, assuming that the data set is appropriate. It is also emphasized in Raines (1999) and Raines and Mihalasky (2002) that the expert delineation suffers from generalization of the tracts, possible inclusion of non-permissive areas and inconsistent tract delineation approaches between different expert groups.

In this study, we will test two MPM approaches for defining the permissive tract, and compare the result to the tract defined manually by experts. One of the approaches uses fuzzy logic based MPM, which will also be implemented in the MAP project. Fuzzy logic has been used for mineral prospectivity modelling since An et al. (1991), and provides means to transform knowledge into numerical form. Fuzzy logic has been one of the most popular MPM methods and different

ways to apply, improve the quality and estimate the uncertainty of the results have been presented in a large number of studies (e.g., Cheng and Agterberg 1999; Yousefi et al. 2012; Lisitsin et al. 2014; Torppa et al. 2015; Yousefi and Nykänen 2016). The other MPM approach uses data clustering with self-organizing maps (Kohonen 2001) and k-means, and defines the prospectivity of clusters based on the frequency of known mineral occurrences and deposits in the clusters. This approach was used by Torppa et al. (2019) in delineating the permissive tract for orogenic gold prospectivity modelling of the Central Lapland Greenstone belt. Clustering geoscientific data using SOM has also been used in several studies, such as Fraser et al. (2006), Torppa et al. (2015) and Carneiro et al. (2018).

Prospectivity values produced by different MPM techniques and computed using different data sets are not generally comparable and there is no universal prospectivity threshold value that could be used to distinguish permissive region from non-permissive. Thus, an important part of the method development is to generate guidelines and justification to specify the threshold for defining what is permissive and what is not.

We will apply MPM for generating the permissive tract for volcanic massive sulfide (VMS) deposits in the Pyhäsalmi and Vihanti Groups in Finland. A manual delineation of the permissive tract for Pyhäsalmi and Vihanti VMS deposits has been carried out before (Rasilainen et al. 2014), and the result obtained using the MPM approach will be compared to the one obtained by the manual generation by experts.

In this paper, we describe the proposed MPM approaches and the data, while the results will be presented in the conference.

2 Permissive tract delineation methods

In the context of the three-part quantitative assessment, a permissive tract represents the surface projection of a volume of rock where geology allows the existence of mineral deposits of one or more specific types. The delineation of the permissive tract using conventional methods requires binary thinking, as the study area is directly divided to permissive and non-permissive parts. Mineral prospectivity modelling methods differ from this in the sense that, even if each single data set would be split to permissive and non-permissive classes, the resulting prospectivity map has a range of prospectivity scores, either discrete or continuous, depending on the modelling method. For generating the permissive tract from the prospectivity map, a prospectivity threshold must be defined. The threshold can be set to exclude the regions that are most likely non-permissive, leaving the rest of the region permissive, or it can be set to include the regions that are most likely permissive, leaving the rest of the region non-permissive. The difference between the tracts defined in these two ways depends on the data sets and MPM methods that were used. In any case, the permissive tract defined using the latter approach is a subset of the tract defined by the former approach. By defining a suitable threshold, the tracts defined manually by an expert, and computationally using MPM should be approximately the same. However, the data used in MPM have higher spatial resolution, producing a more detailed permissive tract.

2.1 Expert delineation

In a three-part assessment process, the permissive tracts are generally delineated by experts using available geological information. Delineation mostly relies on the lithological map that is used to manually select the regions that are expected to contain or not to contain the deposit of interest. In addition to the lithological map, also drill core, geochemical and geophysical data are used if applicable, to refine tract boundaries. The criteria for the delineation are expressed in the descriptive deposit model, which contains the characteristic features of the deposit type and its geological environment. As the purpose of the permissive tract is to represent a surface projection of the permissive volume, the geology below the surface is in principle defined as well. However, the workflow usually starts with first defining the 2D surface projection, and then extending this down wards, rather than starting with generating a 3D model and then projecting this to the surface. In the assessments carried out by the GTK, 1 km is usually used as the assessment depth.

2.2 Computational delineation

We use two MPM approaches (fuzzy logic and clustering with training data) to define the prospectivity of the study area, and divide the area to non-permissive and permissive parts, based on the prospectivity scores. A fuzzy logic based approach is used to calculate a continuous prospectivity score, in which case a threshold is needed to be defined for splitting the prospectivity values to permissive and non-permissive. The clustering based approach provides areas with discrete prospectivity values, and the zero prospectivity class is used to represent the non-permissive region and all the other clusters the permissive region.

2.3 Fuzzy logic

The idea of fuzziness is used in the fuzzy logic MPM to define the membership values for each input data set. Instead of making just a binary division of the data to favorable and non-favorable, continuous membership values are defined according to how the values of each data set correspond to or are expected to correspond to the occurrence of a specific mineral. The major advantage of the approach is that the membership values can be defined based on expert knowledge, without using any known mineral occurrences as training data. Memberships, however, can also be defined using training data by finding the function that describes the frequency of known occurrences as a function of the data value (Torppa et al. 2019). In an

optimal case the fuzzy logic prospectivity maps computed from memberships generated by expert and those computed using training data are the same. However, due to restrictions in both the number of known occurrences and expert knowledge, the maps may differ significantly.

We use ArcGIS Fuzzy Overlay functions to combine the fuzzy memberships. One of the overlay functions OR, AND, SUM, PRODUCT and GAMMA is used, depending on does the existence of minerals require a high membership of only one or of all the evidence data sets, or does the prospectivity increase as any of the evidence memberships increases.

A drawback in the membership approach is, that it assumes each data set to be independently correlated to the occurrence of minerals, which does not generally apply.

2.4 Clustering

The main idea of the clustering approach is to divide the study area into regions with internally homogenous geological properties, and define the prospectivity for each region. Clustering is a mathematical procedure that requires no geological modelling or assumptions. The success of clustering in representing the variation in geology depends purely on the choice of the data sets. A single data cluster can be a single solid region in the geospace or, more commonly, it can form several spatially separate regions with similar properties.

The prospectivity of each cluster can be defined either knowledge-based or empirically. In the knowledge-based approach, the expert uses the distribution of data within each cluster to evaluate whether the cluster represents geology favourable for the occurrence of mineral deposits or not. The empirical approach uses the frequency of known mineral deposits and occurrences in the clusters to compute the favourability.

We use the unsupervised clustering methods self-organizing maps (SOM) and k-means to define the clusters, and known mineral deposits and occurrences to define the prospectivity score for each cluster. SOM is applied for generating a large number (of order 10000) of proto-clusters to reduce the size of the data set and to remove outliers. SOM proto-clusters are further clustered with k-means to produce of order 10-20 clusters that represent the variation in geology of the study area.

3 VMS deposits in the study area

GTK has previously assessed the undiscovered resources in VMS deposits in Finland (Rasilainen et al. 2014). For the present study, we selected an area in the central part of Finland, which contains the important Vihanti and Pyhäsalmi VMS areas in Finland (Fig. 1). The study area contains four permissive tracts delineated by GTK experts during the previous assessment. Two of the tracts (Vihanti tract, Pyhäsalmi tract) are delineated for the felsic-type VMS deposits (Mosier et al. 2009), and they contain 11 well-known VMS deposits, five of which have been mined, and 41 occurrences. The other two tracts (Rauhala tract, Upper Svecofennian tract) belong to the bimodal-mafic-type and contain one well-known deposit and 11 occurrences.

4 Data available for VMS permissive tract delineation using MPM

The study area has a good coverage of geochemical and geophysical data. It contains over 7000 diamond drill holes, and large part of it has been actively explored for VMS, gold and nickel deposits since the early 1900s.

Based on the report by Leväniemi and Karell (2013), gravity, magnetic, electromagnetic and possibly radiometric data as well may be useful to indicate the locations of VMS deposits. Magnetic, electromagnetic and radiometric data are extracted from GTK's low altitude airborne geophysical survey data products. Gravimetric measurements have been carried out across the entire study area by the Finnish Geospatial Research Institute (Kääriäinen and Mäkinen 1997), and supplementary gravity measurements across part of the study area have been carried out by GTK.

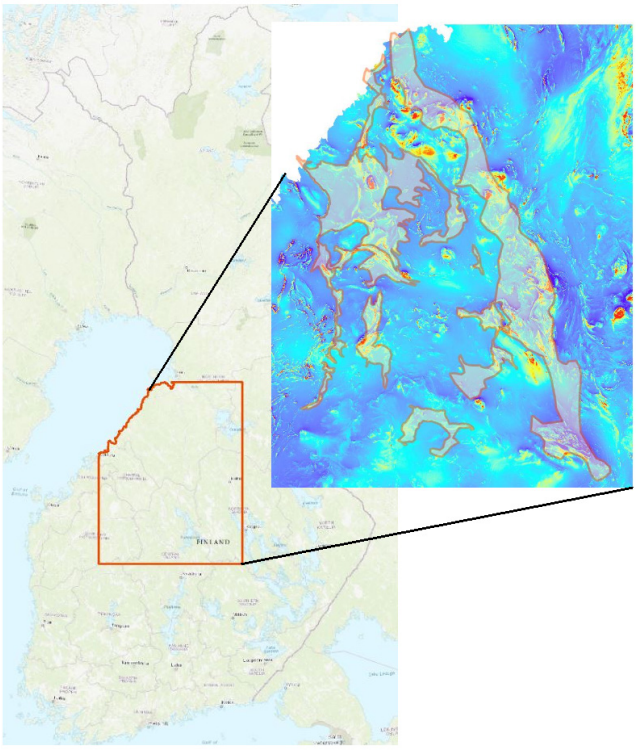

Figure 1. Location of the study area in Finland, and the magnetic anomaly map with the manual delineation of VMS deposits.

Geochemical data are available from both till and whole rock samples. Till geochemical data are available from the GTK regional till geochemical survey from the entire study area with approximately 2 km sampling point spacing. The data, thus, provides average concentrations in till with low resolution compared to geophysical data. Whole rock geochemical data of the

Rock Geochemical Database of Finland (Rasilainen et al. 2007) are available from the whole study area. The data are unevenly distributed with approximately 7 km sampling point spacing. Geochemical data from drill cores and outcrop samples are also available. Due to the low spatial density of the samples with whole rock geochemistry, the data will not be used as interpolated concentrations, but as an indicator of existence and non-existence, based on a specified concentration threshold of the elements. The indicator elements for VMS prospectivity modelling include all the main ore metals (Cu, Zn and Pb). In addition, the applicability of several other trace elements, including S, Se, Ag, Au and Fe, will be tested.

Geological map will be used to rule out certain areas. Since VMS deposits are hosted by volcanic-sedimentary sequences, rocks not belonging to such sequences are not permissive. Within the study area, the 1.93–1.91 Ga lower Svecofennian volcanic and sedimentary rocks of the Pyhäsalmi and Vihanti groups, and the 1.88 Ga upper Svecofennian supracrustal rocks define the minimum boundaries of the permissive areas.

References

Agterberg FP (1989) Computer programs for mineral exploration. Science 245(4913):76-81.

Agterberg FP (1990) Estimating the probability of occurrence of mineral deposits from multiple map patterns. *in*: Kurzl H, Merriam DF (eds) Use of Microcomputers in Geology, Computer Applications in the Earth Sciences, Springer, Boston, MA.

An P, Moon WM, Rencz A (1991) Application of fuzzy set theory for integration of geological, geophysical and remote sensing data. Canadian Journal of Exploration Geophysics 27:1–11.

Bonham-Carter GF, Agterberg FP, Wright (1990) Weights of evidence modelling: a new approach to mapping mineral potential, *in:* Statistical applications in the earth sciences. Geol. Survey Canada Paper 89-9:171-183.

Carneiro C, Fraser S, Crósta A, Silva A, Barros C (2018) Semiautomated geologic mapping using self-organizing maps and airborne geophysics in the Brasilian Amazon. Geophysics 77 (4):17-24.

Carranza EJM (2017) Natural Resources Research publications on geochemical anomaly and mineral potential mapping, and introduction to the special issue of papers in these fields. Natural Resources Research 26:379–410.

Cheng Q, Agterberg FP (1999) Fuzzy weights of evidence method and its application in mineral potential mapping, Natural Resources Research 8:27-35

Fraser S, Mikula P, Lee M, Dickson B, Kinnersly E (2006) Data mining data – Ordered vector quantization and examples of its application to mine geotechnical data sets, i*n*: Dominy S. (ed), 6th International Mining Geology Conference AusIMM Publication Series 6/2006:259-268.

Kohonen T (2001) Self-organizing maps. Springer Series in Information Sciences.

Kääriäinen J, Mäkinen J (1997) The 1979-1996 gravity survey and results of the gravity survey of Finland 1945-1996, Publications of the Finnish Geodetic Institute 125.

Leväniemi H, Karell F (2013) Geophysical indications of VMS deposits in the Häme Volcanic Belt. Geological Survey of Finland, Archive Report 152.

Lisitsin V, Porwal A, McCuaig TC (2014) Probabilistic fuzzy logic modeling: Quantifying uncertainty of mineral prospectivity models using Monte Carlo simulations. Mathematical geosciences 46:747-769.

Mosier D, Berger V, Singer D (2009) Volcanogenic massive sulfide deposits of the world; database and grade and tonnage models. U.S. Geological Survey Open-File Report 2009-1034.

Raines GL (1999) Evaluation of weights of evidence to predict epithermal gold deposits in the Great Basin of the Western United States. Natural Resources Research 8:257-276.

Raines GL, Mihalasky MJ (2002) A reconnaissance method for delineation of tracts for regional-scale mineral-resource assessment based on geologic-map data. Natural Resources research 11(4):241-248.

Rasilainen K, Eilu P, Halkoaho T, Karvinen A, Kontinen A, Kousa J, Lauri L, Luukas J, Niiranen T, Nikander J, Sipilä P, Sorjonen-Ward P, Tiainen M, Törmänen T, Västi K (2014) Quantitative assessment of undiscovered resources in volcanogenic massive sulphide deposits, porphyry copper deposits and Outokumpu-type deposits in Finland. Geological Survey of Finland, Rep Invest 208.

Rasilainen K, Lahtinen R, Bornhorst TJ (2007) The Rock Geochemical Database of Finland manual. Geological Survey of Finland, Rep Invest 164.

Singer DA (1993) Basic concepts in three-part quantitative assessments of undiscovered mineral resources. Nonrenewable Res 2:69−81.

Singer DA, Menzie WD (2010) Quantitative mineral resource assessments: An integrated approach. Oxford University Press, New York.

Torppa J, Middleton M, Hyvönen E, Lerssi J, Fraser S (2015) A novel spatial analysis approach for assessing regional-scale mineral prospectivity in northern Finland, Geological Survey of Finland, Special Paper 57:87-120.

Torppa J, Nykänen V, Molnár F (2019) Unsupervised clustering and empirical fuzzy memberships for mineral prospectivity modelling. Ore Geology Reviews 107:58-71.

Yousefi M, Kamkar-Rouhani A, Carranza EJ (2012) Geochemical mineralization probability index (GMPI): A new approach to generate enhanced stream sediment geochemical evidential map for increasing probability of success in mineral potential mapping. Journal of Geochemical Exploration 115:24-35.

Yousefi M, Nykänen V (2016) Data-driven logistic-based weighting of geochemical and geological evidence layers in mineral prospectivity mapping. Journal of Geochemical Exploration 164:94-106.